RECEIVED
LAWRENCE
RADIATION LABORATORY

UCRL-18597 Rev.

c.2

DOCUMENTS SECTION

DIFFUSION AND MIGRATION IN ELECTROCHEMICAL SYSTEMS

Limin Hsueh
(Ph.D. Thesis)

December 1968
(Corrected March 1971)

AEC Contract No. W-7405-eng-48

TWO-WEEK LOAN COPY

This is a Library Circulating Copy which may be borrowed for two weeks. For a personal retention copy, call Tech. Info. Division, Ext. 5545

LAWRENCE RADIATION LABORATORY
UNIVERSITY of CALIFORNIA BERKELEY

UCRL-18597 Rev.
c.2

DISCLAIMER

This document was prepared as an account of work sponsored by the United States Government. While this document is believed to contain correct information, neither the United States Government nor any agency thereof, nor the Regents of the University of California, nor any of their employees, makes any warranty, express or implied, or assumes any legal responsibility for the accuracy, completeness, or usefulness of any information, apparatus, product, or process disclosed, or represents that its use would not infringe privately owned rights. Reference herein to any specific commercial product, process, or service by its trade name, trademark, manufacturer, or otherwise, does not necessarily constitute or imply its endorsement, recommendation, or favoring by the United States Government or any agency thereof, or the Regents of the University of California. The views and opinions of authors expressed herein do not necessarily state or reflect those of the United States Government or any agency thereof or the Regents of the University of California.

DIFFUSION AND MIGRATION IN ELECTROCHEMICAL SYSTEMS

Contents

ABSTRACT v

I. INTRODUCTION 1

II. MASS TRANSFER IN A BINARY ELECTROLYTIC SOLUTION 6

2.1 Limiting Current Density in a Concentrated Solution . . . 6

2.2 Differential Diffusion Coefficients 19

III. MASS TRANSFER IN A MULTICOMPONENT ELECTROLYTIC SOLUTION 26

3.1 The Justification of the Use of an Integral Diffusion Coefficient 27

3.2 The Equation of Convective Diffusion at High Schmidt Number 28

A. Boundary Layer Model 28

B. Penetration Model 32

3.3 Integral Diffusion Coefficient 34

IV. THE EFFECT OF MIGRATION IN A MULTICOMPONENT ELECTROLYTIC SOLUTION 42

4.1 Comparison of Complete and No Dissociation of Bisulfate Ion 43

4.2 Partial Dissociation of Bisulfate Ion 53

V. TRANSIENT BEHAVIOR IN A STAGNANT DIFFUSION CELL 58

5.1 Mathematical Analysis 58

5.2 Numerical Calculation Method 62

5.3 Theoretical Results 64

VI. EXPERIMENTAL WORK-----Electrical Measurement 71

6.1 Experimental Method in a Stagnant Diffusion Cell 71

A. Cell Construction 71

B. Preparation and Analysis of Solution 71

C. Circuit Diagram 74

D. Control Panel 74

6.2 Experimental Procedure 76

6.3 Results and Discussion 77

A. Transient Behavior at Very Short Times 83

B. Current Behavior at Very Large Times----the effect of Migration 87
VII. EXPERIMENTAL WORK----Optical Measurement 91
7.1 Experimental Method 91
A. Cell and Electrode 92
B. Cell Cleaning 95
C. Photography 97
D. Counting the Number of Fringes 97
7.2 Evaluation of Proportionality Constants k_A and k_B 99
7.3 Surface Concentration in a Binary Electrolyte 106
7.4 Concentration Profile in a Binary Electrolyte 113
7.5 Surface Concentration in a Multicomponent Solution . . . 116
7.6 Concentration Profile in a Multicomponent Solution . . . 120
VIII. CONCLUSIONS AND RECOMMENDATIONS 124
ACKNOWLEDGEMENTS 129
APPENDICES 130
A. Physical Properties of $CuSO_4$-H_2SO_4 Solutions at 25°C. 130
B. Analysis of Copper Sulfate and Sulfuric Acid Solutions 139
C. Data Processing of a Magnetic Tape 143
D. Magnetic Tape Handling 156
E. Computer Programs 157
F. Control Panel in Electrical Measurement 172
G. Analytic Solution of the Effect of Migration in Nernst Diffusion Layer 175
NOMENCLATURE 182
REFERENCES 186

DIFFUSION AND MIGRATION IN ELECTROCHEMICAL SYSTEMS

Limin Hsueh

Inorganic Materials Research Division, Lawrence Radiation Laboratory
Department of Chemical Engineering
University of California, Berkeley, California

March 1971

ABSTRACT

The limiting current and concentration profile in a stagnant diffusion cell are calculated for a concentrated copper sulfate solution with consideration of the variation of physical properties and nonzero interfacial velocity. The calculated concentration profile is compared with that observed optically in a cell with a stagnant electrolyte at the limiting current. The possibility and the method for obtaining differential diffusion coefficients from the limiting current measurements are explored.

The use of integral diffusion coefficients in multicomponent electrolytic solutions at high Schmidt numbers is justified on the basis of hydrodynamic considerations. Integral diffusion coefficients are measured by a rotating disk and a stagnant diffusion cell over a concentration range of copper sulfate 0.01M to 0.6M, and sulfuric acid 0.0 to 2.5M.

In a copper sulfate, sulfuric acid solution, sulfate ions as well as bisulfate ions are present in the solution as anions. The effect of migration on the limiting current and the concentration difference between bulk and surface is measured and compared with calculated values from the incomplete dissociation of bisulfate ions.

The theory of transient behavior of current density and surface concentration in a stagnant diffusion cell is discussed. The experimental results agree well with the theory, within the accuracy of available electrochemical kinetic parameters and the experimental error.

I. INTRODUCTION

In modern electrochemical industries, such as electroplating, electrorefining, and electromachining, the rate of electrochemical reactions is mostly limited by mass transfer. The three general directions to increase the operating efficiency of an electrochemical process are;

i. Increase the concentration of electrolyte,

ii. Add a proper amount of supporting electrolyte or special addition agents, and

iii. Apply appropriate stirring.

The stirring helps to increase the mass transfer rate and prevents the buildup of concentration gradients, whereas the supporting electrolyte increases the rate of charge transfer and makes the current distribution more uniform. Since the mass transfer rate is approximately proportional to the concentration of electrolyte, the more concentrated the electrolyte is, the shorter the residence time of operations.

There is no way to study the stirring unless the hydrodynamics are well defined. In the past decades, several well-known hydrodynamic flow conditions have been subjected to electrochemical mass transfer study. Two well-written review papers in this area are due to Newman[1] and Ibl.[2]

The advantage of using an electrochemical system in a mass transfer study is that the concentration or mass flux can be easily measured or controlled in terms of current density or voltage. On the other hand, the surface overpotential, concentration overpotential, and

ohmic resistance are likely to complicate the boundary conditions in solving the equation of convective diffusion.

In a previous paper,[3] a concentrated electrolyte was studied with a rotating disk electrode with consideration of the variation of physical properties in the diffusion layer, the nonzero interfacial velocity due to the high mass transfer rate, and the Schmidt number correction. There was no way to measure the concentration profile near the electrodes or to invert the measured integral diffusion coefficient into the differential diffusion coefficient. Consequently, a simpler geometry and hydrodynamic system-----a stagnant diffusion cell (see Fig. 6-1)----is chosen for study, thus keeping the assumptions in solving the diffusion equation as few as possible, in order to improve our understanding of the basic laws of mass transfer in electrolytic solutions.

A metal deposition reaction, namely, copper from a copper sulfate solution or from a copper sulfate plus sulfuric acid solutions is chosen for this study.

In chapter 2, the rigorous method of calculating the limiting current and concentration profile of a concentrated binary electrolyte (electrolyte consists of one salt and one solvent) is carried out for a stagnant diffusion cell with consideration of all the previously mentioned conditions. The inverse procedure of calculating the differential diffusion coefficient from the measured limiting current can be done by means of correlations and iterative procedure for a complete concentration range of a binary electrolyte.

However, as one extends the problem to a ternary electrolyte, i.e., a solution consisting of one salt, one supporting electrolyte, and one solvent, the number of transport coefficients increase greatly. The actual rigorous calculation of a limiting current is tedious and almost impossible because of the lack of data of transport properties as function of concentration.

In chapter 3, integral diffusion coefficients for the multicomponent, concentrated solution are defined and measured. An integral diffusion coefficient measured by a simple hydrodynamic setup can be used for other hydrodynamic conditions according to their classifications.

Because of the difficulty of treating all effects in a multicomponent solution simultaneously, the effect of migration is separated out and treated in chapter 4 with the assumptions of constant physical properties and dilute solution theory. The incomplete dissociation of bisulfate ion was ignored in a copper sulfate and sulfuric acid solution in most previous work. Its effect on the migration and the concentration difference of supporting electrolyte between the bulk and electrode surface is discussed.

In limiting current measurements in a solution with <u>little</u> or <u>no</u> supporting electrolyte, the behavior of polarization curves, measured by a rotating disk or a stagnant diffusion cell, is not as ideal as was found in most of the work that has been done in this area with a large amount of supporting electrolyte (5 to 1000 times more than the reacting electrolyte).

For a solution with little supporting electrolyte, the overall voltage with a rotating disk is high and the plateau of the polarization curve tends to become a point of inflection. Moreover, the limiting current, or the point of inflection, varies with respect to the rate of increase of applied current. For the same solution, measurements of log current vs. log time in a stagnant diffusion cell have only a small portion of the curve with a slope of $-\frac{1}{2}$.

The quantitative description of the non-uniformity of current distribution by Newman,[1,33,34] at a rotating disk electrode and at a plane electrode was a major step toward the solution of the paradox. In chapter 5, a similar treatment is applied to the study of the transient behavior in a stagnant diffusion cell. The surface concentration of the reacting ion will not be assumed to have a step drop to zero,[7] but will be a function of time. Both ohmic resistance and surface and concentration overpotentials are included as boundary conditions.

In chapter 6, the detailed experimental procedure of the measurement of current as a function of time in a simple capillary tube is described. The results are compared with the theoretical prediction from chapters 4 and 5.

In chapter 7, concentration profiles and surface concentrations for deposition of copper from stagnant copper sulfate solutions in an optical cell are measured at the limiting current. O'Brien has observed concentration profiles by an optical technique at constant current in a cell of finite length (0.313 cm) with cathode over anode. His results deviate significantly from classical solution based on constant physical properties.

In summary, the objectives of this work are

1. To study the rate of mass transfer in electrolytic solutions at various hydrodynamic conditions in terms of the relationship between limiting current and diffusivity.

2. To observe the concentration profiles in a stagnant diffusion cell at the limiting current and to compare it with the numerical solutions which account for the concentration dependence of transport properties.

3. To study the role of bisulfate ion and its effect on migration in $CuSO_4/H_2SO_4$ system from the measurements of limiting current and the surface concentration change of surface acid.

4. To study the transient behavior of current density and surface concentration of a binary electrolyte as a function of time in a stagnant diffusion cell.

II. MASS TRANSFER IN A BINARY ELECTROLYTIC SOLUTION

2.1 Limiting Current Density and Concentration Profile in a Concentrated Electrolyte

The limiting current density is a quantity that is of general interest in the mass transfer study in an electrochemical system. Since this quantity expresses the maximum rate of mass transfer of the reactants to the electrode or of the products being removed from the electrode, the limiting current is thus defined as the highest permissible current that may cross an electrode without a secondary electrode process occurring. When an electrochemical system is operated at limiting current, either the concentrations of reactants become zero or the products reach the saturation concentration in the solvent.

In convective diffusion, the limiting current is generally proportional to the concentration of electrolyte and inversely related to the thickness of the diffusion layer which is in turn inversely related to the rate of stirring.

In a concentrated, binary electrolyte, the limiting current calculation is complicated by the effect of variation of physical properties, the nonzero interfacial velocity, and Schmidt number corrections. The problem has been solved for a rotating disk electrode in a previous paper.[3] The theoretical analysis of a stagnant diffusion cell is similar to the analysis of a rotating disk electrode.

For one dimensional, unsteady state diffusion, the concentrated electrolyte theory shows[4] that a binary electrolyte in a solution carrying a current i_y obeys the equation

$$\rho\left(\frac{\partial\omega}{\partial t} + v_y \frac{\partial\omega}{\partial y}\right) = \frac{\partial}{\partial y}\left(\rho D \frac{\partial\omega}{\partial y}\right) - \frac{M_s i_y}{z_+ \nu_+ F} \frac{\partial t_+}{\partial y} \quad , \tag{2-1}$$

where y is the distance from the electrode in the direction perpendicular to the electrode surface; v_y is a mass average velocity which arises from the high mass transfer flux; M_s is the molecular weight of salt. Subscripts + or - refer to cations or anions respectively. The mass fraction* is used for consistency with the mass average velocity v_y.

Since the density of the solution depends on the concentration, the velocity is determined by the equation of continuity,

$$\frac{\partial\rho}{\partial t} + \frac{\partial}{\partial y}\left(\rho v_y\right) = 0 \quad . \tag{2-2}$$

With the assumption of constant surface concentration, the boundary conditions are

$$\begin{aligned} &\omega = \omega_\infty && t \geq 0 \quad \text{at } y \to \infty \\ &\omega = \omega_o \ , \ v_y = \frac{i_y M_+}{\rho_o F z_+} && t > 0 \quad \text{at } y = 0 \end{aligned} \tag{2-3}$$

For a metal deposition reaction, the fluxes of anions and solvent are zero at the interface; therefore the current is directly related to the flux of cations. The flux in a <u>concentrated</u> binary electrolyte is (see e.g., Eq. (84) in Ref. 4.)

$$\frac{i_y}{F z_+} = N_+ = -\nu_+ \frac{D_o \rho_o}{M_s} \frac{\partial\omega}{\partial y} + \frac{i_y t_+}{F z_+} + \frac{\rho_o}{M_+} \omega_+ v_y \tag{2-4}$$

---

*mass fraction is related to molarity by $c_i = \frac{\rho}{M_i} \omega_i$.

where t_+ is transference number of the cation and the subscript o refers to the physical properties at z=0.

Substituting the nonzero interfacial velocity of Eq. (2-3) into Eq. (2-4) and solving for current density give

$$i_y = \frac{\rho_o D_o F z_+ \nu_+}{M_s(1-t_+-\omega_+)} \frac{\partial\omega}{\partial y}\Big|_{y=0} \tag{2-5}$$

With the dimensionless variables

$$\xi = \frac{y}{\sqrt{4D_\infty t}} \quad , \qquad H(\xi) = 2v_y\sqrt{\frac{t}{D_\infty}} \tag{2-6a,b}$$

and the assumption that ω is function of ξ only, and hence the same for all the other fluid properties (ρ, D, t_+), Eqs. (2-1) and (2-2) are then reduced to two ordinary differential equations

$$\left[\frac{\rho}{\rho_\infty}(H-2\xi) + I\frac{dt_+}{d\omega}\right]\frac{d\omega}{d\xi} = \frac{d}{d\xi}\left(\frac{\rho D}{\rho_\infty D_\infty}\frac{d\omega}{d\xi}\right) \quad , \tag{2-7}$$

and

$$\frac{dH}{d\xi} = \frac{2\xi-H}{\rho}\frac{d\rho}{d\xi} \quad , \tag{2-8}$$

where I is a dimensionless current density which is

$$I = \frac{2M_s i_y}{\rho_\infty \nu_+ z_+ F}\sqrt{\frac{t}{D_\infty}} \quad . \tag{2-9}$$

Two integrations of Eq. (2-7) give the concentration profile

$$\frac{\omega-\omega_o}{\omega_\infty-\omega_o} = \int_0^\xi \frac{1}{S} e^B d\xi \Big/ \int_0^\infty \frac{1}{S} e^B d\xi \tag{2-10}$$

$$S = \rho D/\rho_\infty D_\infty$$

$$B = \int_0^\xi \left(\frac{P}{S} - \frac{2D_\infty}{D}\xi\right) d\xi$$

$$P = \frac{\rho}{\rho_\infty} H + I\frac{dt_+}{d\omega}$$

Integration of Eq. (2-8) gives the velocity profile

$$H = 2\xi - \frac{2}{\rho}\int_0^\xi \rho d\xi + \frac{H_o\rho_o}{\rho} \tag{2-11}$$

Combining Eqs. (2-5), (2-6a) and (2-9) gives the relation of dimensionless current and concentration derivative at the surface

$$I = -\frac{\rho_o D_o}{\rho_\infty D_\infty}\frac{1}{(1-t_+-\omega_+)}\frac{d\omega}{d\xi}\Big|_{\xi=0} \tag{2-12a}$$

Combining Eqs. (2-3), (2-6b) and (2-9) gives the relation of dimensionless current and mass flux

$$I = \frac{\rho_o}{\rho_\infty}\frac{M_s}{M_+\nu_+} H(0) \tag{2-12b}$$

The integration of Eqs. (2-10), (2-11) and the differentiation of Eq. (2-12) were performed numerically with a digital computer. The physical properties of the binary electrolyte of copper sulfate at 25°C were obtained from the literature and are linearly correlated as a

function of ω^5

$$\rho = 0.99669 + 0.026901\,\omega^{\frac{1}{2}} + 0.74771\omega + 0.80718\,\omega^{\frac{3}{2}}$$

$$t_+ = 0.40293 - 3.57889\,\omega + 8.21995\,\omega^{\frac{3}{2}}$$

$$D = 0.207\,\exp\,(-29.0\,\omega^{\frac{1}{2}}) + 0.638 - 0.580\,\omega^{\frac{1}{2}} \qquad (2\text{-}13)$$

The computer program CONCEN was written for this calculation and is presented in Appendix E1. For a 0.4M $CuSO_4$ solution, the concentration profile in terms of c/c_∞ is tabulated as a function of the dimensionless distance ξ in Table 2-1. This is compared with the concentration profile calculated without consideration of variation of physical properties and nonzero interfacial velocity, which is independent of the nature of the electrolytic solution and can be expressed as

$$\frac{c}{c_\infty} = \frac{1}{\Gamma(\frac{3}{2})} \int_0^{\xi} e^{-\xi^2} d\xi = \text{erf}\,(\xi) \qquad (2\text{-}14)$$

The numerical value of the error function erf(ξ) is also given in Table 2-1 for comparison. For more detailed numerical tabulations, see Ref. 44.

For the same solution, the concentration profile was also calculated for a rotating disk, the details of formulas and calculations are given in Ref. 5. For this case, the dimensionless distance becomes

$$\xi = y\left(\frac{a\nu}{3D_\infty}\right)^{\frac{1}{3}}\sqrt{\frac{\Omega}{\nu}} \qquad (2\text{-}15)$$

and the concentration profile of constant physical properties becomes

$$\frac{c}{c_\infty} = \frac{1}{\Gamma(\frac{4}{3})} \int_0^{\xi} e^{-\xi^3} d\xi \tag{2-16}$$

The detailed tabulation of Eq. (2-16) can also be found in Ref. 44. All four concentration profiles are plotted in Fig. 2-1. The solid lines refer to the exact concentration profiles, whereas the dashed lines are those from Eqs. (2-14) and (2-16), i.e., with the assumption of constant physical properties and nonzero interfacial velocity and, for the disk, large Schmidt numbers.

A normalized flux at the electrode is defined as $(1/c_\infty)dc_\infty/d\xi$ at $\xi = 0$. It is a constant of $1/\Gamma(3/2)$ or 1.12838 for a stagnant diffusion cell and $1/\Gamma(4/3)$ or 1.1198 for a rotating disk electrode when the physical properties are assumed constant, interfacial velocity is zero and, for the disk, the Schmidt number is large. In actuality, it decreases as concentration increases, the numerical values being tabulated in Table 2-2 and plotted in Fig. 2-2. Again, the solid lines and dashed lines have the same meanings as in Fig. 2-1.

Since the flux is not an easily measurable quantity, it is desirable to find the concentration dependence of the dimensionless limiting current density I_L. The I_L was defined in Eq. (2-9) and actually calculated from the differentiation of Eqs. (2-10) and (2-12) with $\omega_+ = 0$. For copper sulfate at 25°C, I_L are tabulated as a function of concentration in Table 2-3 and $i_L\sqrt{t}$ were calculated accordingly from the definition of I_L in Eq. (2-9).

For the case of the rotating disk electrode, the detailed mathematics have been discussed[3,5] in a similar manner; only the result

has been transferred here for comparison. The numerical values and plots are again put in parallel with the stagnant diffusion cell in Table 2-3 and Fig. 2-3.

Comparisons were also made for the case of constant physical properties and nonzero interfacial velocity and, for the disk, large Schmidt numbers. For a stagnant cell[7]

$$i_L\sqrt{t} = -\frac{nFc_\infty}{(1-t_+)}\sqrt{\frac{D}{\pi}} \tag{2-17}$$

and for a rotating disk electrode, it is the Levich equation[8]

$$\frac{i_L}{\sqrt{\Omega}} = 0.62048\left(\frac{\nu}{D}\right)^{-\frac{2}{3}}\frac{nFc_\infty\sqrt{\nu}}{(1-t_+)} \tag{2-18}$$

In summary, with the knowledge of ρ, t_+, and D_+ as functions of concentration (e.g., Eqs. (2-13)), the concentration profile can be established numerically by Eq. (2-10). The dimensional limiting current (see Eq. (2-9)) can be calculated from the slope of the concentration profile at the electrode surface by Eq. (2-12), thus making it possible to predict $i_L\sqrt{t}$ as a function of concentration in a stagnant diffusion cell.

From a practical point of view, it is desirable to predict D from the experimental measurements of $i_L\sqrt{t}$ or $i_L/\sqrt{\Omega}$. This is what will be discussed in the next section, i.e., how to invert the experimental measurements of $i_L\sqrt{t}$ or $i_L/\sqrt{\Omega}$ into differential diffusion coefficients.

Table 2-1. Concentration profile of 0.4M $CuSO_4$ at 25°C.

ξ	c/c_∞ stagnant diffusion cell (Penetration Model)		c/c_∞ Rotating Disk Electrode (Boundary Layer Model)	
	CPP[a]	Exact	CPP[a]	Exact
0	0.0	0.0	0.0	0.0
0.2	0.22270	0.1703	0.22352	0.1786
0.4	0.42839	0.3566	0.44090	0.3857
0.6	0.60386	0.5327	0.63776	0.5897
0.8	0.74210	0.6832	0.79616	0.7635
1.0	0.84270	0.8000	0.90429	0.8866
1.2	0.91031	0.8827	0.96410	0.9565
1.4	0.95228	0.9360	0.98973	0.9868
1.6	0.97635	0.9676	0.99786	0.9970
1.8	0.98909	0.9848	0.99968	0.9995
2.0	0.99532	0.9933	0.99996	0.9999
2.5	-	0.9994	1.0	-
4.0	-	0.9999	1.0	-

[a]Constant physical properties.

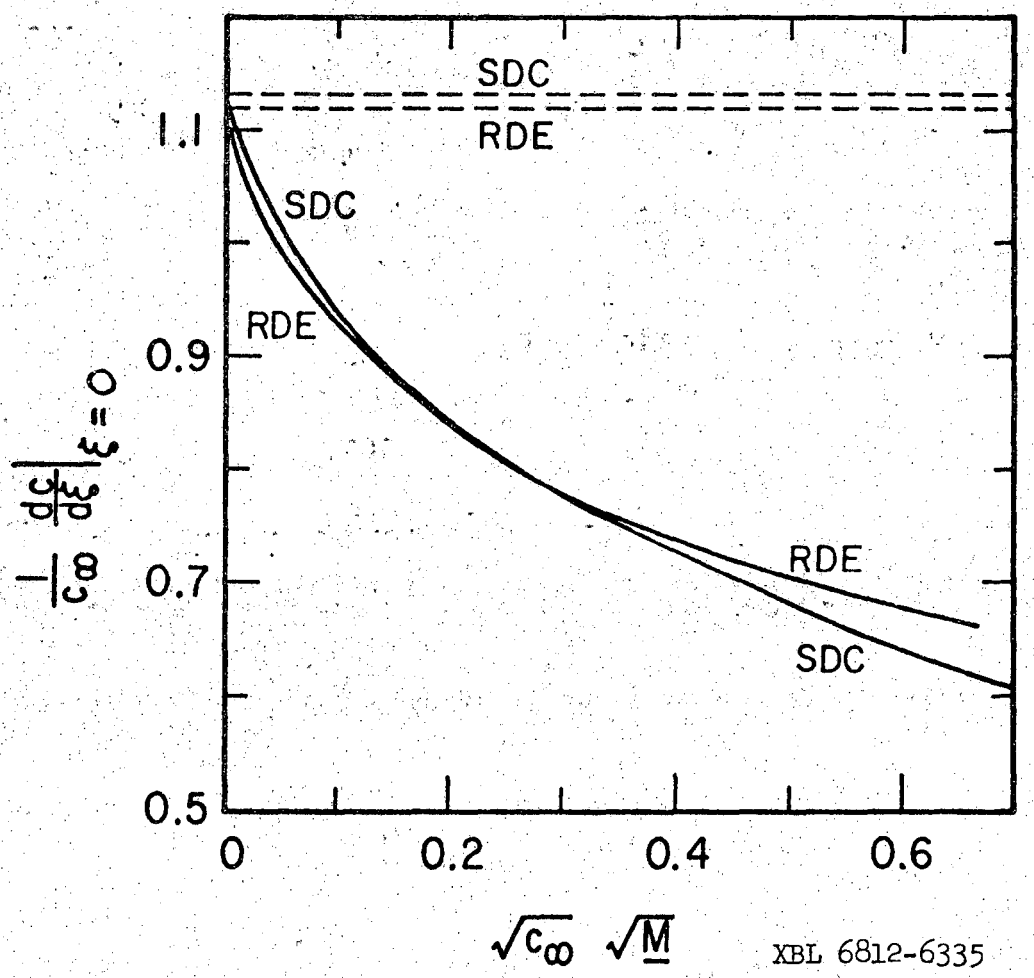

Fig. 2-2. Concentration dependence of the flux for copper sulfate solutions at 25°C.

Table 2-3. Limiting current density as a function of concentration for $CuSO_4$ at 25°C.

				SDC (Penetration)			RDE (Boundary Layer)	
c_∞	ω_∞	$t_{+\infty}$	D_∞	I_L	$i_L\sqrt{t}$		$i_L/\sqrt{\Omega}$	
M	10^{-2}		$10^{-6}\frac{cm^2}{sec}$		$\frac{mA}{cm^2}\sqrt{sec}$		$\frac{mA}{cm^2}/\sqrt{\frac{rad}{sec}}$	
					Exact	CPP[a]	Exact	CPP[a]
0.009984	0.1595	0.3978	6.80	-0.003122	-4.916	-4.707	1.608	1.563
0.01986	0.3168	0.3901	6.46	-0.006206	-9.542	-9.055	3.135	2.995
0.04969	0.7887	0.3805	6.02	-0.01530	-22.84	-21.43	7.443	6.986
0.1000	1.575	0.3628	5.71	-0.03001	-44.93	-40.82	14.13	13.05
0.2000	3.102	0.3368	5.37	-0.05748	-82.89	-76.11	26.66	23.91
0.2985	4.561	0.3198	5.14	-0.08300	-118.9	-108.4	38.34	33.71
0.4000	6.020	0.3089	4.96	-0.1082	-154.4	-140.3		
0.4989	7.403	0.3036	4.80	-0.1320	-188.2	-170.9	61.07	51.51

[a]CPP constant physical properties.

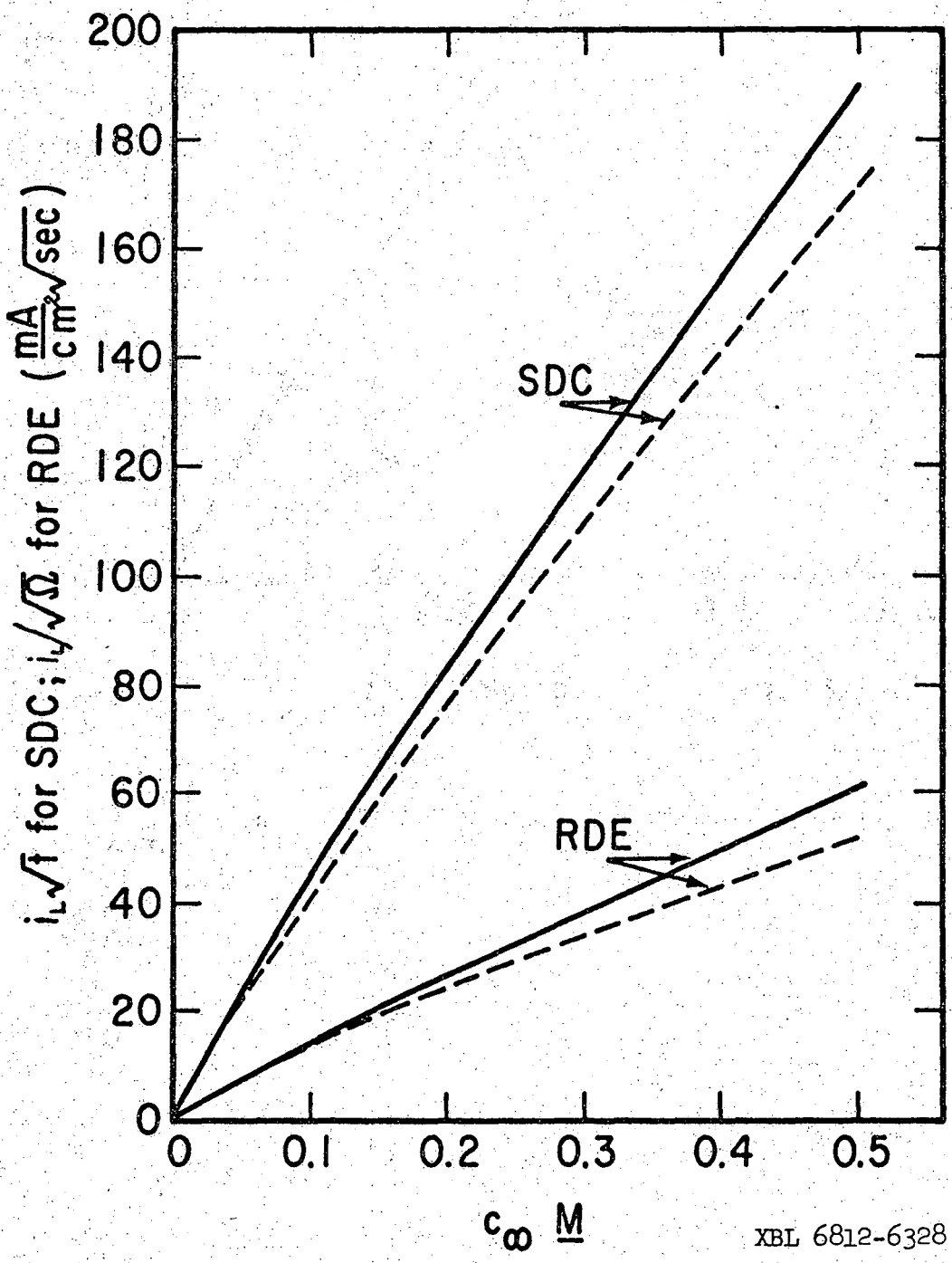

Fig. 2-3. Limiting currents for copper deposition from copper sulfate at 25°C.

2.2 : Differential Diffusion Coefficients

For decades, a considerable amount of work has been done in the measurement of diffusivities with various methods. The most common methods appear to be those utilizing optical methods or a diaphragm cell. The diaphragm cell has the inconvenience of being calibrated with a known system occasionally, in addition to the lengthy time for one measurement and the precision analysis of the concentration of solution. An optical method, however, generally involves the use of special precision equipment.

A stagnant diffusion cell, or a rotating disk electorde has the advantage of relatively simple experimental setup and easily measured quantities, current density and time or rotation speed. With modern instruments, no difficulty is involved in obtaining four to five signifcant figures in the above quantities. Thus the measurement of diffusivity is greatly facilitated.

To invert the measured values of $i_L\sqrt{t}$ (or $i_L/\sqrt{\Omega}$ for the case of a rotating disk electrode) into differential diffusion coefficients requires a numerical iteration procedure. In order to illustrate this procedure, let us take the exact values of $i_L\sqrt{t}$ from Table 2-3 and regard them as measured values from actual experiments.

From the measured values of $i_L\sqrt{t}$ and Eq. (2-17) we are able to calculate a first approximation to values of $D^{(1)}$ with the known values of t_+ taken from the literature. The superscript refers to the

number of iterations from here on. The calculated values of $D^{(1)}$ are then linearily regressed as a function of concentration; mass fraction is used here for consistency with the previous section

$$D^{(i)} = a_o^{(i)} + a_1^{(i)}\omega^{\frac{1}{2}} + a_2^{(i)}\omega + a_3^{(i)}\omega^{\frac{3}{2}} + a_4^{(i)}\omega^2 \qquad (2\text{-}19)$$

Once we have all the physical properties, density, t_+ and $D^{(1)}$ as a function of concentration, i.e., Eq. (2-13), it is possible to calculate $I^{(1)}$ from Eq. (2-12a) by the computer program CONCEN and the steps listed in the previous section.

With the measured values of $i_L\sqrt{t}$ and $I^{(1)}$, it is possible to go one step forward to the differential diffusion coefficient $D^{(2)}$ at concentration c_∞ from Eq. (2-9). At this point, one may recall that Eq. (2-9) is the definition of I, but $I^{(1)}$ was calculated from (2-12), and not (2-9). At different experimental concentrations, different values of $D^{(2)}$ are obtained. They are again subjected to the linear regression program, i.e., to fit them as a function of concentrations as Eq. (2-19). The process is repeated until the values of $D^{(i)}$ converge, i.e., when the difference of $D^{(i-1)}$ and $D^{(i)}$ is smaller than a specified tolerable error. This final step yields the differential diffusion coefficients.

Figure 2-4 shows how the values of $D^{(i)}$ calculated from Eq. (2-17) are converted to differential diffusion coefficients for the binary electrolyte of copper sulfate at 25°C with the exact values of $i_L\sqrt{t}$ given in Table 2-3. The numbers labeled in Fig. 2-4 represent the iteration. It took six iterations to converge satisfactorily to the

differential diffusion coefficient measured by Eversole.[43] The detailed computer program DIFF is given in Appendix E2.

A similar procedure would also be possible to invert the measured values of $i_L/\sqrt{\Omega}$ into differential diffusion coefficients for the case of a rotating disk electrode.

Despite the good convergence to the literature data of copper sulfate at 25°C, no one seems ever (no literature found) to have made any limiting current measurements of binary electrolyte by a stagnant diffusion cell. Neither has anyone pointed out the difficulties or failure of such measurements. Many of this kind of measurements were done at very low concentrations and with a large amount of supporting electrolyte.[10,11,42] Systems with supporting electrolyte are discussed in the next chapter.

In the remainder of this section, the difficulty of the measurement of limiting current density in a stagnant diffusion cell and its possible resolution are discussed. For the experimental setups and procedure, one should refer to chapter 6.

For a solution with a large amount of supporting electrolyte, a typical plot of log current vs log time curve consists of two parts, the horizontal part which corresponds to the ohmic resistance of the solution and the decreasing part of slope $-\frac{1}{2}$ where the concentration of electrolyte near the electrode surface drops to zero. (See Eq. (2-17) or (2-9))

With a copper sulfate solution of 0.100M without any supporting electrolyte, and a voltage of 0.3 to 0.4 volt*, the decreasing part would

*This is the voltage range which is used for most other measurements of the solutions with sufficient amount of H_2SO_4 as supporting electrolyte; see chapter 6.

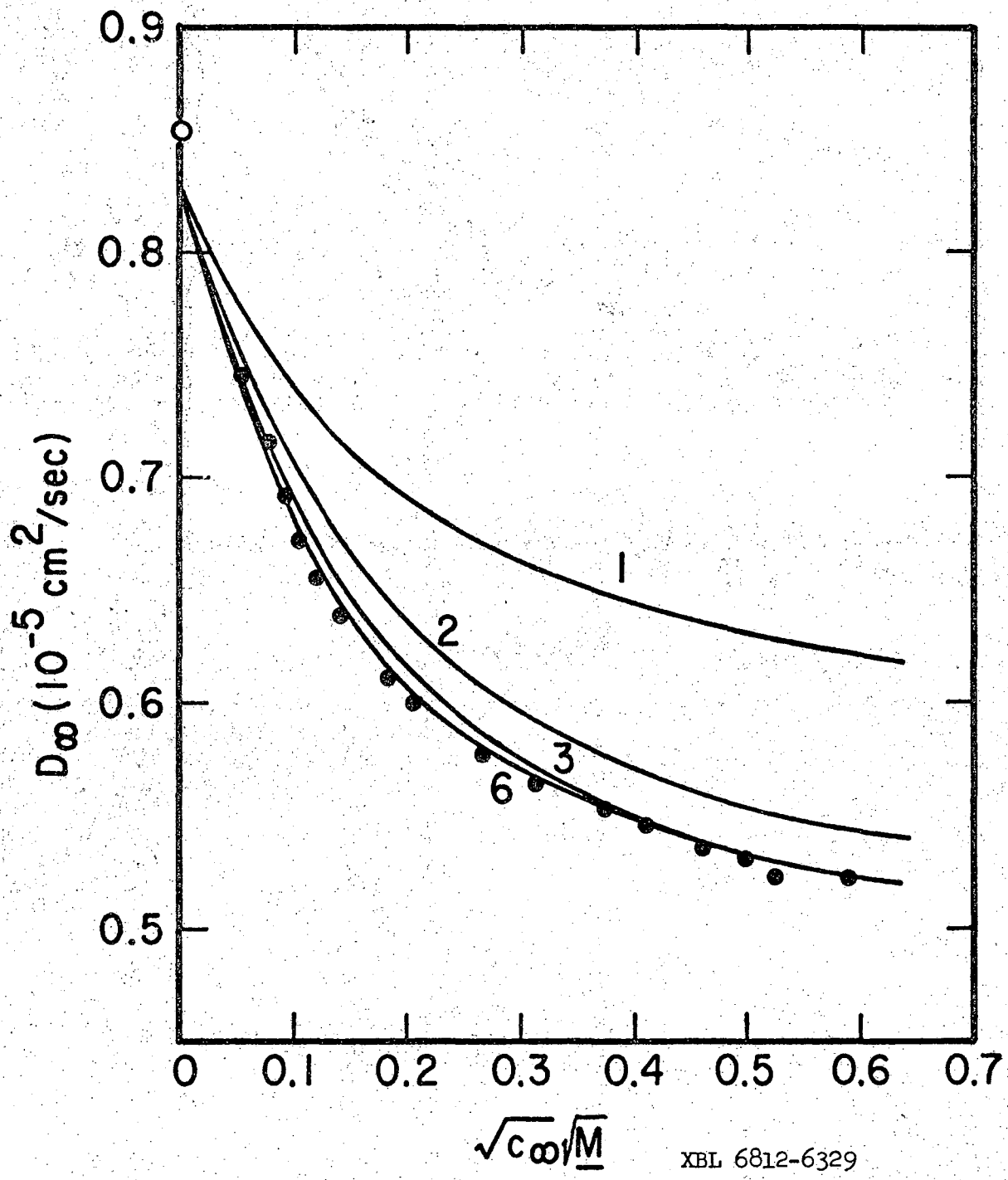

Fig. 2-4. The inversion of $i\sqrt{t}$ to differential diffusion coefficients for a stagnant diffusion cell at 25°C

o Nernst limiting value

● differential diffusivities (Eversole[43]).

not show up until several hundreds thousand seconds, i.e., several days. This is almost at the same order of magnitude of time as is needed with a diaphragm cell.

If the applied voltage is raised, the flat part becomes shorter. A constant voltage of 1.0 volt was applied to the above solution in a stagnant cell. A plot of log i vs. log t for several different-sized capillary tubes is shown in Fig. 2-5. Instead of a monotonic decrease at slope of $-\frac{1}{2}$, the curve wavers up and down, which makes the quantity $i_L\sqrt{t}$, presumably a constant, not easy to define.

The same solution was again run in the capillary C except that the voltage was decreased manually step by step as it is shown in the lower part of Fig. 2-6. This time the straight line of the decreasing part becomes longer than the one in Fig. 2-5. The curve does not waver until at 10,000 sec when the source voltage remaining unchanged at 0.8 volt after 5,500 sec.

These experiments lead us to believe that a power source, the output voltage of which starts to decrease with respect to the square root of time when the concentration of electrolyte near the electrode has dropped to zero, affords a possible method of measuring $i\sqrt{t}$ in a binary electrolyte.

One would also notice that all four curves in Figs. 2-5 and 2-6, overshoot above the line of slope $-\frac{1}{2}$, which is in harmony with the curves observed in solutions with supporting electrolyte in chapter 6. This phenomenon also agrees with what is predicted in the theoretical calculations in chapter 5.

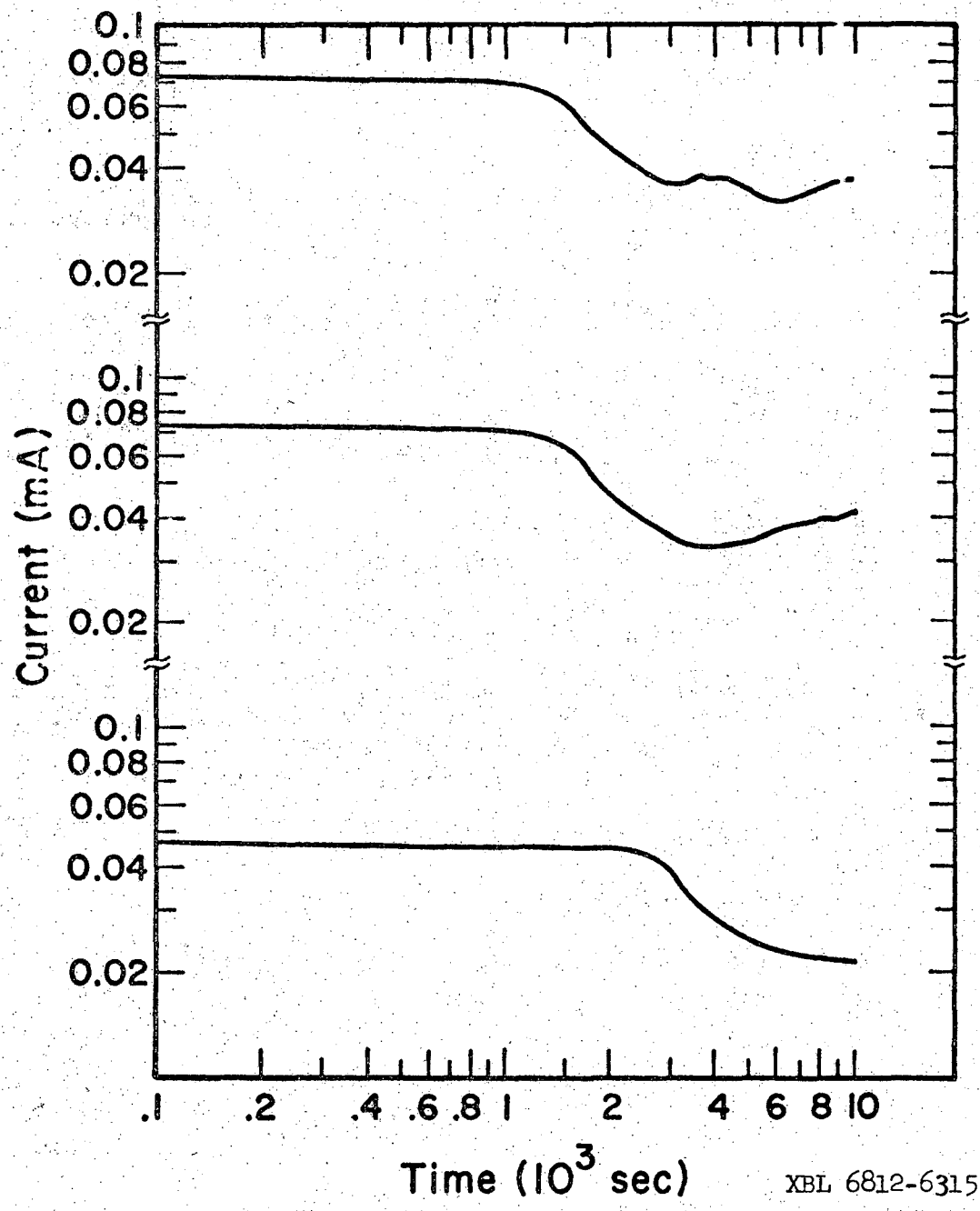

Fig. 2-5. Current-time behavior in a stagnant diffusion cell of binary electrolyte.
(Run 202; Solution 101, $CuSO_4$ 0.1001M; From top to bottom, capillary H, F, C, see Table 6-1)

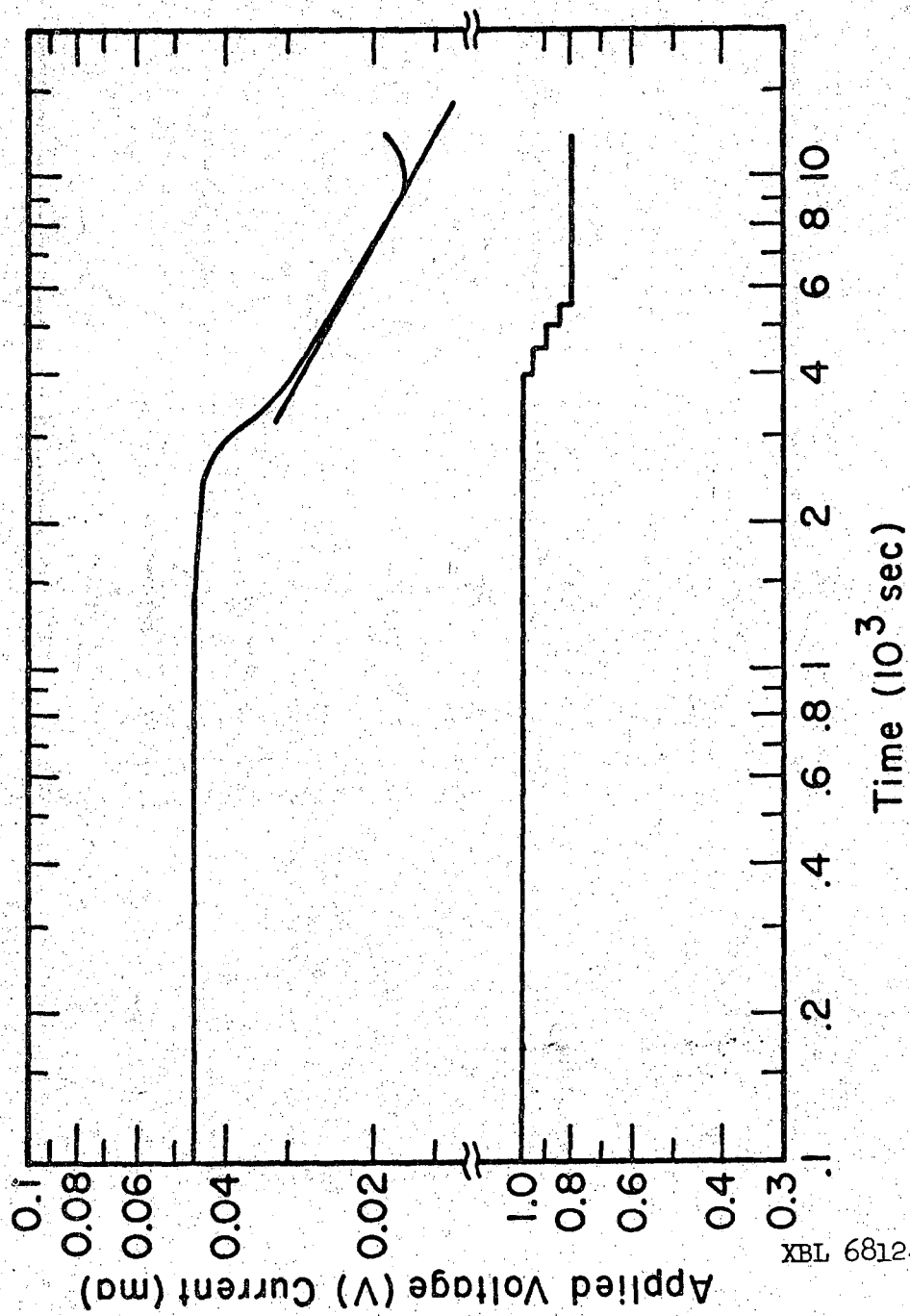

XBL 6812-6330

Fig. 2-6. Current response for stepwise changes in voltage (Run 206; Solution 101; Capillary C).

III. MASS TRANSFER IN A MULTICOMPONENT ELECTROLYTIC SOLUTION

In our laboratory, there exist several different experimental setups of different hydrodynamic conditions for the study of mass transfer in multicomponent electrolytic solutions. The common problem we face is how we define a diffusion coefficient and calculate the limiting current density under these different hydrodynamic conditions and different concentrations of supporting electrolyte.

Until recently, most literature have employed the differential diffusion coefficient measured by a diaphragm cell or an optical method directly to an electrochemical system with supporting electrolyte. There is no justification of this except one of expediency. On the other hand, the polarographic diffusion coefficients of Brasher and Jones[42] have been largely ignored.

In the previous chapter, it has been shown how the limiting current in a binary electrolyte could be calculated for a stagnant diffusion cell or for a rotating disk electrode. One could see how difficult it would be to extend the calculations to a ternary electrolyte. For example, for an aqueous copper sulfate solution with the presence of supporting electrolyte of sulfuric acid, the fundamental transport properties consist of three independent sets of diffusion coefficients (corresponding to binary interactions between $CuSO_4$ and water, H_2SO_4 and water, and $CuSO_4$ and H_2SO_4), two transference numbers of three ionic species (Cu^{++}, $SO_4^{=}$, H^+), the conductivity, and the viscosity. If all these properties as well as the density were known as functions of composition, it would then be possible to calculate the limiting current.

However the necessary data usually are not available for most cases. Addition agents would certainly make the problem much more complicated.

In this chapter, we will discuss how to treat the mass transfer in multicomponent electrolytic solutions by means of integral diffusion coefficients. In section one, the factors that justify the use of integral diffusion coefficients are discussed. In section two, the hydrodynamic configurations that are frequently used for electrolytic mass transfer studies are classified into two, namely, the boundary layer model and the penetration model. Efforts are devoted to prove how the equation of convective diffusion can be reduced to an identical dimensionless equation according to this classification under the assumption of large Schmidt number of electrolytic solution. This is also the basis, in the final section, that leads us to believe that an integral diffusion coefficient measured by one hydrodynamic condition can also be applied to the others according to this classification. Some measured data for a stagnant diffusion cell as well as a rotating disk electrode are also included.

3.1 The Justification of the Use of an Integral Diffusion Coefficient

The use of an integral diffusion coefficient is influenced by the following effects;

i. the value of the Schmidt number,

ii. the nonzero interfacial velocity,

iii. the effect of ionic migration, and

iv. the variations of transport properties.

Each effect has been treated individually by several workers, mostly in nonelectrolytic systems. The Schmidt number correction was

treated by Newman.[13] For electrolytic systems, the correction is usually no more than a few percent.

The effect of nonzero interfacial velocity due to the high mass transfer rate can also be expressed as a correction factor to the mass transfer coefficient in the absence of an interfacial velocity for a rotating disk.[3] If the Schmidt number is very large, the correction factor has been shown to be a function of mass flux ratio for an arbitrary, two-dimensional boundary layer model[9,15] and in a generalized penetration model.[16]

Similarly, the effect of ionic migration in the diffusion layer can also be expressed as a correction factor to the mass transfer rate in the absence of migration.[14] For large Schmidt number, one correction factor has been shown to apply to the hydrodynamics of a boundary layer model and another to situations obeying the penetration model.[17]

As to the effect of variations of physical properties, there is no general correction factor except under the assumption that the properties follow a logarithmic function.[18] However, for an solution of given composition the correction should be identical for any arbitrary boundary layer model and for a penetration model at high Schmidt numbers, as shown by Acrivos[12] for the boundary layer model case.

3.2 The Equation of Convective Diffusion at High Schmidt Number

A. Boundary Layer Model

For an electrolytic system, the Schmidt number is invariably large, being on the order of 1000. In steady state, boundary layer convective diffusion, the diffusion layer is very thin compared with the

hydrodynamic boundary layer. Consequently, one frequently uses the first term of the series expansion of the velocity profile of various hydrodynamic conditions as an asymptotic form for mass-transfer-rate calculations. They can be expressed as

$$v_x = y\beta(x) \tag{3-1}$$

$$v_y = -\frac{1}{2}\frac{d\beta(x)}{dx}y^2 + v_o \tag{3-2}$$

where $\beta(x)$ is the velocity derivative $\partial v_x/\partial y$ evaluated at the wall ($y=0$). The two expressions also satisfy the two dimensional equation of continuity.

Hydrodynamic configurations which are commonly used in electrochemical mass transfer studies and fall into this category are

i. Two-dimensional diffusion layers in laminar forced convection.
   1. a flat plate in a free stream[24]
   2. a cylinder in a free stream[22b]
   3. stagnation in plane flow (Hiemenz flow)[22a, 23]

ii. Axisymmetric diffusion layer in laminar forced convection
   1. a rotating disk electrode[22]
   2. a sphere in a free stream[9]
   3. flow through an annulus[1] and its special cases, a circular tube or two parallel plates

For steady state, two dimensional or axisymmetric boundary layer hydrodynamic configurations, the general equation of convective

diffusion for an ionic species i in a multicomponent electrolytic solution is[4]

$$v_x \frac{\partial c_i}{\partial x} + v_y \frac{\partial c_i}{\partial y} = z_i F \frac{d}{dy} \left(u_i c_i \frac{d\phi}{dy}\right) + \frac{\partial}{\partial y}\left(D_i \frac{\partial c_i}{\partial y}\right) \tag{3-3}$$

In this equation, ϕ is the electrostatic potential, u_i is the mobility of ionic species i and the remaining symbols have their usual meanings. The terms involving the second order partial derivatives of concentrations and potential with respect to x have been dropped on the basis of order of magnitude comparisons with the terms that are retained.[17]

Here the dilute solution theory of mass transfer has been used. This is not only because of its simplicity but also its widespread use in the literature. For the multicomponent, concentrated solution theory, which involves the inversion of the Stefan-Maxwell flux matrix and the use of electrochemical potentials instead of concentrations, one should refer to the papers by Smyrl and Newman.[4,19]

The y component of the flux of ionic species i, N_{iy}, consists of three contributions, i.e., diffusion, migration, and convection,

$$N_{iy} = -D_i \frac{dc_i}{dy} - z_i u_i F c_i \frac{d\phi}{dy} + c_i v_y \tag{3-4}$$

The y component of the current density is the sum of the species fluxes multiplied by the charge

$$i_y = F \Sigma z_i N_{iy} \tag{3-5}$$

The mass average interfacial velocity[9] v_o at the electrode-solution interface is

$$v_o = \frac{\Sigma\rho_i v_{iy}}{\Sigma\rho_i} = \frac{\Sigma M_i N_i}{\rho} \tag{3-6}$$

For a metal depositon reaction, the mass flux at the electrode surface is zero for all ionic species except the reacting ion, (e.g., in the $CuSO_4$-H_2SO_4 system, copper ion is the reacting ion) or in mathematical notations

$$N_{iy} = 0 \qquad \text{where } i \neq R \qquad \text{at } y = 0 \tag{3-7}$$

Equations (3-5) to (3-7) can be combined to yield a relationship between the interfacial velocity and the current density

$$v_o = \frac{i_y M_R}{F z_R \rho} \tag{3-8}$$

where subscript R refers to the reacting ion. If the results of Eqs. (3-8) and (3-5) are introduced into Eq. (3-4) at y = 0, there then follows

$$\frac{i_y M_R}{F z_R \rho} = -\frac{z_R u_R F c_R}{\left(\frac{\rho}{M_R} - c_R\right)} \frac{d\phi}{dy}\Big|_{y=0} - \frac{D_R}{\left(\frac{\rho}{M_R} - c_R\right)} \frac{dc_R}{dy}\Big|_{y=0} \tag{3-9}$$

According to Eq. (3-8), the left hand side of the above equation is exactly v_o. Next, we replace v_o in Eq. (3-2) by (3-9) and introduce the

Lighthill transformation*[20]

$$\xi = \frac{y\sqrt{\beta(x)}}{[9D_R\int_0^x\sqrt{\beta(x)}\,dx]^{1/3}} \tag{3-10}$$

for a two dimensional boundary model and assume that c_R and ϕ depend only on ξ. Equation (3-3) then reduces to

$$\frac{d}{d\xi}\left(\frac{z_1u_1Fc_1}{D_R}\frac{d\phi}{d\xi}\right)+\frac{d}{d\xi}\left(\frac{D_1}{D_R}\frac{dc_1}{d\xi}\right)+[3\xi^2+Q]\frac{dc_1}{d\xi}=0\,, \tag{3-11a}$$

where

$$Q=\frac{z_Ru_RFc_R}{D_R(\frac{\rho}{M_R}-c_R)}\frac{d\phi}{d\xi}\Big|_{\xi=0}+\frac{1}{(\frac{\rho}{M_R}-c_R)}\frac{dc_R}{d\xi}\Big|_{\xi=0} \tag{3-11b}$$

B. Penetration Model

In this model, the diffusion layer grows as time elapses. The fluid velocity normal to the interface can be expressed, in general, as a function of the time-dependent surface area S(t)

$$v_y = -y\,\frac{d\ell nS(t)}{dt} + v_o \quad . \tag{3-12}$$

This was first proposed by Angelo, Lightfoot and Howard[21] as a generalized penetration theory.

---

*For an axisymmetric boundary layer model, the Lighthill transformation has the same form but with $\beta(x)$ replaced by $r\beta(x)$, where r is the normal distance of the surface from the axis of symmetry.

Hydrodynamic configurations belonging to this category are

i. a stagnant diffusion cell, and

ii. a growing mercury drop in polarographic study.

For this model, the equation of convective diffusion of ionic species i is

$$\frac{\partial c_i}{\partial t} + v_y \frac{\partial c_i}{\partial y} = z_i F \frac{d}{dy}\left(u_i c_i \frac{d\phi}{dy}\right) + \frac{\partial}{\partial y}\left(D_i \frac{\partial c_i}{\partial y}\right) \tag{3-13}$$

The same equations of interfacial velocity, Eqs. (3-8) and (3-9) are still valid for this model in a metal deposition reaction.

Again, we introduce a similarity variable

$$\xi = \frac{yS(t)}{[4D_R \int_0^t S^2(t)dt]^{1/2}} \tag{3-14}$$

Equation (3-13) becomes

$$\frac{d}{d\xi}\left(\frac{z_i u_i F c_i}{D_R} \frac{d\phi}{d\xi}\right) + \frac{d}{d\xi}\left(\frac{D_i}{D_R} \frac{dc_i}{d\xi}\right) + [2\xi+Q]\frac{dc_i}{d\xi} = 0 \tag{3-15}$$

where Q is exactly the same expression as in Eq. (3-11b).

In summary, the equation of convective diffusion reduces to Eq. (3-11) for those hydrodynamic configurations classified under the boundary layer model, and reduces to Eq. (3-15) for those belonging to the penetration model under the assumption of high Schmidt number.

The equation of convective diffusion would then be solved together with the electroneutrality equation. If the transport

properties are known as functions of composition, it is then possible to obtain the concentration profile or potential distribution for each ionic species. The current density is solved from Eq. (3-9).

3.3 Integral Diffusion Coefficient

We have proved that for each category of hydrodynamic configurations, there is an unique equation of convective diffusion at high Schmidt number. However, in a concentrated multicomponent solution, the transport coefficient data are usually not available as functions of composition, which makes it impossible to solve Eqs. (3-11) and (3-15).

The alternative means to approach this problem is to measure the limiting current density of this solution in a simple but typical experimental setup which characterizes its category of hydrodynamics. The measured result is then applied to other hydrodynamic systems.

Let us define an integral diffusion coefficient which follows the equation of convective diffusion

$$v_x \frac{\partial c_R}{\partial x} + v_y \frac{\partial c_R}{\partial y} = \bar{D} \frac{\partial^2 c_R}{\partial y^2} \quad , \tag{3-16}$$

for a boundary layer model and

$$\frac{\partial c_R}{\partial t} + v_y \frac{\partial c_R}{\partial y} = \bar{D} \frac{\partial^2 c_R}{\partial y^2} \quad , \tag{3-17}$$

for a penetration model. v_x and v_y retain the same expressions as in Eqs. (3-1), (3-2), and (3-12), except that there is no v_o in these equations. There are no physical properties involved in the derivations of the above two Eqs. (3-16) and (3-17). This is because for a solution

of given composition, the nonzero interfacial velocity correction, the effect of variation of physical properties, and the migration effect are identical for each category of hydrodynamics,[3,9,15-18] as we have discussed in the first section of this chapter.

If we use the Lighthill transformation (see Eqs. (3-10) and (3-14) except that D_R is now replaced by $\bar{D}$), Eqs. (3-15) and (3-16) are then reduced to

$$\frac{d^2c_R}{d\xi^2} + 3\xi^2\frac{dc_R}{d\xi} = 0 \quad ,$$

and

$$\frac{d^2c_R}{d\xi^2} + 2\xi\frac{dc_R}{d\xi} = 0 \quad .$$

respectively. The concentration profiles are the same as in Eqs. (2-16) and (2-14). The current density is

$$i_y = \frac{nF\bar{D}c_\infty}{s_R}\frac{\partial c_R}{\partial y}\Big|_{y=0}$$

where s_R is a stoichiometric coefficient in the electrode reaction.

In Table 3-1, the first terms of the velocity profile and limiting current density have been summarized for the boundary layer model electrochemical systems. In the table, R is the radius of a sphere, cylinder or circular tube, κ is the ratio of the radii of inner to outer cylinder, $\langle v \rangle$ is an average velocity over the conduit, and x is the distance measured along an electrode surface and y is normal distance from the surface.

In Table 3-2, the fluid velocity normal to the interface and current density are summarized for the penetration model electrochemical systems. For the case of a growing mercury drop, the same approximations made by Ilkovič[25] were adopted.

Because of the simplicity of experimental setup, we have chosen the rotating disk electrode and the stagnant diffusion cell to represent the boundary layer model and penetration model respectively. The limiting current densities in copper sulfate and sulfuric acid solutions were measured with a rotating disk electrode as well as in a stagnant diffusion cell.

The integral diffusion coefficients of a rotating disk are calculated from the measured $i_L/\sqrt{\Omega}$ by the equation in Table 3-1: The results are tabulated in Table 3-3. They agree generally well with the measurements by Arvia[35] et al. However, we have covered much wider concentration ranges of sulfuric acid and copper sulfate. The detailed experimental method has been discussed in Ref. 5.

The integral diffusion coefficients of a stagnant diffusion cell are calculated from the measured $i_L\sqrt{t}$ by the equation in Table 3-2. They are tabulated in Table 3-4. The results should be identical with polarographic diffusion coefficients.

Brasher and Jones[42] have measured the diffusion coefficient polarographically at a copper ion concentration of 0.00009M with sulfuric acid concentrations varying from 0.005M to 9.075M (50 to 10^5 times more than the reacting ion concentration) in their measurements, the viscosity of the solutions dominate over the limiting current. The diffusivity becomes as low as 1.1×10^{-6} cm^2/sec in the sulfuric acid solution of

9.075M. On the other hand, as the amount of supporting electrolyte decreases to equal or less than the concentration of the reacting ion, the effect of migration would dominate over the limiting current. The integral diffusion coefficients calculated in this manner may reach as high as 14.4×10^{-6} cm^2/sec (solution 102 in Table 3-4). One should notice that integral diffusion coefficients of the copper ion defined here do not approach the diffusion coefficient of the binary electrolyte as the concentration of supporting electrolyte approaches zero. The detailed experimental setup will be discussed in chapter 6.

Table 3-1. Velocity profile and limiting current density in a boundary layer model of hydrodynamics.

	Velocity Profile (first term)				limiting current
	V_x	V_y	a	η	$i\,\Gamma\left(\frac{4}{3}\right)\frac{S_R}{nF\bar{D}C_{\infty}}$
A rotating disk	$a x \Omega \eta$	$-a\sqrt{\nu\Omega}\,\eta^2$	0.51023	$\sqrt{\frac{\Omega}{\nu}}\,y$	$\left(\frac{a}{3}\right)^{\frac{1}{3}}\left(\frac{\Omega}{\nu}\right)^{\frac{1}{2}}\left(\frac{\nu}{\bar{D}}\right)^{\frac{1}{3}}$
A plane flow potential flow $V_x = kx$; $V_y = -ky$	$a k x \eta$	$\frac{a}{2}\sqrt{k\nu}\,\eta^2$	1.232588	$\sqrt{\frac{k}{\nu}}\,y$	$\left(\frac{a}{6}\right)^{\frac{1}{3}}\left(\frac{k}{\nu}\right)^{\frac{1}{2}}\left(\frac{\nu}{\bar{D}}\right)^{\frac{1}{3}}$
A flat plate	$\frac{a}{2}u_{\infty}\eta$	$\frac{a}{2}\left(\frac{\nu}{y}\right)\eta^3$	1.32824	$\sqrt{\frac{u_{\infty}}{\nu x}}\,\frac{y}{2}$	$\left(\frac{a}{48}\right)^{\frac{1}{3}}\left(\frac{u_{\infty}}{\nu x}\right)^{\frac{1}{2}}\left(\frac{\nu}{\bar{D}}\right)^{\frac{1}{3}}$
A cylinder near front	$2a u_{\infty}\frac{x}{R}\eta$	$-a\sqrt{\frac{u_{\infty}\nu}{2R}}\,\eta^2$	1.232588	$\sqrt{\frac{2u_{\infty}}{\nu R}}\,y$	$\left(\frac{a}{6}\right)^{\frac{1}{3}}\left(\frac{2u_{\infty}}{\nu R}\right)^{\frac{1}{2}}\left(\frac{\nu}{\bar{D}}\right)^{\frac{1}{3}}$
A sphere in stokes flow	$\frac{3}{2}u_{\infty}\frac{y}{R}\sin\frac{x}{R}$	$-\frac{3}{2}u_{\infty}\frac{y^2}{R^2}\cos\frac{x}{R}$			$\frac{1}{R}\sin\frac{x}{R}\left[\frac{u_{\infty}R}{\bar{D}\left(3\frac{x}{R}-\frac{3}{2}\sin 2\frac{x}{R}\right)}\right]^{\frac{1}{3}}$
An annulus Special case	$4\frac{\langle V_x\rangle}{(1-\kappa)R}ay$	0	Outer electrode $a=\frac{1}{k_2}(1-k_1)$ Inner electrode $a=\frac{1}{k_2}\left(-\kappa+\frac{1}{\kappa}k_1\right)$ where $k_1=\frac{1-\kappa^2}{2\ln 1/\kappa}$ $k_2=\frac{1+\kappa^2}{1-\kappa}-\frac{1+\kappa}{\ln 1/\kappa}$		$\left(\frac{4}{9}\right)^{\frac{1}{3}}\left[\frac{\langle V_x\rangle a}{(1-\kappa)R\bar{D}x}\right]^{\frac{1}{3}}$
A circular tube	$4\frac{\langle V_x\rangle}{R}y$	0	$a=1.0$ $\kappa=0$		$\left(\frac{4}{9}\right)^{\frac{1}{3}}\left[\frac{\langle V_x\rangle a}{R\bar{D}x}\right]^{\frac{1}{3}}$
Two parallel plates	$6\frac{\langle V_x\rangle}{h}y$	0	$a=1.5$ $(1-\kappa)R=h$		$\left(\frac{2}{3}\right)^{\frac{1}{3}}\left[\frac{\langle V_x\rangle}{h\bar{D}x}\right]^{\frac{1}{3}}$

Table 3-2. Velocity normal to the interface and current density in a penetration model of hydrodynamics.

	V_y	S in Eq. (3-14)	$i\Gamma(\frac{3}{2})\frac{s_R}{nFDc_\infty}$
A Stagnant Diffusion Cell	0	1	$\frac{1}{2\sqrt{Dt}}$
A Growing Mercury Drop	$-\frac{2y}{R}\frac{dR}{dt}$	$R^2(t)$	$\frac{R^2(t)}{[4D\int_0^t R^4 dt]^{1/2}}$
Special Case Growing at a Constant Rate of Increase of Volume	$-\frac{2y}{3t}$	$\gamma^2 t^{\frac{2}{3}}$	$(\frac{7}{12})^{\frac{1}{2}}\frac{1}{\sqrt{Dt}}$

Table 3-3. Integral diffusion coefficient of boundary layer model of $CuSO_4$-H_2SO_4 system at 25°C.

Solution #	$CuSO_4$ M	H_2SO_4 M	Density g/ml	Viscosity c.p.	Relative Index (λ=5893Å)	$\bar{D}_{BL} \times 10^6$ cm^2/sec
9	0.0093	0.476	1.0298	0.982		5.61
2	0.00956	0.980	1.0612	1.080		4.98
4	0.00976	1.469	1.0917	1.186		5.21
11	0.00947	1.946	1.1206	1.296		4.67
13	0.00943	2.434	1.1489	1.422		4.11
44	0.0200	0.996	1.0621	1.081	1.3454	6.31
10	0.0460	0.492	1.0361	1.003		5.42
3	0.0461	0.991	1.0670	1.101		4.86
5	0.0488	1.463	1.0968	1.204		4.93
12	0.0462	1.936	1.1252	1.319		4.41
14	0.0466	2.420	1.1547	1.460		3.88
39	0.0967	0.500	1.0438	1.030	1.3413	6.56
15	0.1017	1.003	1.0760	1.151	1.3461	5.48
40	0.0997	1.253	1.0892	1.180	1.3488	5.68
16	0.1031	1.514	1.1086	1.257	1.3513	5.16
41	0.1001	1.769	1.1201	1.303	1.3537	5.04
17	0.1024	2.013	1.1378	1.377	1.3592	4.82
42	0.1015	2.551	1.1658	1.511	1.3610	4.52
6	0.2273	1.451	1.1227	1.321		5.38
18	0.2520	0.995	1.0973	1.224	1.3493	5.98
19	0.2565	2.006	1.1585	1.490	1.3593	5.14
20	0.2561	2.535	1.1900	1.654	1.3654	4.59
7	0.4018	1.464	1.1486	1.454		5.66
21	0.4536	0.988	1.1271	1.366	1.3554	6.03
8	0.6394	1.468	1.1835	1.666		5.81

Table 3-4. Integral diffusion coefficient of penetration model of $CuSO_4$ -H_2SO_4 at 25°C.

Solution	$CuSO_4$ M	H_2SO_4 M	Density g/ml	Viscosity c.p.	Refractive Index (λ=5893Å)	$\bar{D}_{PM} \times 10^6$ cm^2/sec
101	0.1001	0.0	1.0131	0.9507		-
102	0.1001	0.005	1.0136	0.9522		14.4
103	0.1001	0.020	1.0146	0.9554		11.9
104	0.0999	0.050	1.0164	0.9587		10.1
105	0.0998	0.100	1.0194	0.9656		9.06
106	0.1000	0.125	1.0209	0.9707		8.87
107	0.1003	0.175	1.0243	0.9800		8.42
108	0.1001	0.250	1.0290	0.9897		8.08
51	0.1024	0.810	1.0624	1.085	1.3441	5.42
61	0.1008	0.888	1.0667	1.100	1.3451	5.34
52	0.0986	0.998	1.0731	1.120	1.3461	5.33
62	0.1005	1.085	1.0790	1.139	1.3470	5.28
53	0.1006	1.195	1.0850	1.162	1.3481	5.18
63	0.1006	1.295	1.0911	1.183	1.3491	5.12
54	0.0999	1.375	1.0963	1.202	1.3503	5.09
64	0.0999	1.473	1.1018	1.224	1.3510	5.01

IV. THE EFFECT OF MIGRATION IN A MULTICOMPONENT ELECTROLYTIC SOLUTION

Since it is difficult to solve Eq. (3-11) or Eq. (3-15) analytically or numerically, we will concentrate our effort on the rôle of migration. The problem has been solved by Newman[14,17] when the assumptions of constant D_i u_i and $Q = 0$ are adopted. In brief, for a solution of three ionic species, Eqs. (3-11) and (3-15) become

$$\frac{D_i}{D_R}\frac{d^2c_i}{d\xi^2} + k\xi^m\frac{dc_i}{d\xi} + \frac{z_i u_i F}{D_R}\frac{d}{d\xi}\left(c_i\frac{d\phi}{d\xi}\right) = 0 \quad . \tag{4-1}$$

There are three such equations, i=1, 2, R and

$k = 2$; $m = 1$ for a stagnant diffusion cell or penetration model,

$k = 3$; $m = 2$ for a rotating disk electrode or boundary layer model.

When Eqs. (4-1) are combined with the equation of electroneutrality,

$$\Sigma z_i c_i = 0 \quad , \tag{4-2}$$

it is possible to solve for c_1, c_2, c_R and the electric potential ϕ with the known ratios of ionic mobilities and diffusivities.

In Ref. 14, the electrolytic system of copper sulfate and sulfuric acid was treated as completely dissociated into $SO_4^{=}$, H^+, Cu^{++}.

In a pure sulfuric acid solution, the sulfuric acid molecule ionizes in two stages; the ionization constants[26] at 25°C are

$$H_2SO_4 \rightarrow H^+ + HSO_4^- \quad ; \quad K_1 = 10^3$$
$$HSO_4 \rightleftarrows H^+ + SO_4^= \quad ; \quad K_2 = 1.04 \times 10^{-2}$$

The second ionization constant is much smaller than the first ionization constant. Consequently, except at extreme dilution, the bisulfate ion would not be completely dissociated.

A simple, dramatic evidence of the existence of bisulfate ions in a copper sulfate and sulfuric acid solution is the conductivity of the solutions (see Appendix A, Fig. A-1). When copper sulfate is added to a solution of sulfuric acid, the conductivity is found to decrease. Qualitatively speaking, this is because the highly mobile hydrogen ions have combined with the sulfate ions from copper sulfate and formed the less mobile bisulfate ions.

4.1 Comparison of Complete and No Dissociation of Bisulfate Ion

In this section, the effect of migration of two extreme cases will be discussed, namely, complete dissociation of bisulfate ion and no dissociation of bisulfate ion. The former case has been carried out in Ref. 14. For the latter case the numerical method is exactly the same as before.

The four coupled, nonlinear differential equations (three equations (4-1) at i=1, 2, R plus equation of electroneutrality (4-2)) were solved numerically by linearization about a trial solution which produces a series of coupled, linear differential equations. In the finite difference form, these give coupled, tri-diagonal matrices, which can be solved on a high speed, digital computer. The detailed mathematics and numerical method have been discussed in Ref. 27.

Let c_A^∞ and c_B^∞ be the concentration of copper sulfate and sulfuric acid of bulk solution; their relationships to the ionic concentration of bisulfate, sulfate, hydrogen, and copper for the two extreme cases are given in Table 4-1.

Table 4-1. Relationship of ionic concentration and molecular concentrations.

i	Complete Dissociation	No Dissociation	
		$c_B \geq c_A; r \geq 0.5$	$c_A > c_B; r < 0.5$
1	$SO_4^= = c_A + c_B$	$HSO_4^- = c_A + c_B$	$HSO_4^- = 2c_B$
2	$H^+ = 2c_B$	$H^+ = c_B - c_A$	$SO_4^= = c_A - c_B$
3	$Cu^{++} = c_A$	$Cu^{++} = c_A$	$Cu^{++} = c_A$

The ionic mobility data were calculated from the ionic conductances at infinite dilution at 25°C which were taken from Refs. 26b and 39. The Nernst-Einstein relation

$$D_i = RTu_i \tag{4-3}$$

was assumed to be valid. The data used in calculation are

	$(z_i u_i F^2)$	$z_i u_i F$ $10^{-4}\ \frac{cm}{sec}/\frac{volt}{cm}$	D_i $10^{-5}\ \frac{cm^2}{sec}$	z_i	s_i
HSO_4^-	50	5.18	1.331	-1	0
$SO_4^=$	80.0	8.29	1.065	-2	0
H^+	349.8	36.24	9.312	1	0
Cu^{++}	54.0	5.595	0.7188	2	1

The result is presumably valid at infinite dilution. However, according to Eq. (4-1), it is the ratios of mobilities and diffusivities

of ionic species with respect to the reacting ion which are important. Therefore, the calculated results are also valid if the ratios are not changed with concentration.

The effect of migration on the limiting current for two hydrodynamic systems is shown in Figs. 4-1 and 4-2 and Table 4-2. The abscissa is a ratio of the concentration of supporting electrolyte to that of the reacting electrolyte, but expressed as

$$r = c_B^\infty/(c_A^\infty+c_B^\infty) \tag{4-4}$$

so that r varies within a finite range of 0 to 1 for any ratio of c_B^∞/c_A^∞. The ordinate is a ratio of limiting current to the limiting diffusion current of a well supported electrolyte (r=1) when the viscosity effect is excluded. The solid lines indicate the two extreme cases of rotating disk electrode (or boundary layer model in general). The effect of migration is considerably higher for no dissociation of bisulfate ion than in the completely dissociated case. The dashed lines are the case of incomplete dissociation and will be discussed in the next section.

For many cathodic metal deposition reactions, the concentration of supporting electrolyte is often higher at the electrode surface than in the bulk solution. Figures 4-3 and 4-4 show the concentration difference of sulfuric acid between the electrode surface and bulk solution for the same electrolytic system. Numerical values are given in Table 4-3. The situation is again substantially different for the

treatments with complete dissociation or no dissociation of bisulfate ions. Moreover, the concentration of sulfuric acid would even decrease near the electrode surface for some values of r when the bisulfate model is used. Qualitatively speaking, the bisulfate ion, containing hydrogen, is driven away from the electrode because of its negative charge.

The computer program[27] failed to converge to a solution of small r for the case of complete dissociation of bisulfate. The program also failed to converge for r close to 0.5 or smaller than 0.5 for the case of no dissociation of bisulfate. An analytic solution was found possible for a special case, a Nernst diffusion layer. This is developed in Appendix G.

Table 4-2. Ratio of limiting current to limiting diffusion current for discharge of copper ions in $CuSO_4/H_2SO_4$ system at 25°C.

	I_L/I_D					
	Complete Dissociation			No Dissociation		
r	RDE*	SDC≠	Nernst	RDE*	SDC≠	Nernst
1	1.0	1.0	1.0	1.0	1.0	1.0
0.9025	1.0247	1.0216	1.0340	1.0709	1.0586	1.10335
0.81	1.0504	1.0440	1.0694	1.1554	1.1283	1.2379
0.7225	1.0773	1.0675	1.1062	1.2617	1.2168	1.3994
0.64	1.1054	1.0921	1.1446	1.4084	1.3413	1.6158
0.5625	1.1350	1.1180	1.1845	1.6565	1.5547	1.9552
0.50	-	-	1.2202	2.6553	2.4981	3.0
0.49	1.1662	1.1455	1.2263	N	N	2.9608
0.36	1.2342	1.2058	1.3153	N	N	2.5625
0.25	1.3113	1.2752	1.4126	N	N	2.3333
0.16	1.3998	1.3563	1.5188	N	N	2.1905
0.09	1.5025	-	1.6346	N	N	2.0989
0	1.8852	1.8303	2.0	1.8852	1.8303	2.0

N Program MIGR1 does not converge

* Rotating disk electrode or boundary layer model in general

≠ Stagnant diffusion cell or penetration model in general

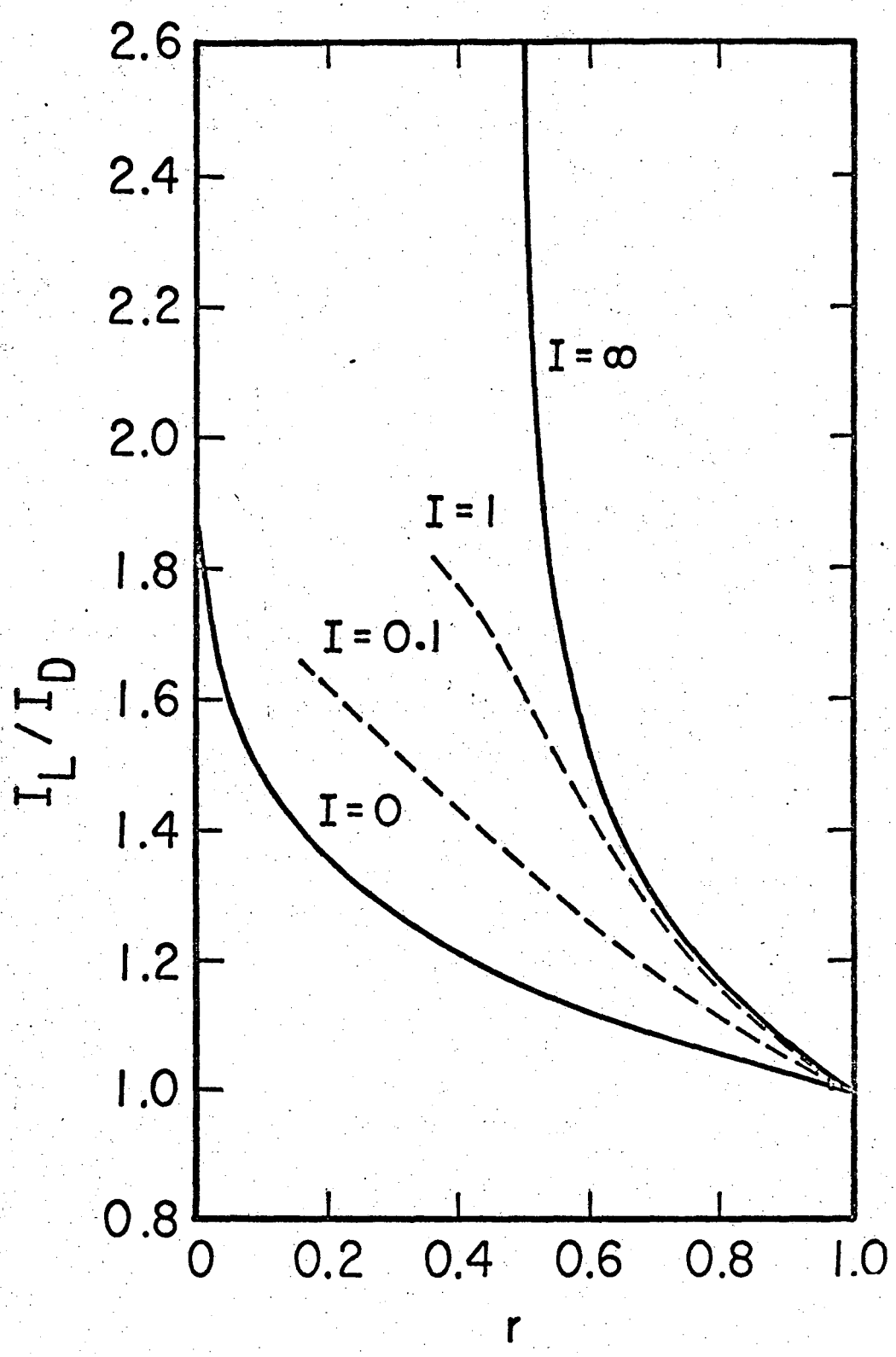

XBL 6812-6331

Fig. 4-1. The effect of migration for a rotating disk electrode.

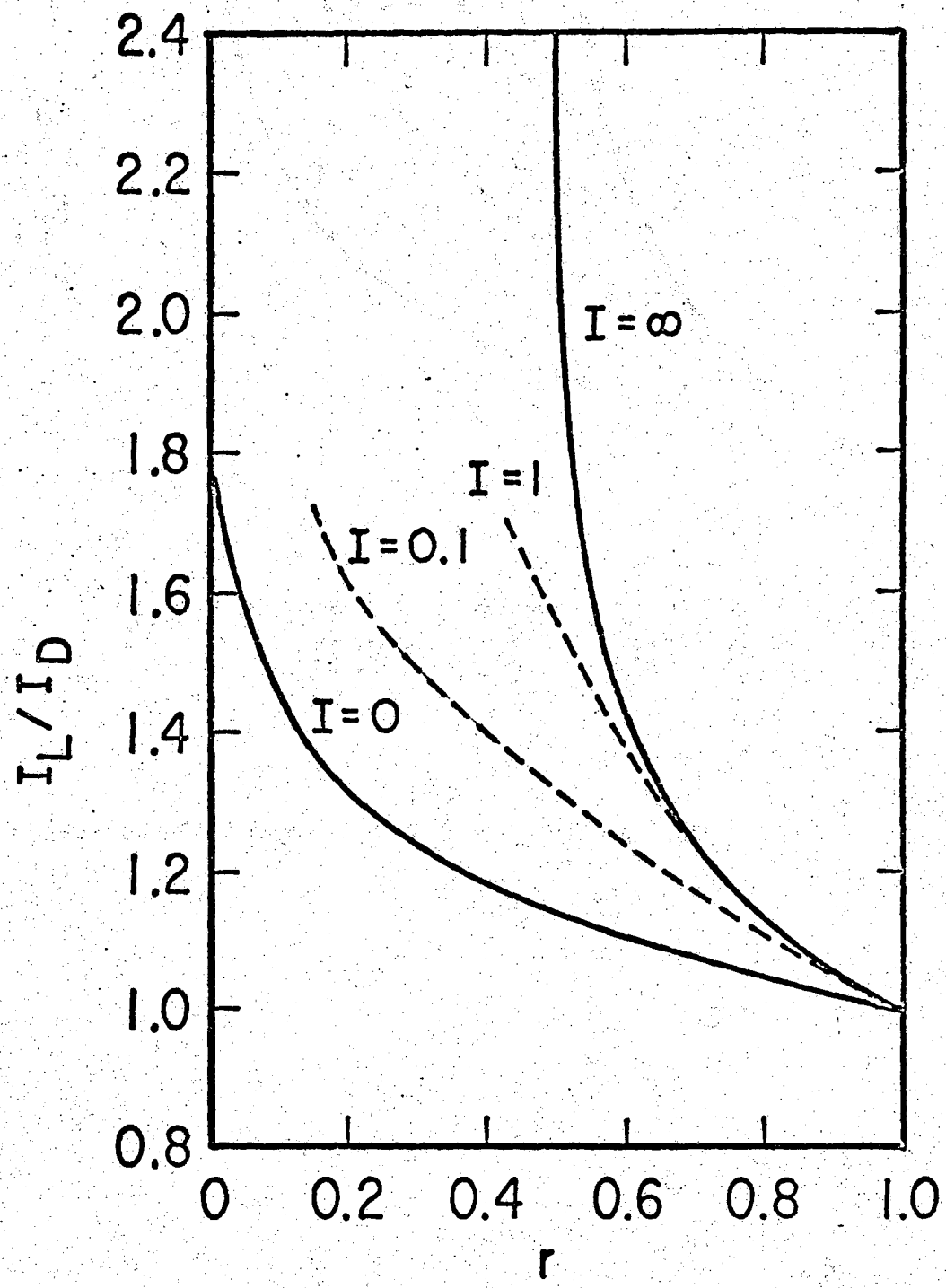

XBL 6812-6332

Fig. 4-2. The effect of migration in a stagnant diffusion cell.

Table 4-3. The surface concentration change of sulfuric acid for discharge of copper ions in $CuSO_4/H_2SO_4$ system at 25°C.

	$(c_B^o - c_B^\infty)/c_A^\infty$					
	Complete Dissociation			No Dissociation		
r	RDE*	SDC≠	Nernst**	RDE*	SDC≠	Nernst**
1	0.43158	0.49893	0.33333	0.16059	0.26781	0.0
0.9025	0.41885	0.48555	0.32200	0.10967	0.21829	-0.05418
0.81	0.40543	0.47136	0.31021	0.04743	0.15661	-0.11894
0.7225	0.39132	0.45630	0.29794	-0.03267	0.07522	-0.19970
0.64	0.37644	0.44028	0.28515	-0.14502	-0.04289	-0.30788
0.5625	0.36073	0.42319	0.27182	-0.33437	-0.24645	-0.47760
0.50	-	-	0.25992	-1.0	-1.0	-1.0
0.49	0.34411	0.40493	0.25791	N	N	-0.96078
0.36	0.30780	0.36435	0.22822	N	N	-0.56250
0.25	0.26683	0.31746	0.19580	N	N	-0.33333
0.16	0.22051	0.26337	0.16038	N	N	-0.19048
0.09	0.16846	-	0.12179	N	N	-0.09890

N Program MIGR1 does not converge

* Rotating disk electrode or boundary layer model in general

≠ Stagnant diffusion cell or penetration model in general

** Nernst diffusion layer see Appendix G

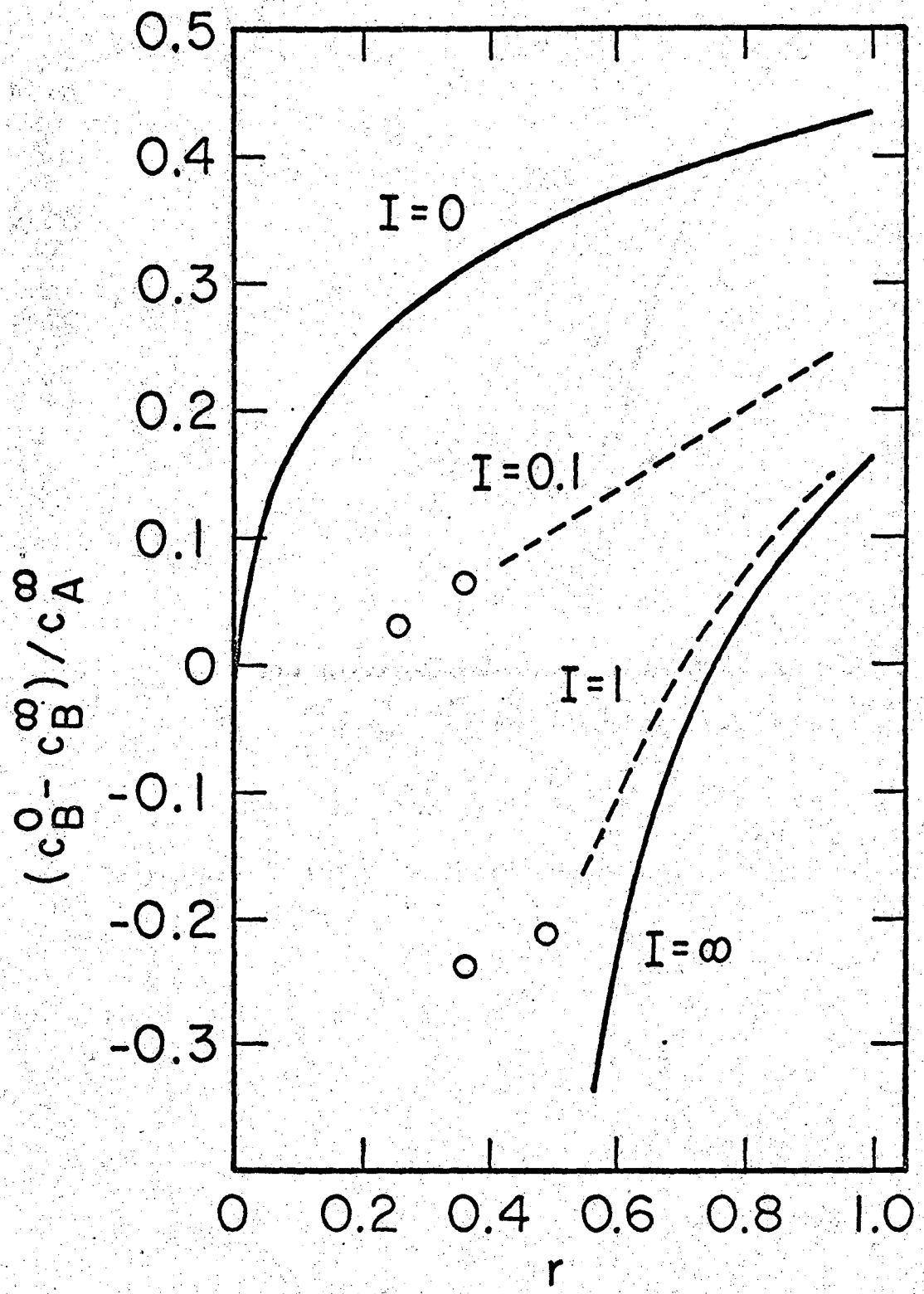

XBL 6812-6333

Fig. 4-3. The surface concentration change for a rotating disk electrode.

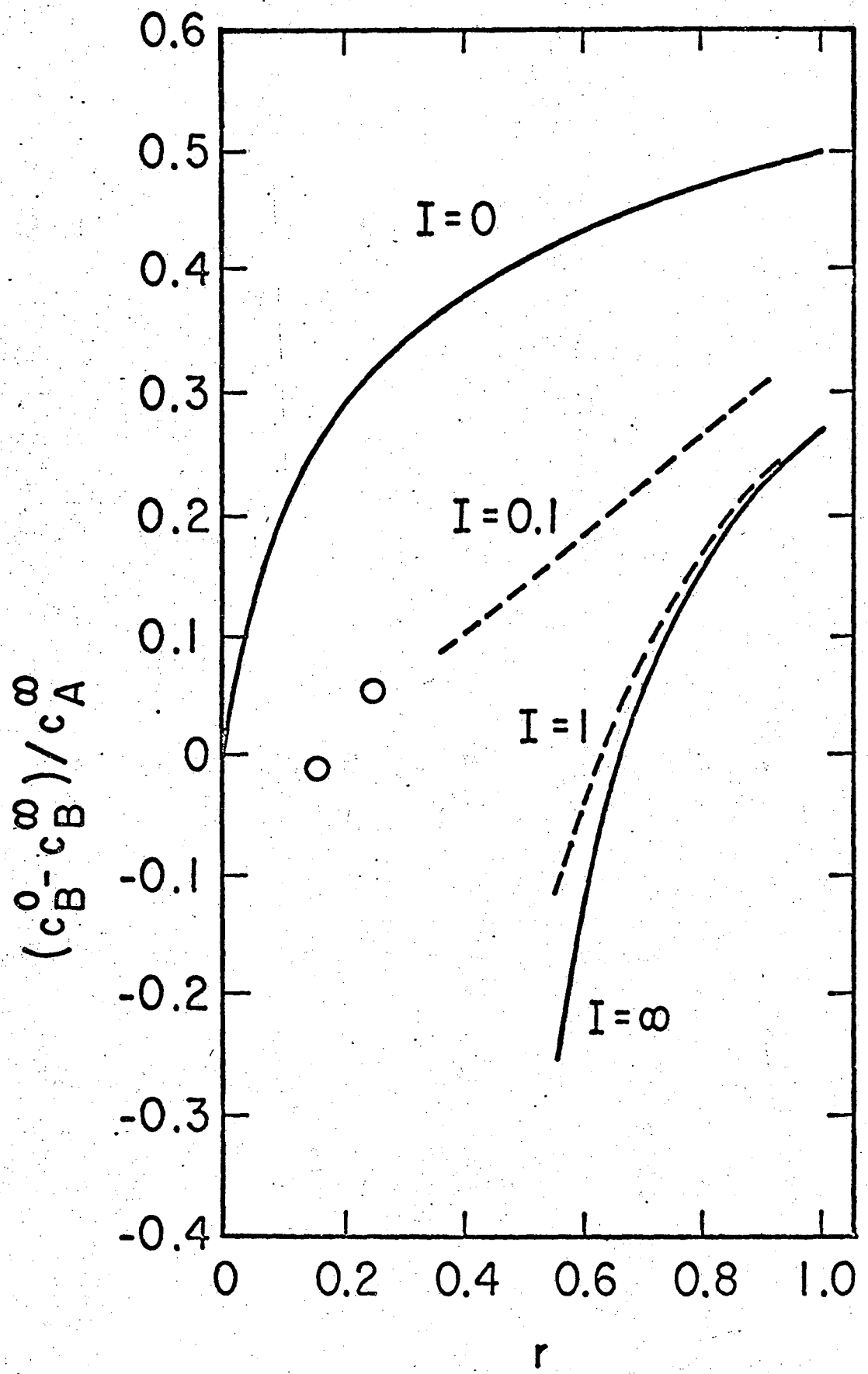

XBL 6812-6334

Fig. 4-4. The surface concentration change in a stagnant diffusion cell.

4.2 Partial Dissociation of Bisulfate Ion

As it was mentioned at the beginning of this chapter, the bisulfate ion is neither completely dissociated nor completely undissociated. For the case of incomplete dissociation, all four ions are present in the solution. Let c_1, c_2, c_3 be the ionic concentrations of bisulfate, sulfate and hydrogen ions respectively, and c_4 be the concentration of reacting ions of copper. c_1, c_2, c_3 are related by the second stage ionization constant K_2

$$K_2 = c_2 c_3 / c_1 \quad . \tag{4-5}$$

The ionic concentrations are related to the molecular concentrations by

$$\begin{aligned} c_1 + c_2 &= c_A + c_B \\ c_1 + c_3 &= 2c_B \\ c_4 &= c_A \end{aligned} \tag{4-6}$$

Equation (4-1) for the incomplete dissociation case is

$$\frac{D_i}{D_4} c_i'' + k\xi^m c_i' + \frac{z_i u_i F}{D_4} (c_i \phi'' + c_i' \phi') + r_i = 0 \tag{4-7}$$

There are four such equations, i=1, 2,3,4; prime refers to the derivative with respect to ξ, and r_i=rate of production of ion i by the second stage of the ionic reaction ($r_1=r$; $r_2=-r$; $r_3=-r$; $r_4=0$ where $r=-k_1c_1+k_2c_2c_3$ and $K_2= k_1/k_2$).

When Eq. (4-7) of i=1 is added to the equation of i=2, the ion production term r_i is cancelled. A similar equation would also be obtained by adding the equation of i=1 and i=3. Thus we have two such equations plus Eq. (4-5) and Eq. (4-7) of i=4 and the equation of electroneutrality, we may be able to solve for the five independent variables c_1 to c_4 and ϕ.

The numerical method is essentially the same as the one discussed in the first section of this chapter. The program MIGR2 is attached to Appendix E3.

The effect of migration and the surface concentration change were plotted in Figs. 4-1 to 4-4, with the ionic strength of the solution as a parameter. Ionic strength is defined as if the solution is totally dissociated into sulfate, hydrogen and copper ions

$$I = \frac{1}{2} \Sigma z_i^2 c_i = 4c_A + 3c_B \qquad (4\text{-}8)$$

The numerical values of the calculated results are given in Tables 4-4 and 4-5. For the calculations the following values were used: $K_2 = 0.01$, total number of mesh points = 402, and mesh size = 0.012 for RDE, 0.03 for SDC.

The two extreme cases (complete and no dissociations of bisulfate ion) discussed in section 4-1 correspond to very large and very small ionic strengths. For an actual solution, the effect of migration and surface concentration changes would fall between the two extremes.

According to the analytic solution of the Nernst diffusion layer in Appendix G, a maximum should appear in the I_L/I_D plot for large values of the ionic strength. However, the poor convergence of MIGR2 at small r and a desire to avoid excessive consumption of computer time prevented us from showing the maxima. For the same reasons, the minima are not shown in the surface concentration difference plots.

(The circles on figures 4-3 and 4-4 were calculated at a very slow convergence rate and are not considered completely reliable.)

Table 4-4. Ratio of limiting current to limiting diffusion current for discharge of copper ions in $CuSO_4/H_2SO_4$ at 25°C.

	I_L/I_D				
	Incomplete Dissociation				
	RDE or Boundary Layer Model		SDC or Penetration Model		
r	I=1	I=0.1	I=1	I=0.1	I=0.01
1	1.0	1.0	1.0	1.0	1.0
0.9025	1.06775	1.05246	1.05709	1.04667	1.02950
0.81	1.14661	1.10799	1.12478	1.09712	1.05990
0.7225	1.24137	1.16642	1.20844	1.15114	1.09116
0.64	1.35778	1.22707	1.31527	1.208126	1.12342
0.5625	1.49602	1.28881	1.44763	1.26692	1.15679
0.49	1.63662	1.35017	1.58834	1.32604	1.19138
0.36	1.82040	1.46623	N	1.44002	1.26482
0.25	N	1.56822	N	1.54669	1.34535
0.16	N	1.65753	N	1.69467	1.43649
0.09	N	-	N	-	-
0	1.8852	1.8852	1.8303	1.8303	1.8303

N Program MIGR2 does not converge

Table 4-5. The surface concentration change of sulfuric acid for discharge of copper ions in $CuSO_4/H_2SO_4$ system at 25°C.

	$c_B^o - c_B^\infty / c_A^\infty$			
	Incomplete Dissociation			
	RDE or Boundary Layer Model		SDE or Penetration Model	
r	I=1	I=0.1	I=1	I=0.1
1.0				
0.9025	0.1315	0.2332	0.2297	0.3047
0.81	0.07690	0.2052	0.1706	0.2705
0.7225	0.01087	0.1772	0.09555	0.2354
0.64	-0.06739	0.1499	0.01680	0.2003
0.5625	-0.1500	0.1246	-0.1046	0.1667
0.49	-0.2139	0.1023	-0.1989	0.1363
0.36	-0.2370	0.06808	N	0.08599
0.125	N	0.04650	N	0.04606
0.16	N	0.03172	N	-0.02197
0.09	N	N	N	-
0	0	0	0	0

N Program MIGR2 does not converge

V. TRANSIENT BEHAVIOR IN A STAGNANT DIFFUSION CELL

In chapter 2, we have mentioned that a typical log current vs. log time curve in a stagnant diffusion cell consists of two parts, the horizontal part and the decreasing part of slope $-\frac{1}{2}$. According to Eq. (2-17), the current density would be infinitely large at the very beginning, and decrease with the square root of time thereafter. Actually, the current at the beginning is limited by the ohmic resistance of the solution. The assumption that the concentration of electrolyte near the electrode surface will drop to zero right after the power supply is switched on is, of course, not true in actual experiments. It must take a certain amount of time before the surface concentration reaches zero, the amount of time required being a function of applied voltage. In this chapter, the main interest is concentrated on the flat part of the i-t curve.

Davis, Horvath and Tobias[10] have treated the problem with consideration of electrochemical kinetics, or surface overpotential only. In this chapter the analysis is extended to include concentration overpotential as well as surface overpotential and ohmic resistance. The analysis is similar to the case of a plane electrode in the wall of a flow channel.[34]

5.1 Mathematical Analysis

With the assumption of constant physical properties, the equation of unsteady diffusion in a stagnant diffusion cell for a solution without supporting electrolyte or with an excess of supporting electrolyte reduces to

$$\frac{\partial c}{\partial t} = D\frac{\partial^2 c}{\partial y^2} \tag{5-1}$$

where $c = c_+/\nu_+ = c_-/\nu_-$;

$D = \dfrac{z_+u_+D_- - z_-u_-D_+}{z_+u_+ - z_-u_-}$ for a binary electrolyte,

and $c = c_R$; $D = \overline{D}$ for a solution with an excess of supporting electrolyte.

Equation (5-1) has to be solved with the initial condition that the concentration is uniform throughout the whole capillary at t=0 and the boundary condition that the surface concentration c_o is not a constant but a function of time, i.e.,

$c = c_o(t)$ for $t > 0$ at $y = 0$

$c = c_\infty$ for $t \geq 0$ at $y = \infty$

If the Laplace transform is taken with respect to t and the converted ordinary differential equation is solved with the above boundary conditions, then the transform of the concentration profile is

$$\overline{c} = \frac{c_\infty}{s} + \left(\overline{c}_o(s) - \frac{c_\infty}{s}\right) e^{-\sqrt{\frac{s}{D}}\, y}$$

where s and bars have their usual meanings in Laplace transform operations. If Eq. (5-2) is differentiated with respect to y, and y is set equal to zero, and the result is inverted by means of the convolution integral to yield the concentration gradient at the surface

$$\frac{\partial c}{\partial y}\Big|_{y=0} = \frac{-1}{\sqrt{D}} \int_0^t \frac{dc_o(t')}{dt'} \frac{1}{\sqrt{\pi(t-t')}}\, dt' \quad , \tag{5-3}$$

where t' is a dummy variable.

The current density at electrode surface is

$$i = \frac{nFD}{(1-t_R)} \frac{\partial c}{\partial y}\Big|_{y=0} \quad . \tag{5-4}$$

The current density is further related to the surface overpotential η_s, concentration overpotential η_c, and ohmic resistance η_{ohm} in a metal deposition reaction by

$$i = i_o \theta^{\gamma}[\exp(\alpha Zf\eta_s) - \exp(-\beta Zf\eta_s)] \quad , \tag{5-5}$$

$$\eta_c = \frac{1}{Zf}[\ell n\theta + t_R(1-\theta)] \quad , \tag{5-6}$$

$$\eta_{ohm} = iL/\kappa_\infty \tag{5-7}$$

$f = F/RT$,

$\theta = c_o/c_\infty$ is a dimensionless surface concentration.

i_o is exchange current density.

α, β, γ are electrode kinetics parameters.

L is the length of the capillary tube.

$Z = - z_+z_-/(z_+-z_-)$ for a binary electrolyte.

$Z = - n$ for solution with an excess of supporting electrolyte.

The total voltage difference between the potential of the electrode and the potential in the bulk solution is the sum of

concentration and surface overpotentials plus the ohmic potential drop in the solution.

Let us introduce dimensionless total voltage V, overpotential η, dimensionless current density I, exchange current density J, and dimensionless time τ as

$$V = Zf(\eta_c+\eta_s+\eta_{ohm}) \tag{5-8}$$

$$\eta = Zf(\eta_c+\eta_s) \tag{5-9}$$

$$I = ZfiL/\kappa_\infty \tag{5-10}$$

$$J = Zf\, i_o\, L/\kappa_\infty \tag{5-11}$$

$$\tau = t/t_c \tag{5-12}$$

where t_c is a characteristic time defined below.

If we substitute Eq. (5-3) into Eq. (5-4) and make it dimensionless, we obtain

$$I = \int_0^\tau \frac{d\theta(\tau')}{d\tau'} \frac{1}{\sqrt{\tau-\tau'}}\, d\tau' \quad , \tag{5-13}$$

where $$t_c = \left[-\frac{nZFfc_\infty L}{(1-t_R)\kappa_\infty}\right]^2 \frac{D}{\pi} \tag{5-14}$$

In dimensionless form, Eqs. (5-5) to (5-7) become

$$I = J\,[\theta^{\gamma-\alpha}\exp(\alpha C) - \theta^{\gamma+\beta}\exp(-\beta C)] \quad , \tag{5-15}$$

where $C = \eta - t_R(1-\theta)$

and $I = V - \eta$. (5-16)

The dimensionless current I, surface concentration θ and overpotential η are nonlinearly related by Eqs. (5-13), (5-15) and (5-16). They can be solved numerically when the six parameters, α, β, γ, J, V, and t_R are known for a given system.

5.2 Numerical Calculation Method

The integral, Eq. (5-13), is solved numerically by the method of Acrivos and Chambré. To change the differential Eq. (5-13) into a difference equation, first, replace $d\theta/d\tau$ by $(\theta_k-\theta_{k-1})/\Delta\tau$ where k starts from 2 to j and $\Delta\tau$ is the time interval,* and then replace $\sqrt{\tau-\tau'}$ by $\sqrt{\tau_j-\tau'}$ and consider $\tau_j = (j-1)\Delta\tau$ as a constant for a given j. Equation (5-13) can now be written as

$$I_j = \sum_{k=2}^{i} \frac{\theta_k-\theta_{k-1}}{\Delta\tau} \int_{(k-2)\Delta\tau}^{(k-1)\Delta\tau} - \frac{d(\tau_j-\tau')}{\sqrt{\tau_j-\tau'}} \quad . \tag{5-17}$$

After integrating Eq. (5-17) and with some mathematical rearrangements, we obtain

$$I_j = \frac{2}{\sqrt{\Delta\tau}} \left[\theta_j - \theta_1 B_{j-1} - \sum_{k=2}^{j=1} \theta_k A_{j-k}\right] \quad , \tag{5-18}$$

where

$$B_j = j^{\frac{1}{2}} - (j-1)^{\frac{1}{2}} \quad ,$$

$$A_{j-k} = 2j^{\frac{1}{2}} - (j+1)^{\frac{1}{2}} - (j-1)^{\frac{1}{2}}$$

*Because all dimensionless quantities (Eqs. (5-8) to (5-12)) are linearly related to their original quantities, the word "dimensionless" is omitted hereafter.

Knowing the initial condition i.e., $\theta=1$ at $\tau=0$ as a starting point of the first mesh point $j=1$, it is possible to solve η from Eq. (5-15) in conjunction with (5-16) by a Newton-Raphson iteration method (see, for example, Ref. 31).

For the first mesh point, let $\eta = V$, $j=1$ and $f(\eta)$ be

$$f(\eta) = \theta^{\gamma-\alpha}\exp(\alpha C) - \theta^{\alpha+\beta}\exp(-\beta C) - \frac{1}{J}(V-\eta) \qquad (5\text{-}19)$$

and

$$\eta_j^{(r+1)} = \eta_j^{(r)} - \frac{f(\eta)}{f'(\eta)} \qquad (5\text{-}20)$$

The calculations are repeated until η_1 converges. I_1 is then calculated from Eq. (5-16). At the next point, the sequence of calculations is as follows,

1. use the previous mesh point values of θ_{j-1} and η_{j-1} as a first guess,
2. calculate $\eta_j^{(r+1)}$ from Eqs. (5-19) and (5-20),
3. calculate $I_j^{(r+1)}$ from Eq. (5-16),
4. calculate $\theta_j^{(r+1)}$ from Eq. (5-18).
5. If the η_j does not converge within a tolerable error, a new θ with a damping factor d is assumed, i.e.,
$$\theta_j = \theta_j^{(r)}d + (1.0-d)\theta_j^{(r+1)} \quad .$$
6. The new values of θ_j, and η_j are used and the calculations are repeated from step 2 until η_j converges.

During the calculations, it was found that the damping factor was extremely important to the convergence of the iterations. The

damping factor is strongly dependent on θ and τ. By experimentation, the optimum d was found to be $(1-\theta)^n$ where n=2 or 3 at small time and n=1 for large time.

Because of the logarithmic nature of the variation of I and θ vs. τ, the computer program CURD1 (see Appendix E4) was designed so that the mesh size $\Delta\tau$ (or H in the program notation) is a variable. The program starts with a total of 101 mesh points at a specified $\Delta\tau$ which covers the first and second decades of time. After all mesh points have been calculated, $\Delta\tau$ is increased by a factor of 10 with the same n number of mesh points. In the third decade of time, the values of I, η, θ of the first 11 mesh points are taken from the mesh points of 1, 11, 21, 31, ...101 of the previous decade. By doing so, this not only results in a saving of the number of calculations at large times but also minimizes the propagation of errors at large times.

5.3 Theoretical Results

The current density I obtained from the preceding numerical calculation procedures is plotted vs. time τ in Fig. 5-1 with V as a parameter; α, β, γ, J and t_R are all assumed equal to 0.5. It shows the higher the total applied voltage V, the shorter the flat part. When V is high, there is an overshooting phenomenon of the slope of curve at the region where the curve starts to decrease.

The decrease of the surface concentration θ with respect to time is plotted in Fig. 5-2 with identical parameters as in the previous plot. The higher the applied voltage the faster the surface concentration drops to zero. The time required for the surface concentration to drop to 10% and 1% of its original concentration is plotted in Fig. 5-3.

Similar to the first two figures, the exchange current density J is plotted as a parameter in Figs. 5-4 and 5-5 at constant V. A higher exchange density means a higher reversibility of an electrode reaction, which helps the surface concentration to decrease to zero in a shorter time.

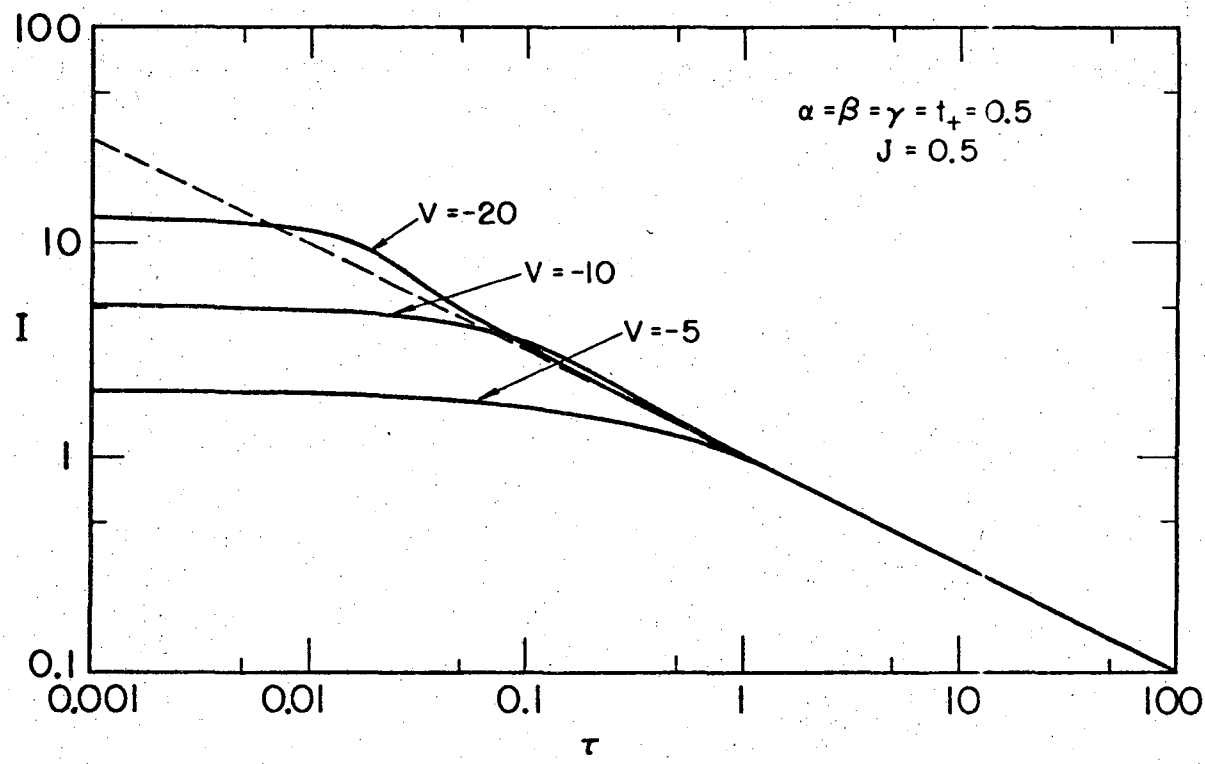

XBL 6811-7263

Fig. 5-1. Decrease of current density in a stagnant diffusion cell (total applied voltage as a parameter).

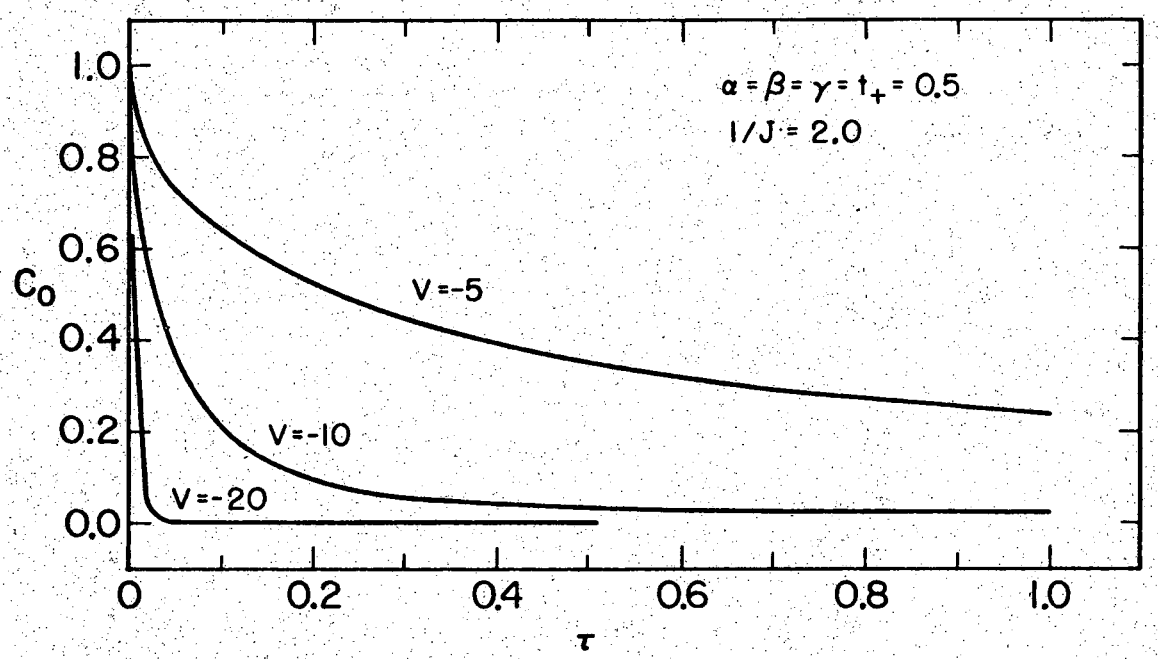

XBL6811-7235

Fig. 5-2. Decrease of surface concentration in a stagnant diffusion cell (total applied voltage as a parameter).

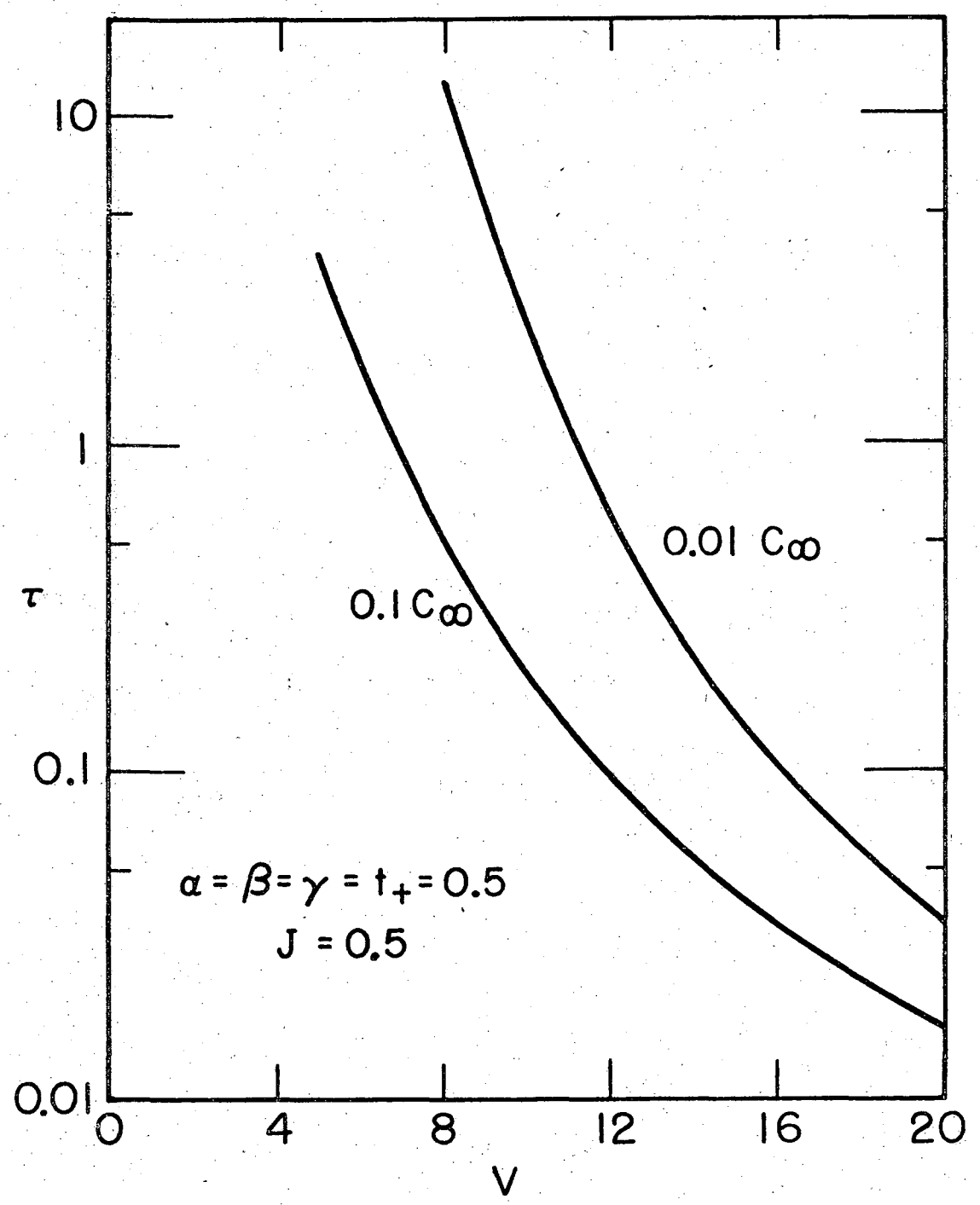

XBL6811-7234

Fig. 5-3. Transient time in a stagnant diffusion cell.

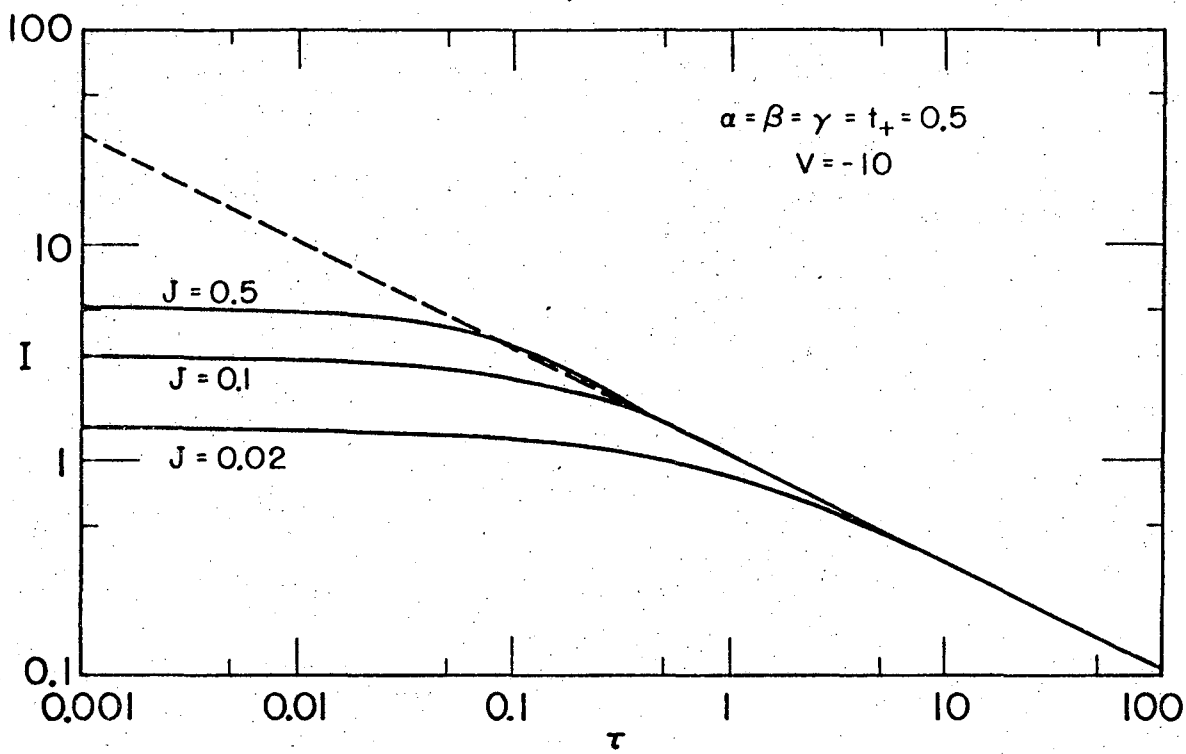

XBL6811-7233

Fig. 5-4. Decrease of current density in a stagnant diffusion cell (exchange current density as a parameter).

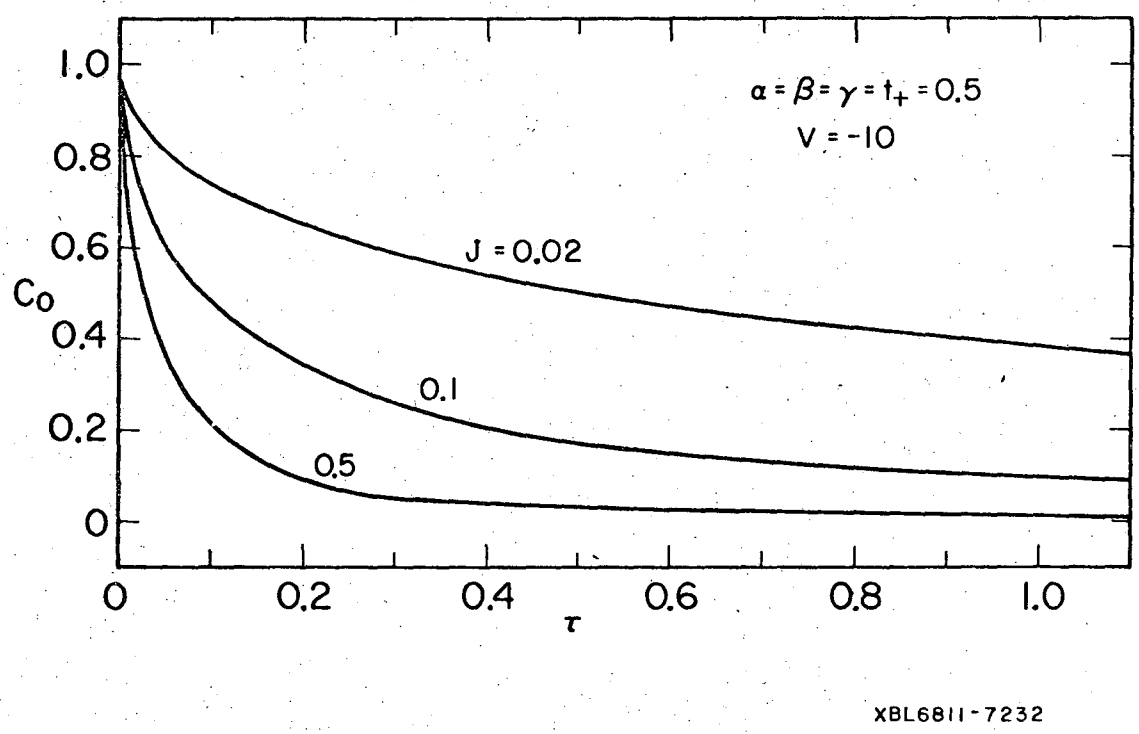

XBL6811-7232

Fig. 5-5. Decrease of surface concentration in a stagnant diffusion cell (exchange current as a parameter).

VI. EXPERIMENTAL WORK----ELECTRICAL MEASUREMENT

6.1 Experimental Method in a Stagnant Diffusion Cell

A. Cell Construction

The cell was made of two pieces of precisely bored glass capillary. The glass capillary tube was chosen because of its good thermal conductivity and ease of cleaning in comparison with lucite. To overcome the poor machinability and sealing problems, the cell was assembled in the following way (see Fig. 6-1).

The tip of the lower part of the capillary (L) was ground in a small angle, the platinum electrode (E) was then glued to the capillary tip by epoxy and set for 24 hours. A short sleeve of glass tubing (S) was fused to the upper part of the capillary (U). The lower part was then glued into the sleeve. Heating was avoided to prevent any change of the shape of the glass tubing. The upper part of the capillary was then filled with mercury for electrical contact. A copper wire was sealed on the top.

Before the lower parts of capillaries were inserted into the sleeves, the diameters were measured on a platform microscope at the Precision Shop of the Lawrence Radiation Laboratory. The diameters and the lengths of capillaries are listed in Table 6-1.

B. Preparation and Analysis of Solutions

Reagent grade $CuSO_4 \cdot 5H_2O$ and concentrated H_2SO_4 of specific gravity 1.84 were used for making all the solutions. All weighings were done on a Mettler analytical balance of ±0.1 mg accuracy. The copper concentration was analysed by the electrogravimetric method, and sulfuric acid was titrated with standardized NaOH solution. The procedure of analysis is given in Appendix B.

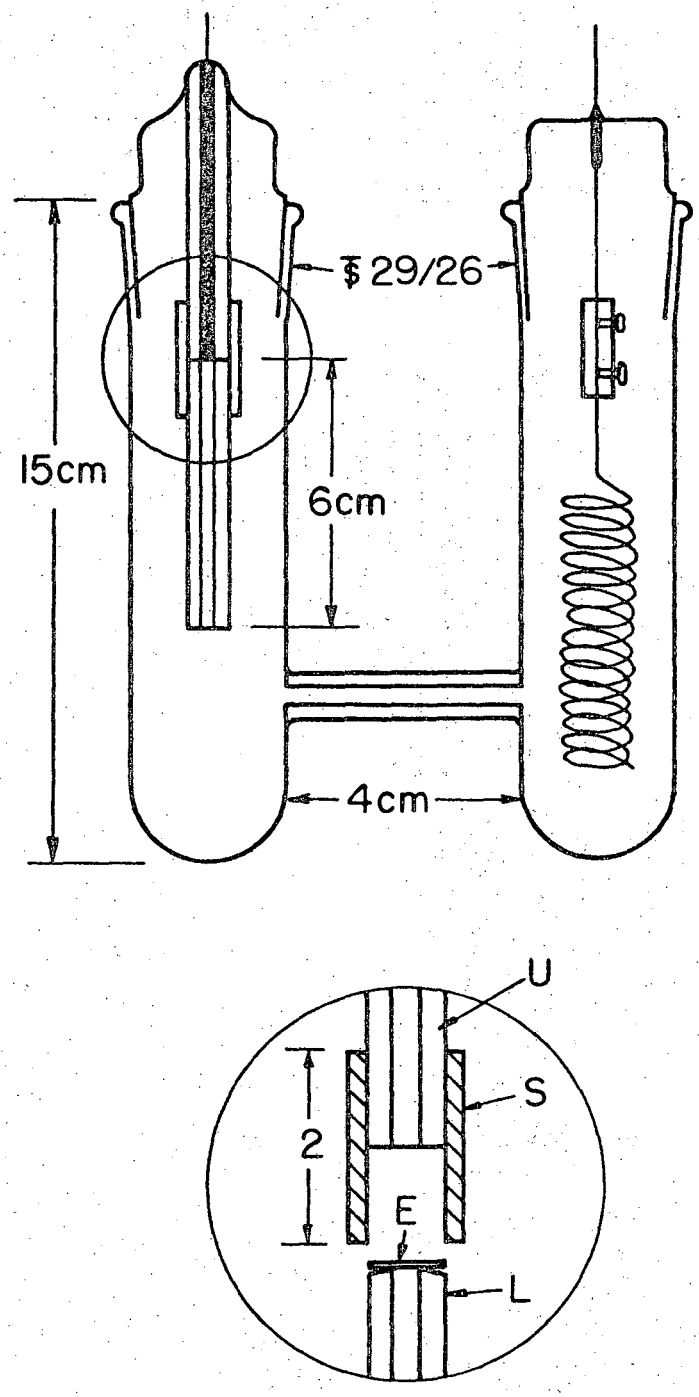

XBL6811-7240

Fig. 6.1. Stagnant diffusion cell.

Table 6-1. The size of diffusion capillaries.

Capillary	Diameter mm	Length cm
B	1.30	7.0
C	2.08	4.0
D	2.03	4.0
E	2.80	5.0
F	2.08	2.0
G	2.78	5.0
H	2.08	2.0
J	3.00	6.0
K	3.00	6.0
L	3.00	6.0
M	3.00	6.0

C. Circuit Diagram

The experiment was designed to measure the current-time behavior of five stagnant diffusion cells at the same time. A schematic diagram is shown in Fig. 6-2. A Transistorized Power Supply (model 5015A made by Power Designs Inc., New York) was used as a constant voltage source. The current flow across each cell was measured by the voltage drop across a known resistance.

The voltages were measured by a VIDAR 520 Integrating Digital Voltmeter (made by VIDAR Corps., Mountain View, California) at a time interval controlled by a VIDAR 625 Electronic Clock. The digital voltmeter has an internal impedence of 1000 MΩ linear accuracy of ±0.005%. The clock has an accuracy of less than one hundredth of a second with a maximum scale of ten thousand seconds.

The measured data from the voltmeter were transmitted either to a FRANKLIN model 1030D High Speed Printer (made by Franklin Electronic Inc., Bridgeport, Pa.) and plotted and analyzed manually or to an AMPEX model 7211 Magnetic Tape Unit and processed by a computer. For the detailed data processing, computer program, and tape handling see Appendices C and D.

D. Control Panel

For convenience in operations, and to start the VIDAR 620 electronic clock and to apply the constant voltage to all cells at the same time, a control panel was built for the stagnant diffusion measurements. The panel was designed to operate five stagnant diffusion cells simultaneously. The detailed operation is discussed in Appendix F.

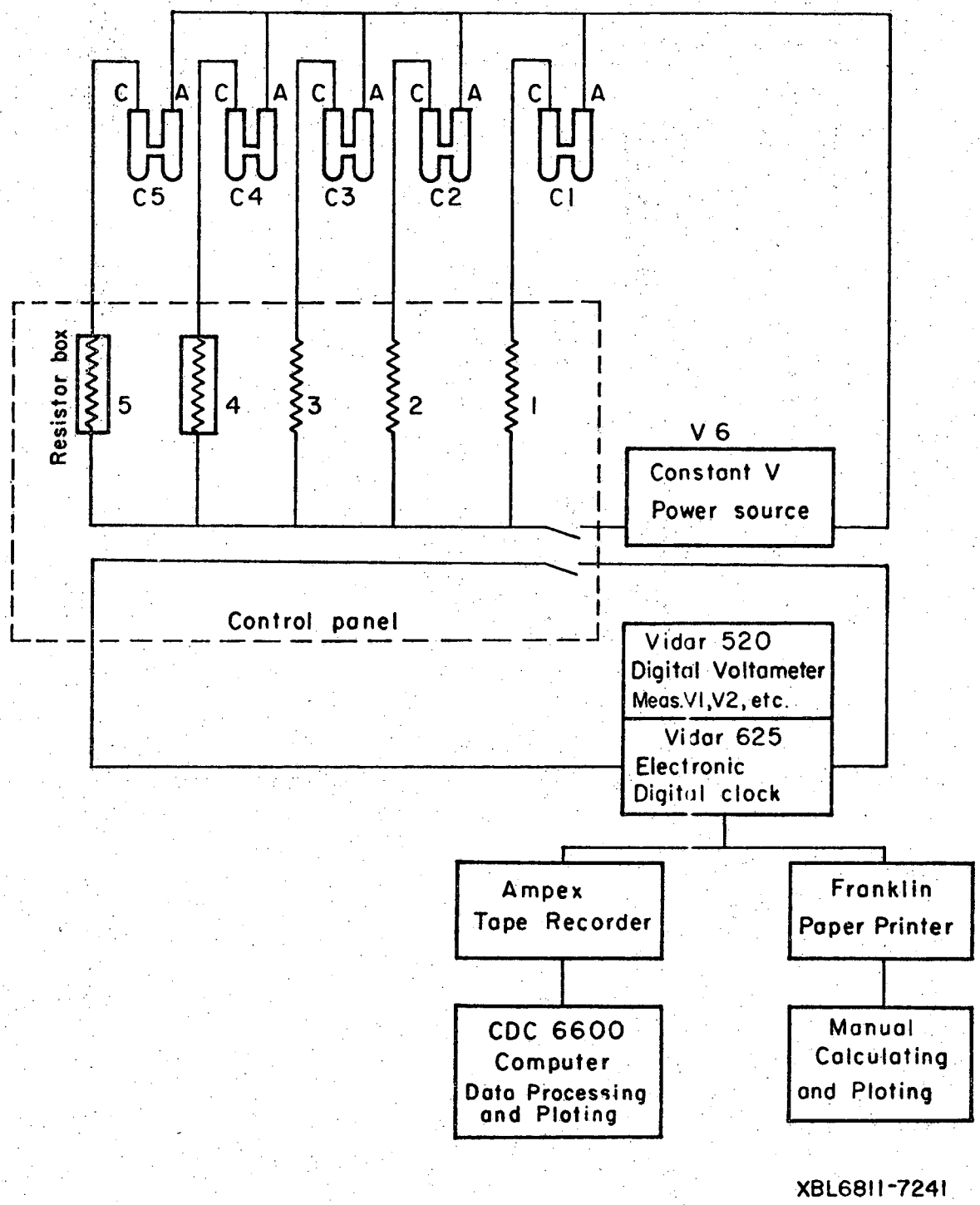

Fig. 6-2. Schematic diagram of stagnant diffusion cell measurement.

6.2 Experimental Procedure

Before each run, the capillary cathode was cleaned with dilute nitric acid to remove all previously deposited copper and rinsed with distilled water followed by the solution. The platinum electrode was then predeposited with copper at a constant voltage of 0.1 volt for one to three minutes in a well supported $CuSO_4$-H_2SO_4 solution. The solution was renewed several times to assure that limiting current was not reached.

Removing and filling solutions or acid were done with a platinum needle and glass-tipped syringe. (The needle was made of 80% platinum, 20% iridium, purchased from the Hamilton Company Inc., Whittier, California). This is necessary because the acidic corrosion and copper replacement reaction would take place with an ordinary stainless steel needle and syringe tip.

The helically shaped anode was made of oxygen free high purity copper wire. To clean the anode, it was dipped into dilute nitric acid, rinsed with distilled water, carefully wrapped dry with a tissue paper, and stored in a vacuum desiccator until ready to be used.

The capillary and cell are then filled with solution, care being exerted that no air bubble was trapped in the cell. The whole assembly was then immersed in a constant temperature bath for at least an hour so that it would reach thermal equilibrium with the bath. The bath was controlled by a Sargent Model S "thermonitor" and monitored with an N.B.S. calibrated thermometer. The temperature variation was less than ±0.02°C.

Both the constant voltage power source and the digital voltmeter were switched on at least thirty minutes before a run actually

started. Pretest, calibration, and checkup of the whole digital system were done from time to time. Cables were connected as shown in Fig. 6-2. The experimental setup and apparatus are shown in Fig. 6-3.

Because of the nature of the behavior of current-time curves, the current density was measured at time intervals of 1 sec for the first 20 seconds, every 10 seconds between 20 and 200 seconds and every 100 seconds thereafter. The gate time is the resolution time of the voltmeter, the longer the gate time is, the more significant figures it measures.

The measured current was then manually plotted on a log-log scale as a function of time. The recorded tapes were processed by computer with the program PROCESS (see Appendix C).

6.3 Results and Discussions

A typical transient behavior of current density and time has two parts; the nearly flat part where the ohmic resistance and surface overpotential dominate the behavior at small times; and the decreasing part where the concentration overpotential dominates the behavior at large times.

In a 0.0986M copper sulfate solution with 1.00M sulfuric acid as supporting electrolyte (solution 52), the transient behaviors are plotted in Fig. 6-4 with the total applied constant voltage across the stagnant diffusion cell as a parameter. The results indicate that the higher is the applied voltage, the higher and the shorter is the flat part. They all converged to a single straight line of slope $-\frac{1}{2}$ at large times.

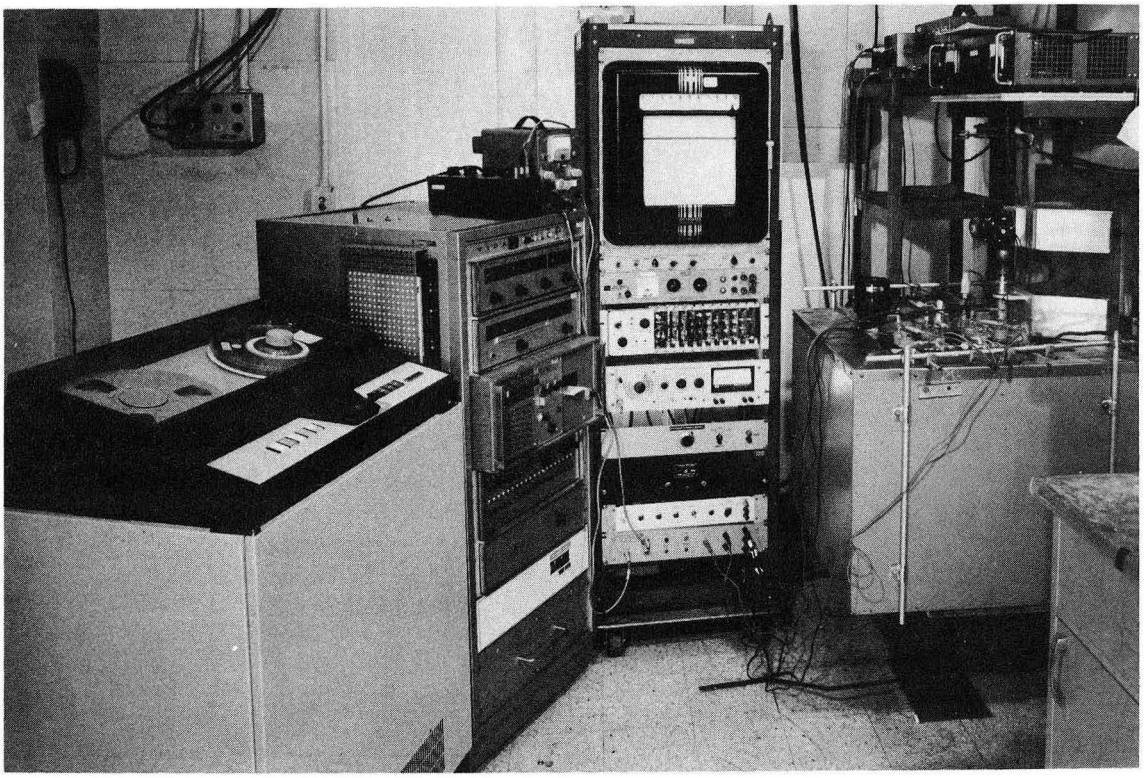

XBB 6811-6775

Fig. 6-3. The experimental setup for electrical measurements in a stagnant diffusion cell.

We should like now to compare these curves with the theoretical predictions from chapter 5. The theoretical curves are specified only if the parameters α, β, γ, t_R, J, and V are known (see Table 6-2). The kinetic parameter data are rare and uncertain. Mattsson and Bockris[32] have reported these parameters in a copper sulfate solution with sulfuric acid concentration of 0.5M. Based on their data, α, β, γ and other parameters are estimated and listed in Table 6-2. The exchange current density is estimated to be between 1 and 10 mA/cm^2 for a cathode surface prepared by electrodeposition.

The conductivity data are calculated from the correlation equation which is given in Appendix 1. Since the solution has excess sulfuric acid, the transference number of copper ion was assumed to be zero.* The integral diffusion coefficients were taken from Table 3-4.

The comparison is made in Fig. 6-5 for one of the voltages shown on Fig. 6-4, i.e., 0.350V. Had all the above estimates been correct, the experimental curves would have fallen between the two theoretically predicted lines corresponding to exchange current densities of 1 and 10 mA/cm^2. Unfortunately, in seven runs (run 41 to 46 and 48) with identical conditions of voltage and concentration of solution, the measured current density is consistently lower than the prediction at small times. Similar inconsistencies are also found in the other experimental curves.

Despite the disagreement of the nearly flat part in the i-t curves, the theory has successfully predicted an overshooting phenomenon at the transition region when the straight line of slope $-\frac{1}{2}$ is extended

---

* When the transference number is calculated from the equation $t_R = z_R^2 u_R c_R / \Sigma z_i^2 u_i c_i$, t_R would be 0.012 if complete dissociation of bisulfate ion is assumed, 0.028 if no dissociation of bisulfate ion is assumed for the solution at that concentration.

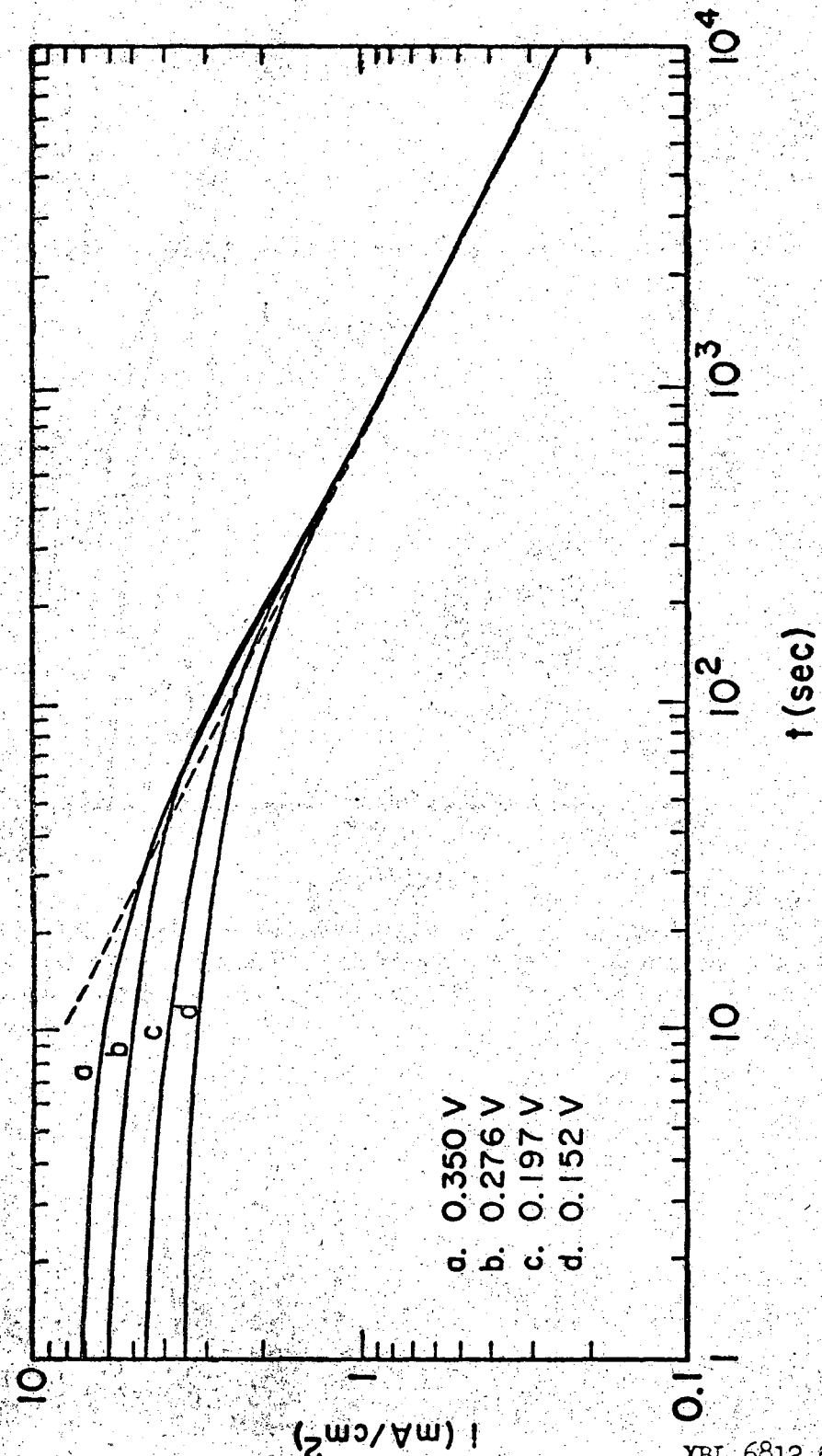

XBL 6812-6313

Fig. 6-4. Observed transient behavior in a stagnant diffusion cell showing the effect of total applied voltage. (Solution 52; curves from top to bottom, run 73, 75, 48, 49)

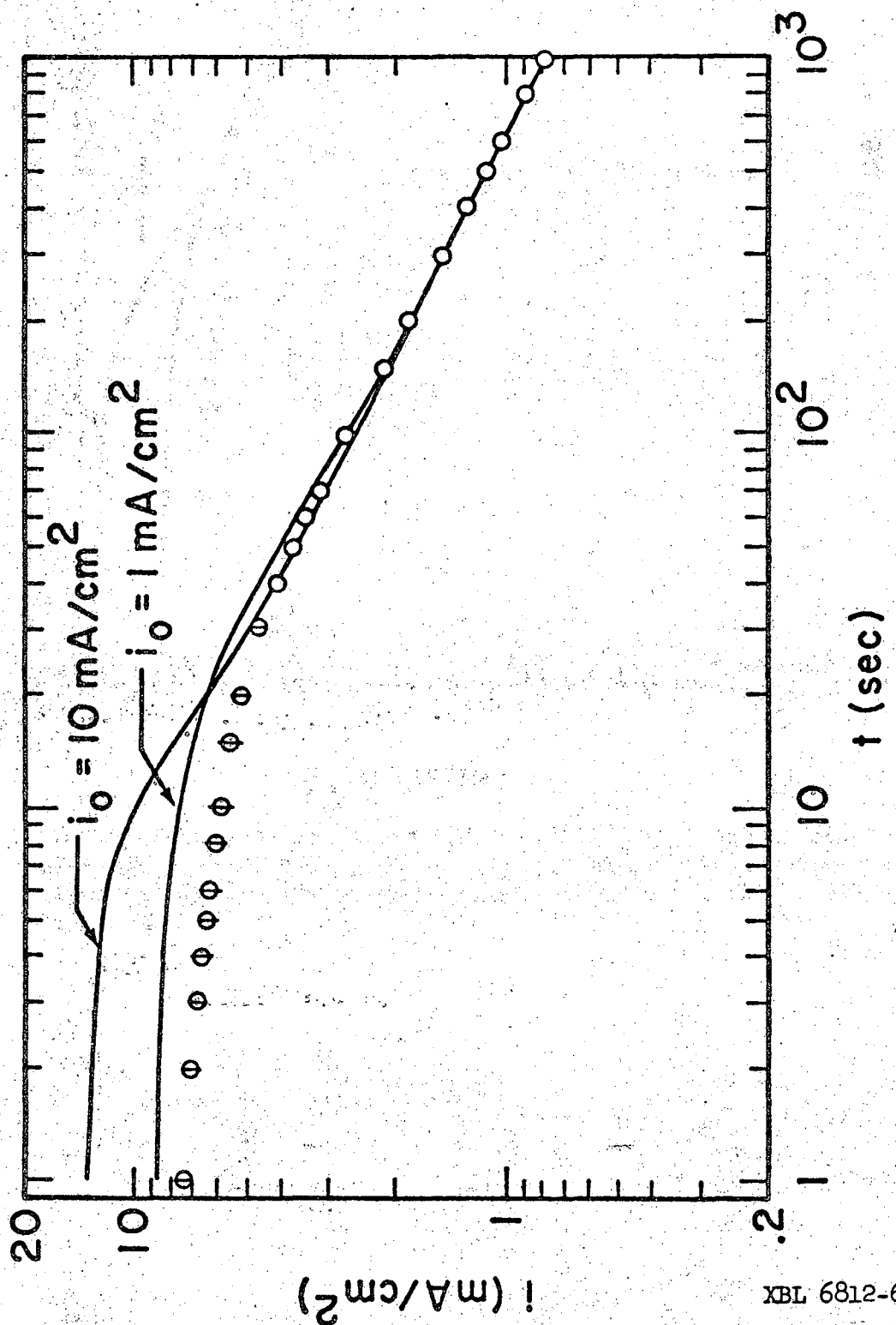

XBL 6812-6326

Fig. 6-5. Comparison of theoretical predictions (solid lines) for exchange current densities of 1 and 10 mA/cm^2 with observed results (open circles). (Solution 52, Run 41 to 46, 48. Total voltage 0.350 V)

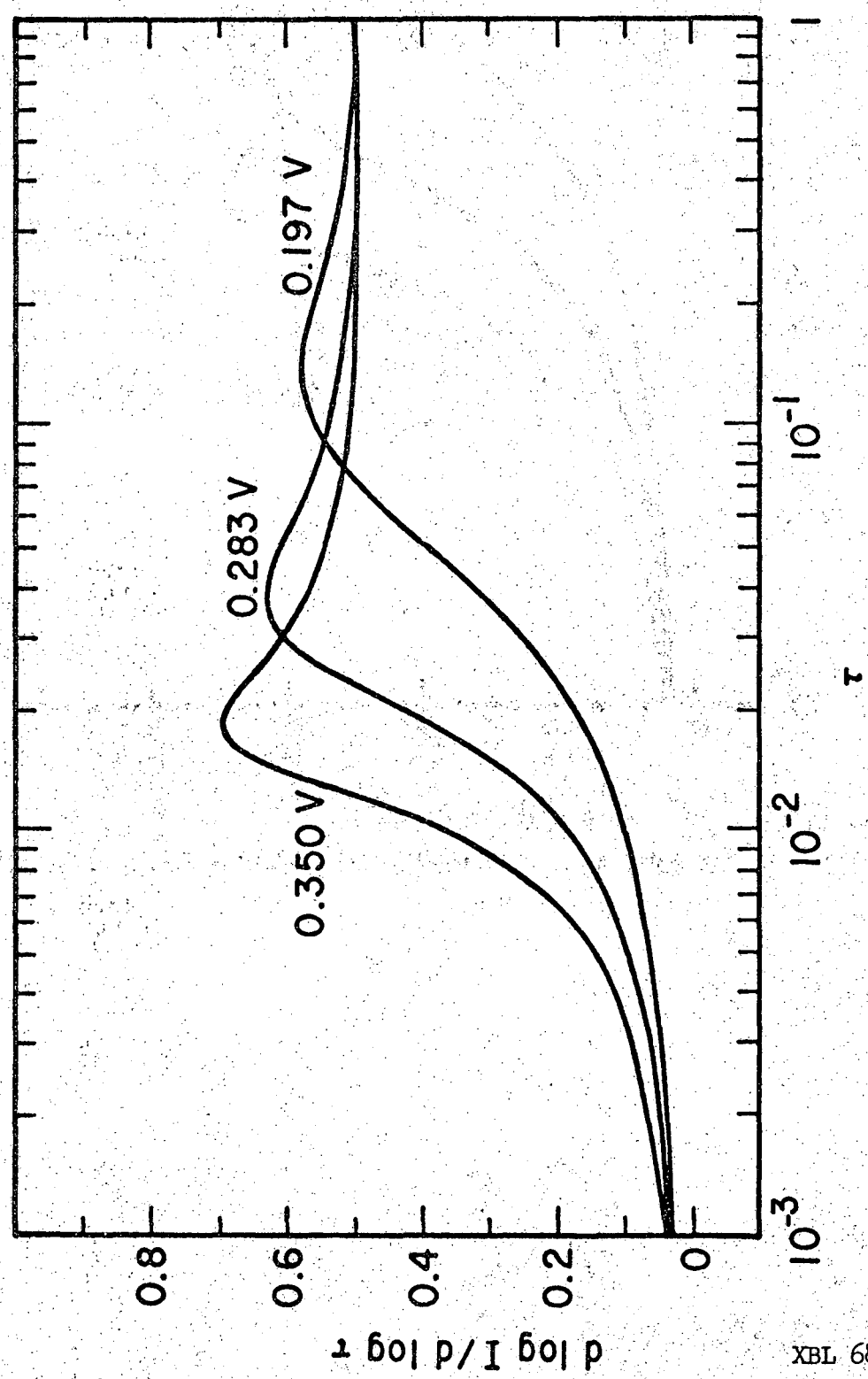

XBL 6812-6327

Fig. 6-6. The overshooting phenomenon in a stagnant diffusion cell.

backwards (the dashed line in Fig. 6-4). In other words, a plot of the slope d log i/d log t would indicate a peak before it reaches the constant value of 0.5. The theoretically predicted slope is plotted vs. time on a semilog scale in Fig. 6-6. The peak tends to smooth off and disappear when the total voltage is decreased.

A. Transient Behavior at Very Short Times

A further investigation of log i - log t behavior at very short times (0.05 to 0.5 sec) of solution 54 reveals that a step drop of current density occurs in this time range. Before the step change of current density, the flat part was found to fall within the theoretical predictions of exchange current density at 1 and 10 mA/cm^2 (see Fig. 6-7, the concentration of the solution, parameters and physical properties used for these calculations have been listed in Table 6-2).

The reason for this step drop of current density is unknown, though the phenomenon was fairly reproducible in a well supported electrolyte. No such step change in a solution with little or no supporting electrolyte was observed. It was suspected to be the charging of the double layer, but a simple calculation shows that the time of charging the double layer should be on the order of 0.5 millisecond.

From the point of view of the system itself, the step drop of current density means additional resistance setting in besides the ohmic resistance of the solution. Since the resistance occurs in the time range of 0.05 to 0.5 sec, it must relate to some change taking place very near to the electrode interface. Let us denote it by R_s.

Two pairs of capillaries (G, E and F, H) of different ratios of length per area were used to measure the i-t curve simultaneously.

Table 6-2. Parameters and physical properties used for the theoretical prediction of transient behavior.

		Solution 52	Solution 54
$CuSO_4$	M	0.0986	0.100
H_2SO_4	M	1.00	1.375
Capillary		B	B
α		0.75	0.75
β		0.25	0.25
γ		0.50	0.50
t_R		0.	0.
κ	mho/cm	0.379	0.493
Z		2	2
$\bar{D}$	10^{-6} cm^2/sec	5.33	5.09
t_c	sec	1270	740
i_o	mA/cm^2	1	1
J		1.437	1.107
i_o	mA/cm^2	10	10
J		14.37	11.07

The total applied voltage is divided by the measured current in the time range of 1 to 10 seconds and tabulated in Table 6-3. Notice that at that time interval, the R_s has already set in.

Table 6-3.

Capillary			G	E	F	H
Area of capillary (cm)			0.061	0.062	0.034	0.034
length/area (1/cm)			82.4	81.2	58.8	58.8
Solution #	$CuSO_4$ M	H_2SO_4 M	V/I Kilohm			
102	0.1001	0.005	14.0		12.0	12.0
103	0.1001	0.020	9.1	9.1	7.4	8.0
104	0.0999	0.050	5.3	5.37	4.9	5.0
105	0.0998	0.100	3.4	3.4	3.4	3.8
106	0.1000	0.125	2.8	3.0	3.3	3.1
107	0.1003	0.175	2.1	2.2	2.3	2.8
108	0.1001	0.250	1.8	2.1	2.2	

For the solution with little supporting electrolyte, the V/I of capillaries G, E are greater than those in F, H. As the concentration of supporting electrolyte increases, the behavior is reversed.

The phenomenon can be explained qualitatively in this manner. We note that R_s is inversely proportional to the area of the electrode, whereas the ohmic resistance is proportional to $L/\kappa A$. When there is little supporting electrolyte, the ohmic resistance of the solution predominates; as the concentration of sulfuric acid increases, the resistivity drops sharply and R_s predominates.

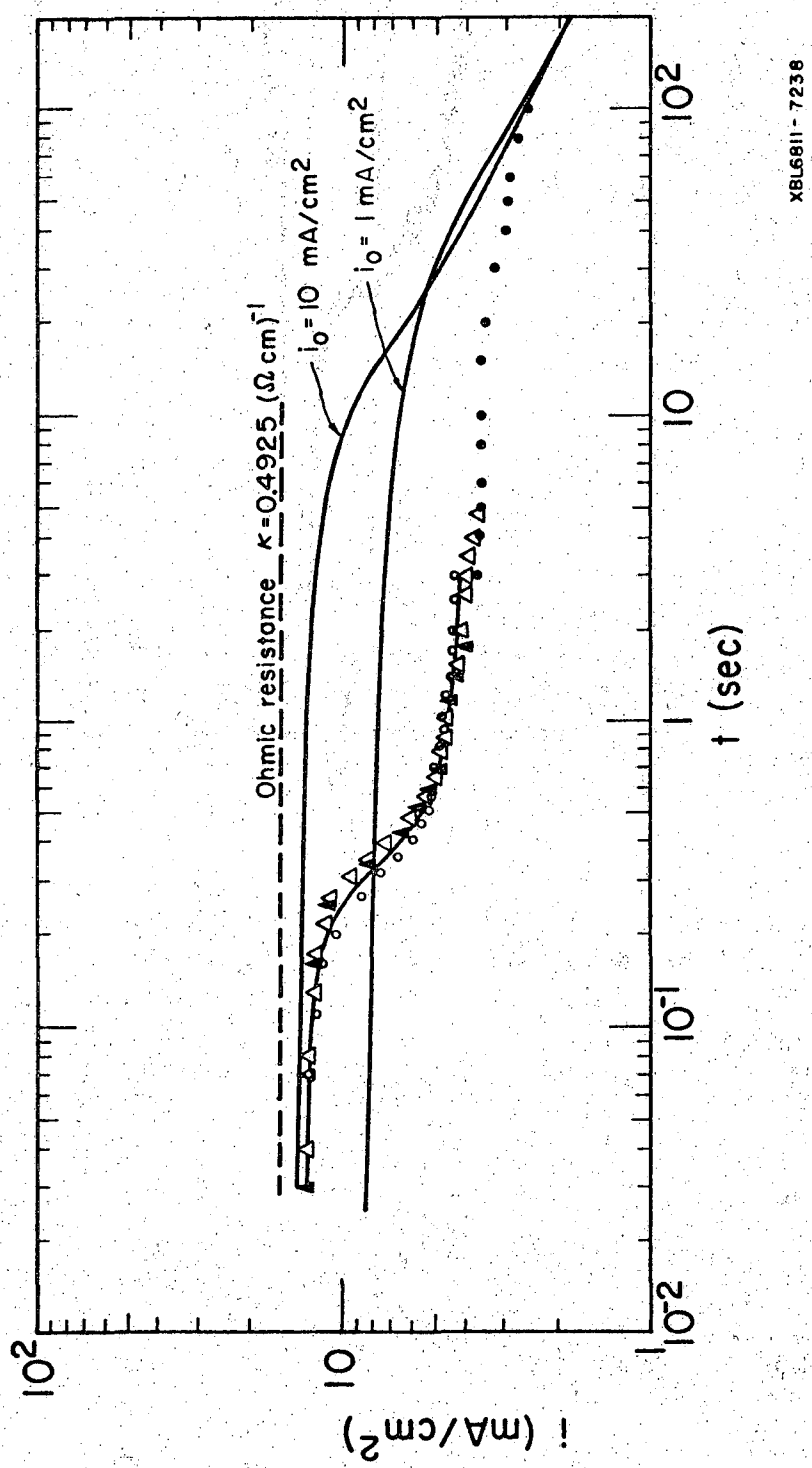

Fig. 6-7. Theoretical and observed transient behavior at very short time (Solution 54, total applied voltage 0.225 V, ● Run 82, o Run 83; ▲ Run 84; △ Run 85.

The step drop of current or the hypothesis involving R_s should be subjected to further investigation before any definitive conclusion could be drawn from it.

B. Current Behavior at large times---- the effect of migration

As the concentration of the reacting ion near the electrode surface gradually decreases to zero, concentration polarization dominates the behavior of the i-t curves. In this region, the current times the square root of time would be a constant. The values of $i\sqrt{t}$ are functions of concentration of copper sulfate and sulfuric acid.

At constant concentration of copper sulfate, the effect of sulfuric acid concentration on the i-t curves is shown in Fig. 6-8. The average values of $i\sqrt{t}$ were evaluated from the recorded tapes in the following manner;

1. Calculate $i\sqrt{t}$ from the voltage drop across the known resistances and the areas of capillaries.
2. At first iteration, calculate the average values and standard deviations of $i\sqrt{t}$ for all channels with t greater than 4000 seconds.
3. The standard deviations and the average values of $i\sqrt{t}$ of the previous iteration are then used as a criterion to check all $i\sqrt{t}$ data. Wherever the deviation of a datum is greater than three times the standard deviation, it is discarded and replaced by -10.0**(5+ITERA), where ITERA is the number of iterations.
4. Repeat the check until no single channel has more than one datum discarded.

5. The maximum number of iterations was set at 8.

The averages of the measured values of $i_L\sqrt{t}$ are tabulated in Table 6-4. Since the diffusion current i_D, the limiting current measured with an infinite amount of supporting electrolyte, could not be measured without introducing a large viscous effect,[42] in comparison with the theory of the effect of migration discussed in chapter 4, the measured $i_L\sqrt{t}$ are adjusted to $i_D\sqrt{t}$ by the theoretically predicted migration factor and if the factor is correct values, $i_D\sqrt{t}$ should be constant.

For the case of complete dissociation of bisulfate ion, the factors I_L/I_D were obtained from Fig. 4-1, and the calculated $i_D\sqrt{t}$ vary from 29.0 to 24.0 $\sqrt{\text{sec}}$-mA/cm^2, with an average value of 26.2 and standard deviation of 2.2. For the case of incomplete dissociation, the factors I_L/I_D was calculated with K_2=0.0104,[26a] and the $i_D\sqrt{t}$ values vary randomly around an average value of 23.4$\sqrt{\text{sec}}$-mA/cm^2, of standard deviation 1.3. These results seem favorable to the assumption of the incompletely dissociation of bisulfate ion in a solution of copper sulfate with sulfuric acid as supporting electrolyte.

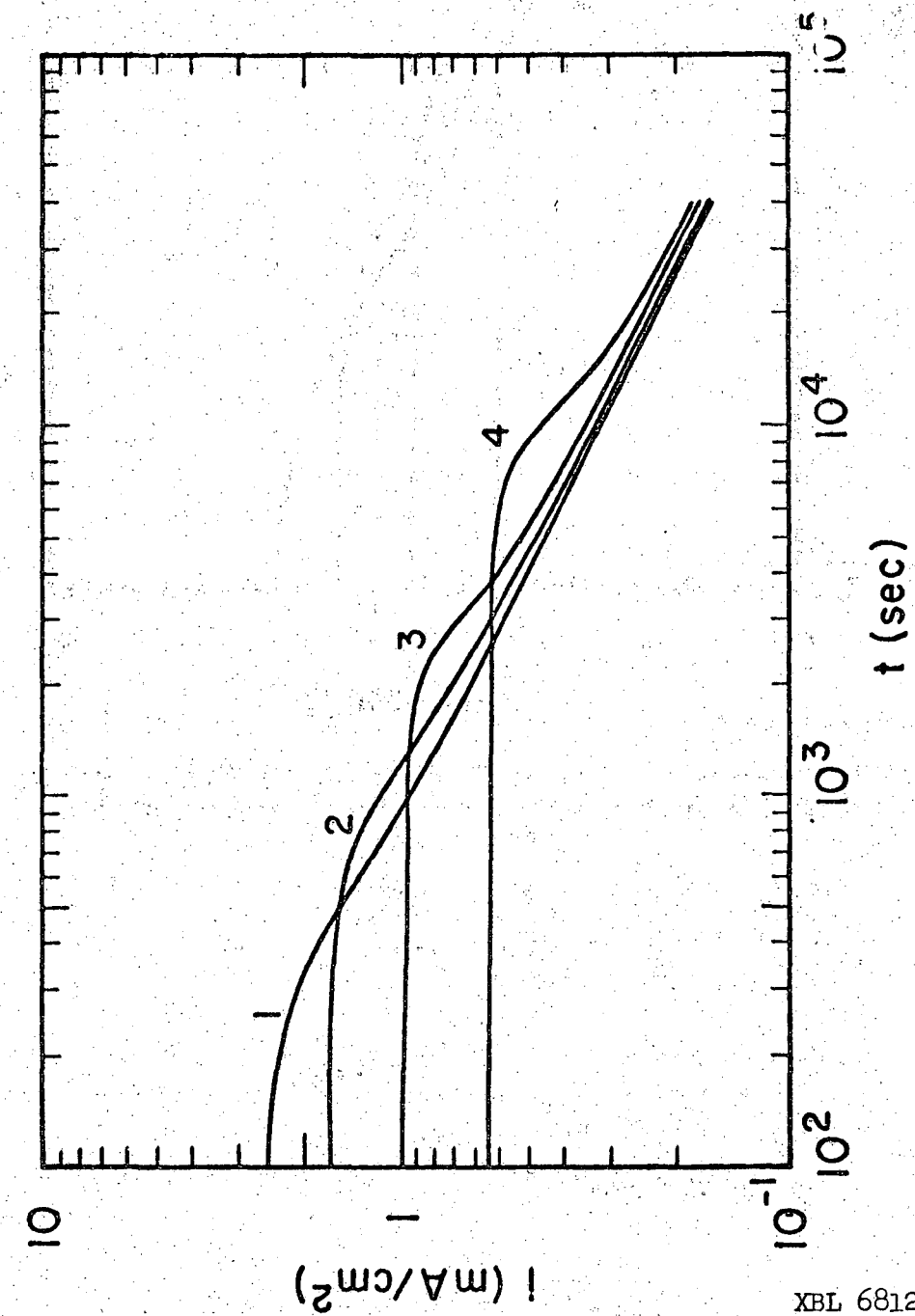

XBL 6812-6314

Fig. 6-8. Observed transient behavior in a stagnant diffusion cell showing the effect of concentration of supporting electrolyte.

	solution #	$CuSO_4$	H_2SO_4	Run #	Applies V.
1	107	0.1003	0.175	175	0.355
2	105	0.0998	0.100	184	0.355
3	104	0.0999	0.050	187	0.355
4	103	0.1001	0.020	190	0.350

Table 6-4. Experimental results of measured $i_L\sqrt{t}$ in a stagnant diffusion cell of copper sulfate and sulfuric acid at 25°C. The effect of migration

Solution* #	r Eq.(4-4)	Measured $i_L\sqrt{t}$ $\frac{mA}{cm^2}\sqrt{sec.}$	# of explts.	Complete dissociation I_L/I_D	Complete dissociation $i_D\sqrt{t}$	Incomplete dissociation I_L/I_D	Incomplete dissociation $i_D\sqrt{t}$
102	0.0471	41.35	2				
103	0.167	37.61	2				
104	0.334	34.60	10	1.20	28.8	1.7259	20.1
105	0.501	32.78	10	1.14	28.8	1.5182	21.6
106	0.555	32.43	11	1.12	29.0	1.4364	22.6
107	0.636	31.59	16	1.095	28.6	1.3179	24.0
108	0.714	30.94	6	1.07	28.9	1.2191	25.4
51	0.888	26.0	3	1.025	25.4	1.0679	24.4
61	0.899	25.4	2	1.022	24.8	1.061	23.9
52	0.912	24.8	3	1.02	24.3	1.053	23.5
62	0.916	25.2	3	1.02	24.7	1.050	24.0
53	0.924	24.9	3	1.018	24.4	1.045	23.8
63	0.927	24.8	2	1.017	24.4	1.043	23.7
54	0.934	24.6	3	1.016	24.2	1.038	23.7
64	0.937	24.4	4	1.015	24.0	1.0365	23.6

*For the concentrations of copper sulfate and sulfuric acid refer to Table 3-4.

VII. EXPERIMENT WORK----OPTICAL MEASUREMENT

In this chapter, the cathodic concentration profile as well as the concentration of electrolyte at the electrode surface in a stagnant diffusion cell are measured at limiting current. The anode is located far enough away so that it does not influence the situation near the cathode. These measurements cannot be observed in a simple, cheap capillary tube, instead an optical cell has to be used for these purposes.

The apparatus used in this experimental work was a Perkin-Elmer Model 238 Electrophoresis Apparatus. The apparatus was originally designed for electrophoresis measurements and producing a Rayleigh interference fringe pattern as well as a Schlieren derivative curve.

The basic principle of Rayleigh interferometry is very simple; two parallel slits are used to split light into two beams which interfere with each other when they are brought together. One of the special features of this interferometer is its multipoint source. Figure 7-1 illustrates the light intensity on the screen of a simple Rayleigh interferometer and its modification. In the modified Rayleigh interferometer, when the monochromatic light from a three point source (P) passes through two slits on a mask (M), each produces a simple interference pattern. If the three point sources are properly spaced, their interference patterns are superimposed upon one another, giving three equally intense fringes on the screen (S).

In the actual apparatus, there are more than 162 point sources, and when the solution in compartments A and B are homogenous, the 162 fringes are straight as in Fig. 7-2. If there is a concentration

difference between the upper part of the cell and the lower part of the cell, the fringes are shifted as in Fig.7-3.

The simple law of interference shows that the number of fringe shifts Δm, is related to the refractive index change Δn by

$$\lambda \Delta m = l \Delta n \tag{7-1}$$

where l is the length of light path across through the cell and λ is the wavelength of the light source. The Rayleigh interference fringe pattern is, therefore, a mapping of the refractive index. Since over a small concentration range, the refractive index is linearly proportional to the concentration of the solution,

$$\Delta m = k \Delta c \quad , \tag{7-2}$$

where k is a proportionality constant, a map of refractive index is essentially a map of concentration.

7.1 Experimental Method

The detailed principles and operations of the apparatus have been discussed in the thesis by Chapman.[37] However, some of the procedures and apparatus features this author wishes to repeat and emphasize.

A. Cells and Electrodes

The optical cells were purchased from the Perkin-Elmer Company. The cell has two channels connected by a U underneath. Each channel has a width of 0.2 cm, length of 0.9 cm in the direction of the light path and depth of 7.9 cm (see Fig. 7-4).

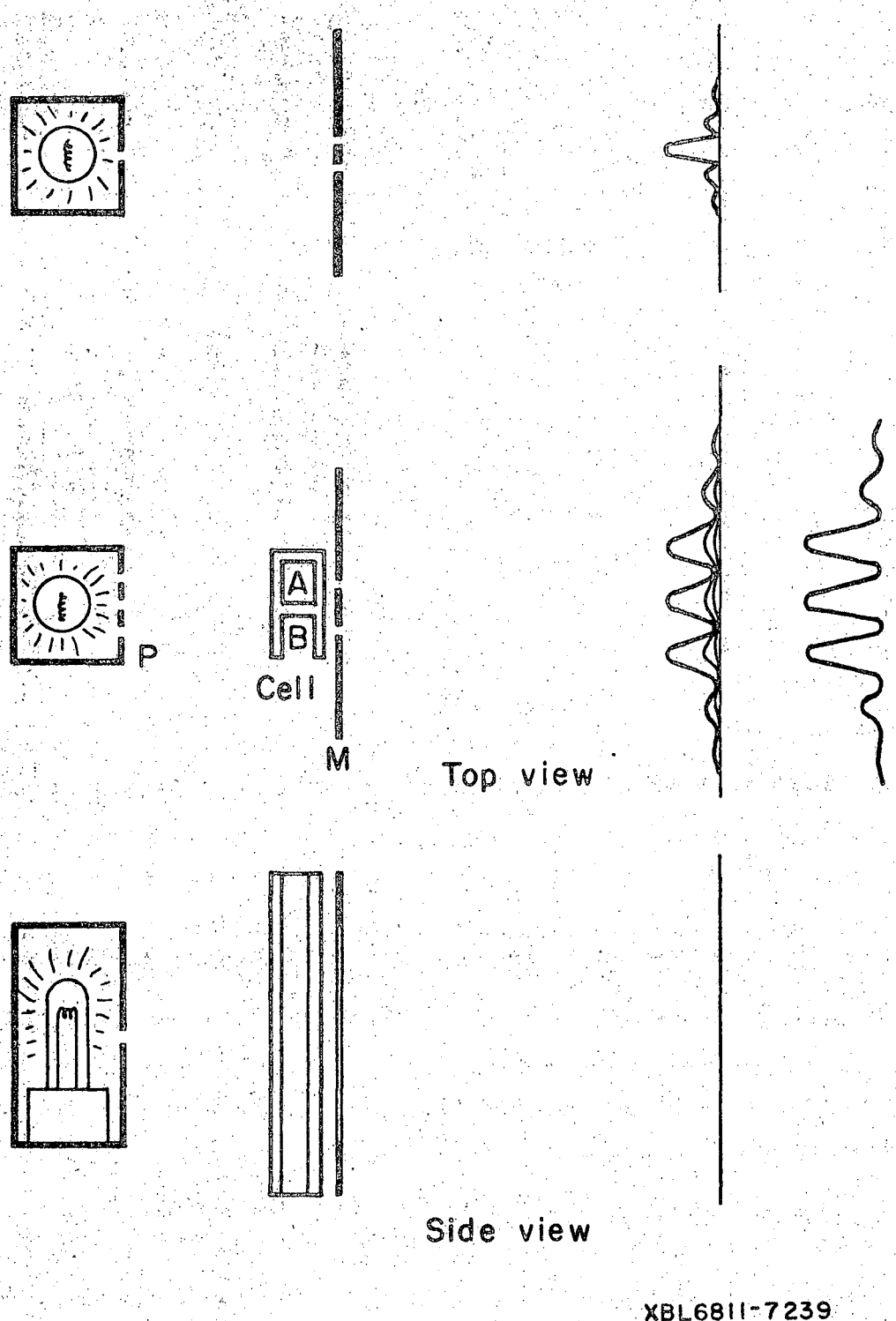

Fig.7-1. A Rayleigh interferometer and a multipoint source.

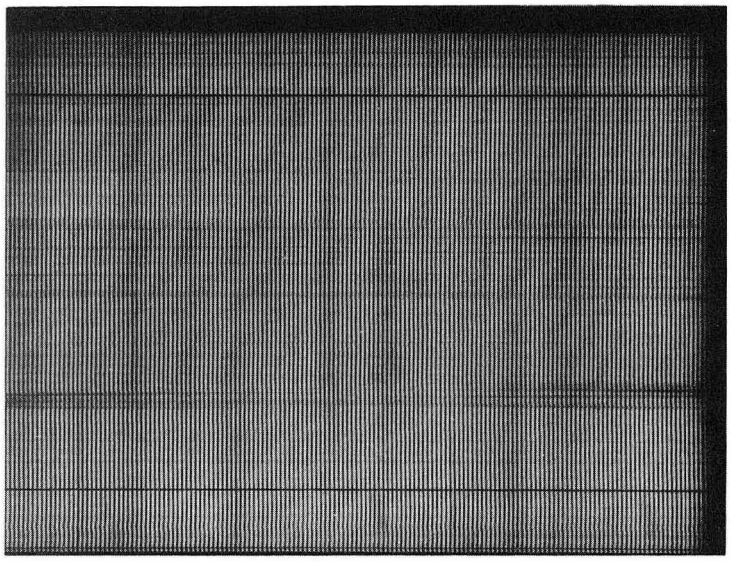

XBB 6811-6718

Fig. 7-2. A Rayleigh interference fringe pattern (162 slits light source).

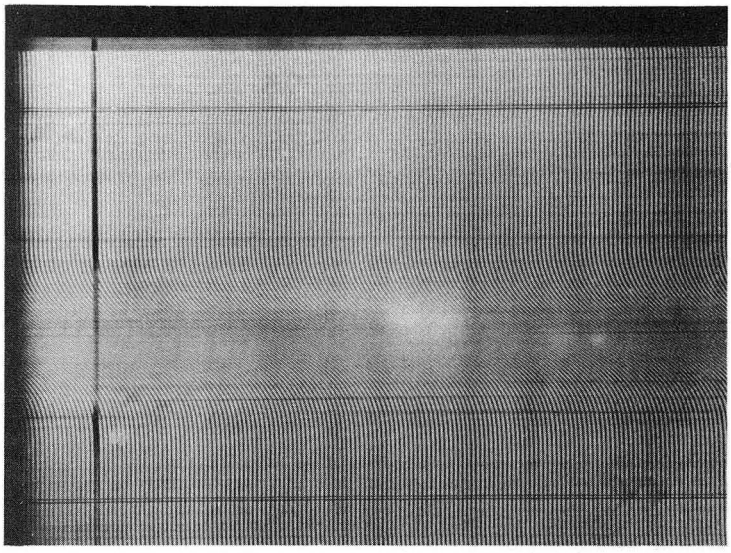

XBB 6811-6717

Fig. 7-3. Fringe shift produced by two solutions of different concentration (Run 17L $1\frac{1}{2}$ hours after forming boundary).

The electrodes were made from an oxygen-free, high-purity copper block. The machining of electrodes was done by the Precision Shop of the Lawrence Radiation Laboratory to fit exactly into the channels, passing a water leak test when the sides of electrodes are properly greased.

A design flaw of the electrode was the extended part of the electrode, which makes the disassembly of the cell very difficult when the ground glass flanges are greased. For future work, a simple rectangular electrode, without the extended part, inserted deep into the channels is recommended.

B. Cell Cleaning

Before each run, the excessive grease was wiped away by a clean tissue paper. The cell was then cleaned with a small amount of cyclohexane to remove all grease on the contacting ground flanges surfaces. The amount of cyclohexane is important in order to prevent any contamination of the cell channels by the dirty solvent. The cell was then washed in a warm Alconox solution and rinsed with distilled water.

Whenever the cell was smeared with grease inside the channels the cell was soaked in a hot chromic acid cleaning solution, (prepared by mixing equal volumes of saturated sodium dichromate solution and technical grade concentrated sulfuric acid) for 3 to 5 minutes to get rid of the grease inside the channels of the cell and perhaps, finger prints on the outside of the glass. Prolonged soaking in acid solution or cleaning with strong solvents may damage the joints of the optical

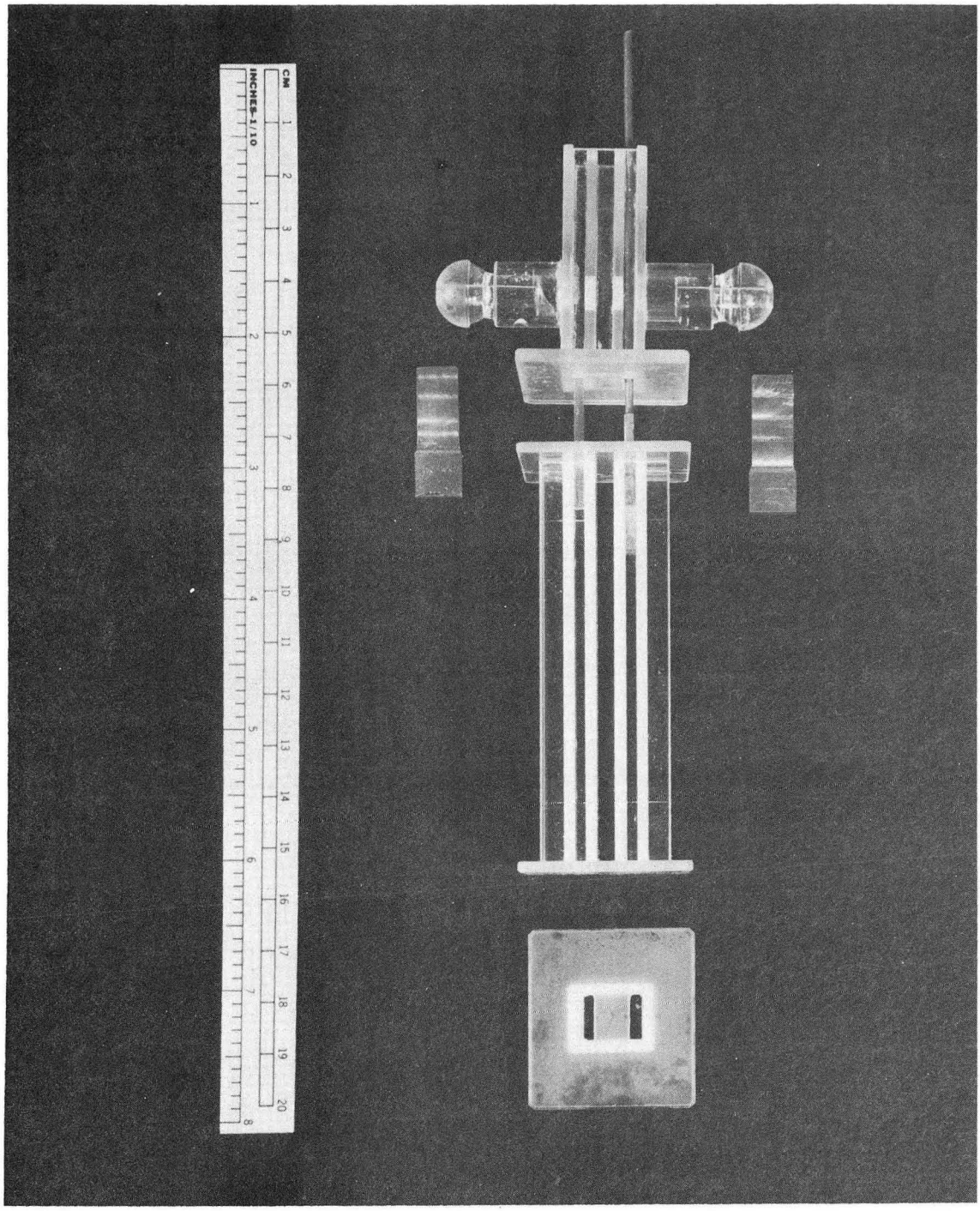

XBB 6811-6777

Fig. 7-4. Optical cell and electrodes.

cell. The cell is then dried in a dust-free dry box overnight at 40-50° C.

A chemically inert Apiezon Type N vacuum grease was used for all sealings.

C. Photography

For periodic checks of the interference fringe pattern, Polaroid Type 47 pictures were taken; this type of film has a speed of ASA equivalent 3000, and an average exposure time of 1 to 2 seconds.

To facilitate counting the fringes on the microphotometer, Kodak Contrast Process Panchromatic Film (ASA speed 100, average exposure time 20 to 30 seconds) was used to take all negative transparent pictures. These films were packed in film holders in total darkness. Each film was identified by a paper label with pencil writing. The exposed films were developed in a fR Cut-Film-Pack Developing Tank with Kodak D-11 developer for 5 minutes, acid stopper for 1/2 minute, and fixer for 5 to 10 minutes at room temperature.

D. Counting the Number of Fringes

The number of fringes was counted by a Jarrell-Ash Recording Microphotometer. The principle of the operation of this photometer is shown in Fig. 7-5. The sample film (F) is placed on a travelling stage (P) with a longitudinal motion driven by a precision motor. A light beam (L) passes through a small portion of the film and is magnified 100 times on a bench underneath. Only a controllable part of the image can pass through the slit (S). Behind the slit is a very sensitive photoelectric cell (C), the signal from which is plotted on a chart

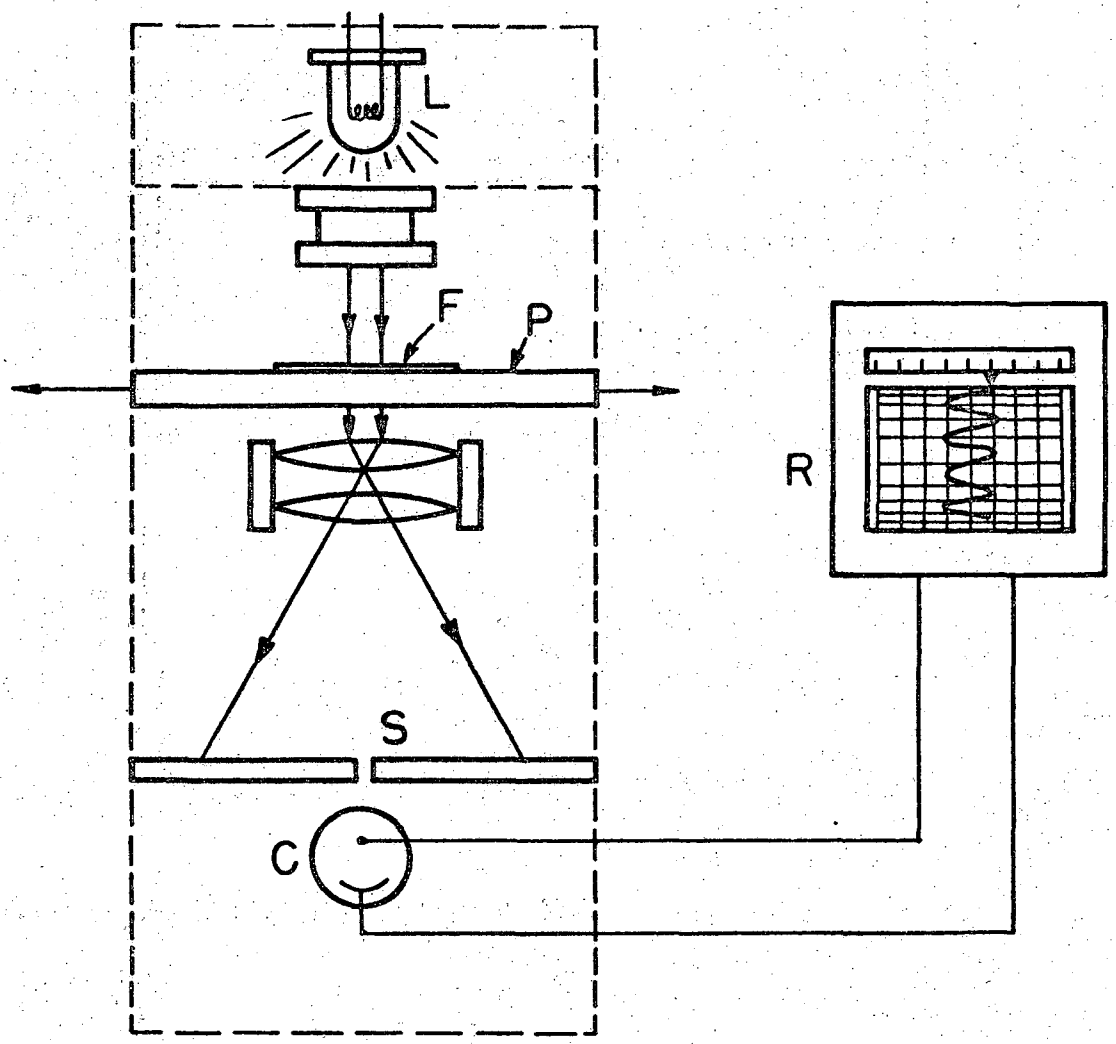

XBL6811-7244

Fig.7-5. A recording microphotometer.

recorder (R). Each dip on the plot corresponds to a dark line on the film.

7.2 Evaluation of Proportionality constants k_A and k_B

The direct application of Eq. (7-1) in the Perkin-Elmer Electrophoresis apparatus suffers the following difficulties;

i. In most literature the refractive index data were measured with sodium d-light of wavelength 5893 Å. The apparatus used in these experiments was equipped with a mercury lamp of wavelength 5461 Å.

ii. The accuracy of most RI data were 5×10^{-5} at best. To calculate the difference of RI means subtracting two roughly equal numbers, thus losing many significant figures.

For these reasons, Eq. (7-2) is adopted to replace Eq. (7-1) and modified to

$$\Delta n = k_A \Delta c_A + k_B \Delta c_B \qquad (7\text{-}3)$$

for multicomponent systems, under the same assumption that the number of fringe shifts is proportional to the concentration difference. Here Δc_A and Δc_B represent the concentration difference of $CuSO_4$ and H_2SO_4 respectively.

To evaluate the constants k_A and k_B, the optical cell is first filled with the heavier solution at the bottom. The lighter solution is carefully placed on top of the heavier solution by means of a syringe which is driven by a slow constant speed motor (see Fig.7-6). The sharpness of the boundary was not important in this case, the straight fringe

lines at both ends are important to assure that there was no mixing of the original homogenous solutions. When the fringes were too close to be distinguished, it was necessary to wait several hours for the boundary to become more diffuse. A typical interference pattern produced with a 1.175M H_2SO_4 solution and a 1.079M H_2SO_4 solution is shown in Fig. 7-3. The number of fringe shifts across the diffusion layer is counted by the previously mentioned microphotometer. The results are tabulated in Table 7-1.

In order to compare with the number of fringe shifts calculated from Eq. (7-1), the values of 5461 Å and 1.81 cm were used for the wavelength λ and the light path l respectively. The length l is chosen because the actual optical setup was such that the light passed twice through a cell of width 0.905 cm.

Some RI data of copper sulfate solutions and sulfuric acid solutions were measured with sodium d-light as follows

Table 7-2. Refractive Index of copper sulfate solutions and sulfuric acid solutions at 25°C.

$CuSO_4$ (M)	RI	H_2SO_4 (M)	RI
0.0385	1.3342	0.7935	1.3416
0.0500	1.3345	0.8850	1.3425
0.0577	1.3347	0.9865	1.3437
0.0963	1.3359	1.0810	1.3447
0.0998	1.3360	1.1800	1.3455

These RI data of copper sulfate together with the data taken from O'Brien[36] are correlated as a function of concentration

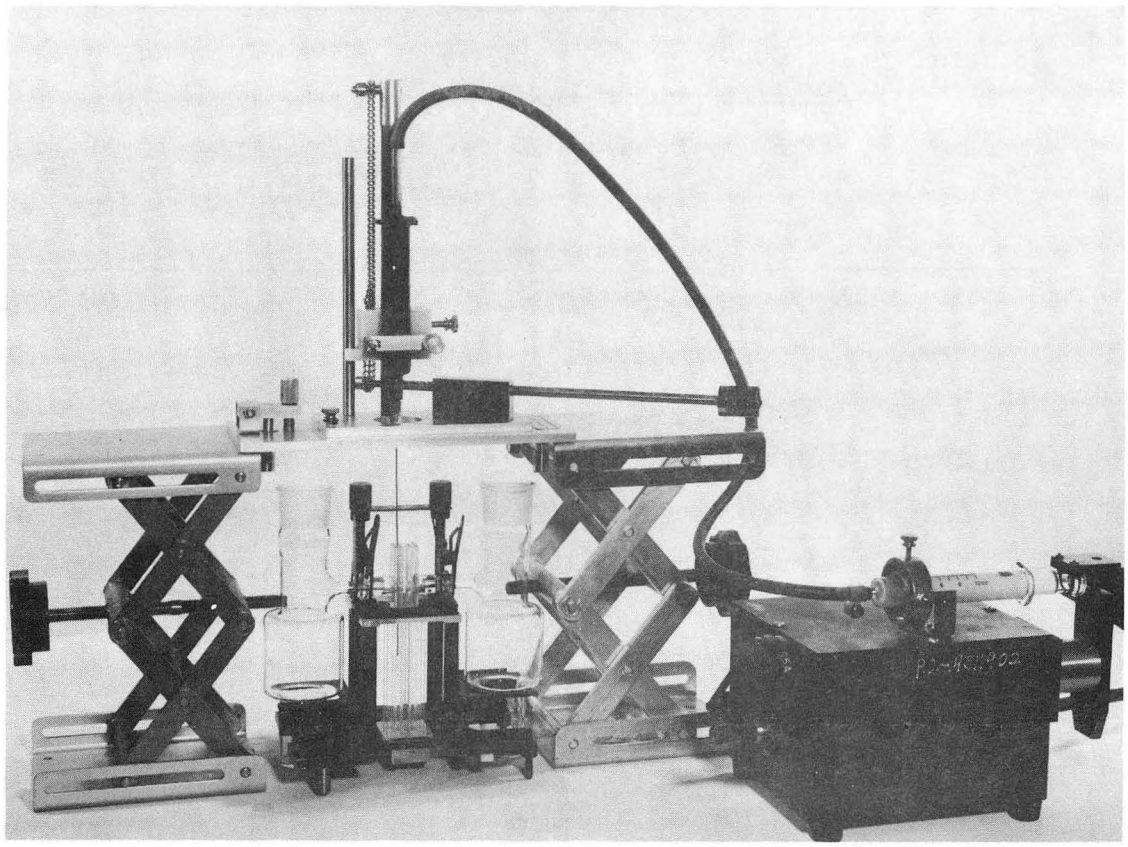

XBB 6811-6776

Fig. 7-6. A motor driven syringe putting a lighter solution on top of a heavier solution.

Table 7-1. Number of fringe shifts across a step change of concentrations.

Solution #	$CuSO_4$ Concentration Upper layer M/ℓ	Lower layer M/ℓ	Film #	Run #	Duffison Time hrs	Number of fringes	Average
114	0.0	0.0385	C-10	10R	0	38	
			D-1	10R	1	37½	
			D-4	10R	2	37½	
			D-2	10L	1	38	
			D-3	10L	2	38	38
112	0.0	0.0481	B-24	6L	0	46½	
			C-13	6L	2¼	47	
			C-16	7L	1½	45	46
113	0.0	0.0571	C-8	9R	2½	54½	
			D-5	11L	0	55	
			D-7	11L	1	56	55
111	0.0	0.0963	C-21	8R	5	86	
			C-23	8R	7	86	86
119/117	1.081	1.180	E-3	16R	0	35	
			E-5	17L	1½	33	34
116/119	0.986	1.081	D-19	13R	2	34½	
			D-22	15L	0	30	
			D-23	13R	5	31	32
118/116	0.885	0.986	E-6	18L	0	32	32
115/116	0.794	0.986	E-7	21R	0	67½	
			E-8	21L	0	65	
			E-10	20L	2	67	
			E-11	20L	0	67	
			E-16	22R	2	66	
			E-17	22R	4½	66	67
115/117	0.794	1.180	D-13	12R	4	127½	
			D-14	12L	4	126	
			D-17	12R	5½	124½	126

$$RI = 1.33256 + 0.041155\ c_A - 0.069305\ c_A^2 \qquad (7\text{-}4)$$

for the copper sulfate concentrations below o.1M. The actual experimental points and the smoothed correlation curve is shown in Fig. 7-7. The RI data of sulfuric acid are correlated as a straight line

$$RI = 1.33343 + 0.01032\ c_B\ , \qquad (7\text{-}5)$$

for sulfuric acid concentrations between 0.8M and 1.2M.

In Table 7-3, the RI values were calculated from Eqs. (7-4) and (7-5), not from Table 7-2. The results show that the actually observed number of fringe shifts of sulfuric acid is quite consistent with the calculated values. This means that the difference of RI is relatively independent of the wavelength of the light source. On the other hand, the blue copper sulfate solutions show considerably less fringe shifts than the calculated values. This means that the difference of RI is smaller in copper sulfate solution for the shorter wavelength of the blue mercury lamp.

The values of k, based on the actually observed number of fringe shifts, were calculated and averaged in Table 7-3. For a binary copper sulfate solution concentration $c_A < 0.05M$,

$$\Delta m = k_A \Delta c_A$$

$$k_A = (0.965 \pm 0.019) \times 10^3 \ \text{fringes/M} \qquad (7\text{-}6)$$

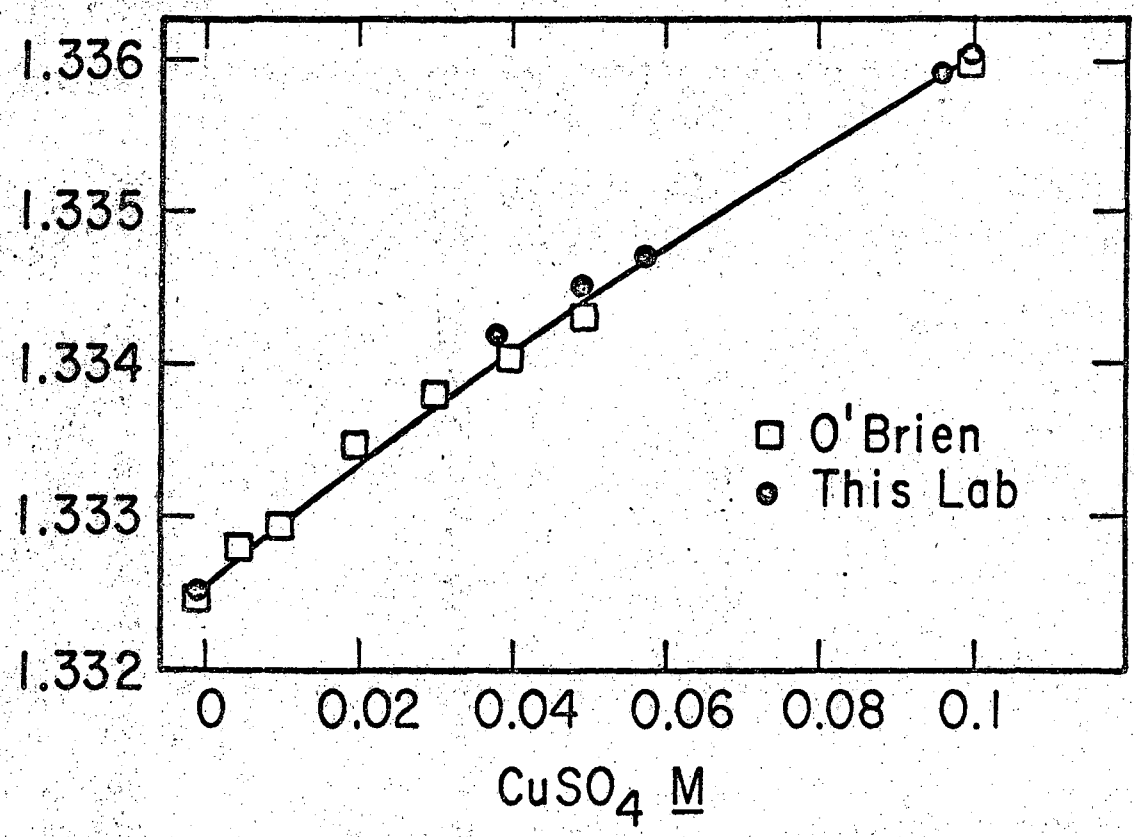

XBL 6812-6316

Fig. 7-7. Refractive index of $CuSO_4$ at 25°C (5893 Å).

Table 7-3. Comparison of observed number of fringe shifts with calculation from Eq. (7-1).

Solution	Concentration		Refractive Index(5893Å)		Number of Fringes		Constant k	
	Upper layer	Lower layer	Upper layer	Lower layer	Calculated	Observed	$10^3 \frac{\text{fringes}}{\underline{M}}$	
$CuSO_4$	0.0	0.0385$\underline{M}$	1.3325^0	1.3340^4	51	38	0.987	
		0.0481		1.3343^8	62	46	0.956	ave. 0.965
		0.0577		1.3347^0	73	55	0.953	
		0.0963		1.3358^8	112	86	0.893	
H_2SO_4	1.081M	1.180$\underline{M}$	1.3446^0	1.3456^2	34	34	0.344	
	0.986	1.081	1.3436^2	1.3446^0	32.4	32	0.339	
	0.885	0.986	1.3425^2	1.3436^2	36.4	32	0.315	avg. 0.334
	0.794	0.986	1.3415^8	1.3436^2	67.5	67	0.348	
	0.794	1.180	1.3415^8	1.3456^2	134	126	0.326	
$CuSO_4/H_2SO_4$	0.0/1.0$\underline{M}$	0.1/1.0$\underline{M}$	1.3437^5	1.3462^1	81.5	79	0.790	

For the copper sulfate solution $c_A < 0.1\underline{M}$, with sulfuric acid $0.8\underline{M} < c_B < 1.2\underline{M}$,

$$m = k_A \Delta c_A + k_B \Delta c_B$$
$$k_A = 0.790 \times 10^3 \quad \text{fringes}/\underline{M} \qquad (7\text{-}7)$$
$$k_B = (0.334 \pm 0.019) \times 10^3 \text{ fringes}/\underline{M}$$

One should notice that k_A and k_B are function of the concentration of copper sulfate and sulfuric acid. They are constant only within small ranges of concentrations. This is why the k_A value in Eq. (7-6) differs from the one in Eq. (7-7).

7.3 Surface Concentration in a Binary Electrolyte

In chapter 5, the term "surface concentration" was repeatedly mentioned in the theoretical analysis; it referred to the concentration of electrolyte right at the interface between the solution and the electrode. In the actual experiments, it is the average concentration at the nearest distance that can be measured. Qualitatively speaking, in an interference measurement the closeness to the interface is limited by the following factors;

i. the wavelength of light source for the interference measurement. It is impossible to measure any distance smaller than the wavelength. For the mercury lamp source in the electrophoresis apparatus, this means 6×10^{-5} cm.

ii. the grain size of negative photo film and the exposure time. These two factors work against each other, the

smaller the grain size, the higher the resolution ability of the film, but the longer the exposure time it needs. The length of exposure time must take consideration of the changing of the diffusion layer with time.

iii. the resolution ability of the microphotometer. For example, the Jarrell-Ash Microphotometer has a smallest resolution area of $10^{-2} \times 10^{-4} cm^2$.

From these three factors, the nearest distance to the electrode which can be measured is estimated to be about 5×10^{-3}cm.* This distance when compared with the time dependent diffusion layer thickness shows that the uncertainty is great at short times. However, the error is relative small at large time when the thickness becomes 1-2 cm.

In an experiment of copper sulfate of concentration 0.0385M, a constant voltage of 0.60 volt was applied across two electrodes in an optical cell. The interference patterns were taken from time to time, a typical fringe pattern is shown in Fig. 7-8. The upper shaded part is the image of the electrode. The number of fringe shifts was counted across the diffusion layer on a microphotometer (see Fig. 7-5). A typical plot from the photometer of the relative light intensity across the diffusion layer is shown in Fig. 7-9. Each peak corresponds to a dark line on a negative film or a bright line on a positive picture.

---

*Fringes spaced at a distance of 5×10^{-3}cm are almost impossible to be distinguished by naked eye. They can only be seen on a negative film under a 100 magnification of the microphotometer.

According to Eq. (7-6), when the surface concentration drops to zero, the total number of fringe shifts across the diffusion layer should be 37.1. Assuming a linear relation between the number of fringe shifts and the concentration, it is possible to calculate $(1-c_o/c_\infty)$ as a function of time from the observed number of fringe shifts. The calculations are tabulated in Table 7-4, and the results are plotted in Fig. 7-10. The experiment with the same solution was repeated also at a constant voltage of 0.80 volt.

To compare the result with theory presented in chapter 5, the following data were used.

	Run 23	Run 24	Source of data
1. conc. of CuSO in bulk	0.0385M		
2. conductivity, κ	4.13×10^{-3} mho/cm		39
3. diffusivity, D	6.07×10^{-6} cm^2/sec		43
4. transference number, t_+	0.383		38
5. Z (see Eq. (5-7))	1		
6. length of cell, L	15 cm		
7. area of electrode	0.178 cm^2		
8. voltage to the cell	0.60 ;	0.80 V	
9. V (see Eq.(5-8))	23.4 ;	31.1	
10. current at short times	0.154	0.244 mA/cm^2	
11. t_c (see Eq. (5-14))	5.60×10^6 sec		
12. exchange current density i_o	0.1 to 1.0 mA/cm^2		
13. J (see Eq. (5-11))	0.07082 to 0.007082		
14. electrochem. kinetic parameters α, β, γ	0.5		

There are no exchange current density data available in the literature for an unsupported $CuSO_4$ solution. The reasonable estimate is that i_o lies between 0.1 and 1.0 mA/cm^2. Theoretical predictions and experimental results are compared in Fig. 7-10. The solid lines are the theoretical calculations at an exchange current density of 0.1 mA/cm^2, whereas the dashed lines are calculated at i_o = 1.0 mA/cm^2. It shows that the solid lines have a satisfactory fit to the experimental result.

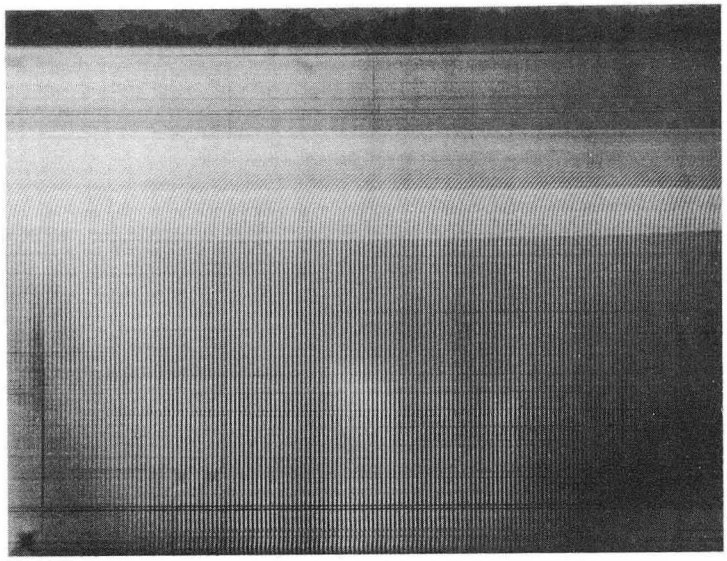

XBB 6812-7570

Fig. 7-8. Fringe pattern of the diffusion layer in a stagnant diffusion cell. The upper shaded part is the image of the electrode (picture taken in run 23, t = 389 minutes).

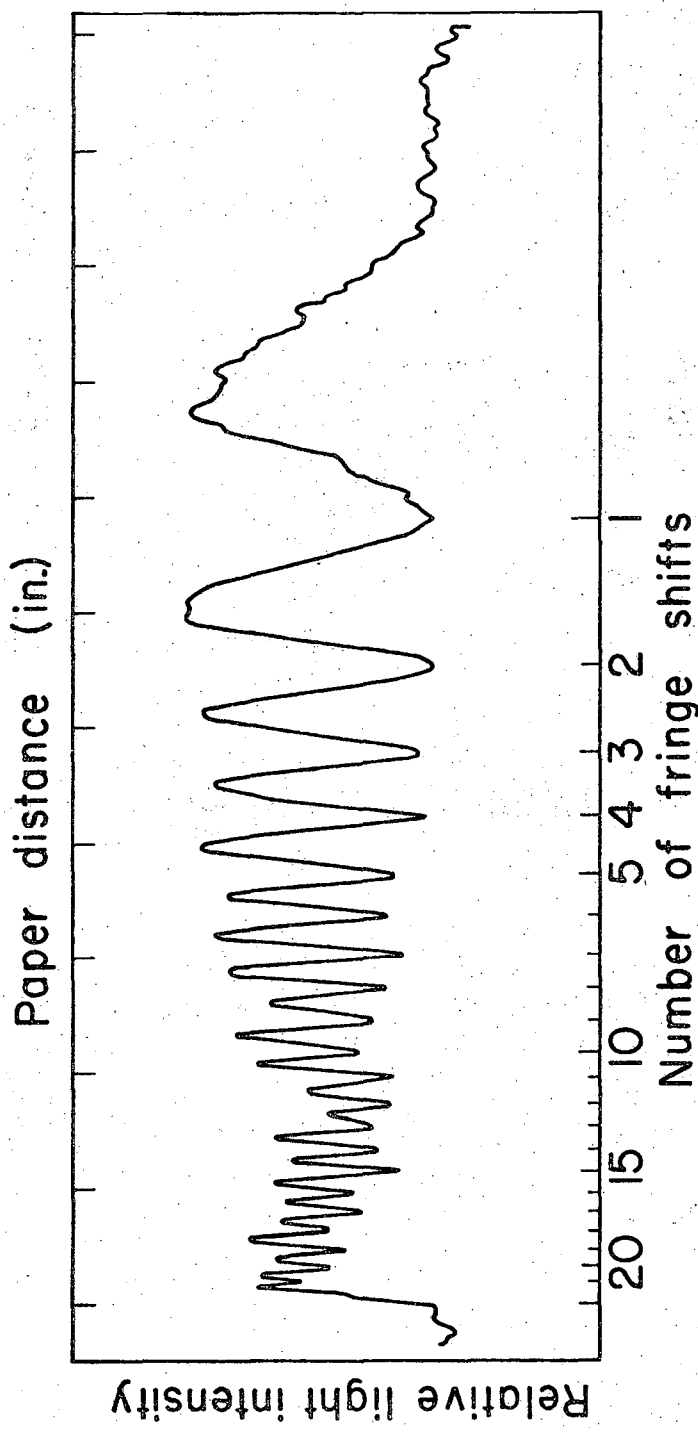

XBL6811-7243

Fig. 7-9. A plot from the recorder of a Jarrelle Ash Microphotometer (Run 24, Film # F-11, Time 6210 sec. film speed 1.5 mm/min, paper speed 2.25 inch/min).

Table 7-4. The number of fringe shifts across a diffusion layer in a stagnant diffusion cell.

t (sec)	Run 23 number of fringe shift	$1 - \frac{c_o}{c_\infty}$	film #	t (sec)	Run 24 number of fringe shift	$1 - \frac{c_o}{c_\infty}$	film #
900	4	0.108	E-18	600	5-7	0.135-0.189	F-6
1200	6	0.162	E-19	1200	7-9	0.189-0.243	F-6
2400	9	0.242	E-20	2400	12-13	0.324-0.350	F-7
3600	11	0.296	E-21	4020	15-17	0.402-0.457	F-9
5610	15	0.405	E-22	5430	20-21	0.540-0.566	F-10
10710	$20\frac{1}{2}$	0.553	E-23	6210	22	0.592	F-11
23400	30	0.807	E-24	9060	$27\frac{1}{2}$	0.743	F-12
23730	32	0.861	F-1	15790	34	0.915	F-13
∞	37.1	1.0		20850	37	0.997	F-14
				23900	37	0.997	F-15
				∞	37.1	10	

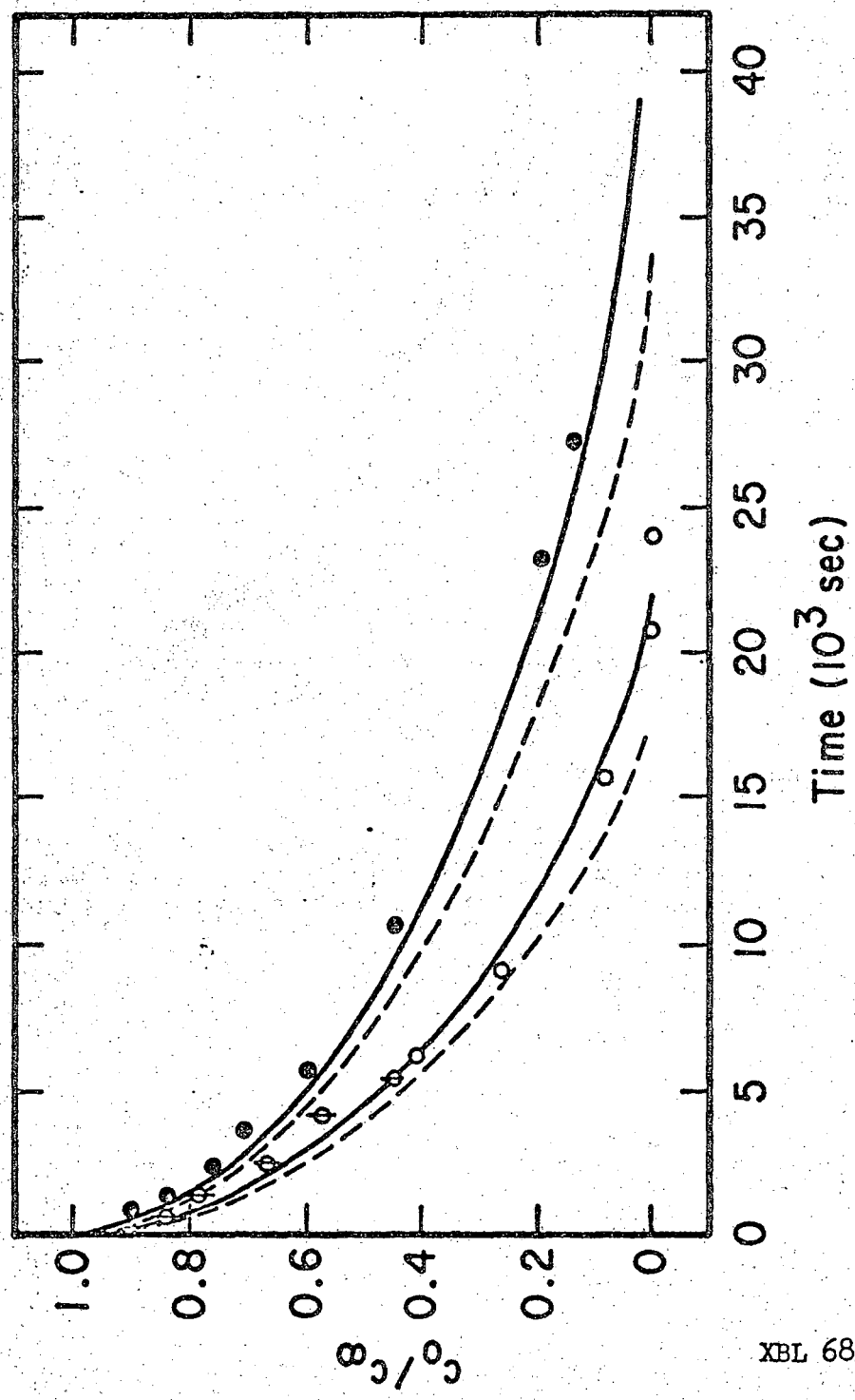

XBL 6812-6317

Fig. 7-10. Transient behavior of surface concentration of copper sulfate (0.0385M) in a stagnant diffusion cell (● Run 23; o Run 24; dashed lines, i_o=1.0 mA/cm^2 solid lines, i_o=0.1 mA/cm^2).

7.4 Concentration on Profile in a Binary Electrolyte

Under the same assumption that the number of fringe shifts is proportional to the concentration change, it is possible to deduce a concentration profile from a plot of Fig. 7-9, since the flat stage of microphotometer, on which the film is placed, is driven by a constant speed motor. If both the film speed and recorder speed are known, it is possible to correlate the length of paper to the distance on the film.

In the original design of the Electrophoresis apparatus, the vertical distance between two points on a film should exactly equal the distance on the optical cell. To avoid any geometrical distortions in the optical system or shrinkage of film, two very fine markings were scribed on the face of the cell. These scratches appeared as fine lines across the photographs of the fringes patterns and thus served as a reliable frame of reference for calculating the ratio of actual distance to the film distance.

The normalized concentration profiles of a copper sulfate solution of concentration 0.0385M at a total applied voltage of 0.80 V are plotted in Fig. 7-11 with time as a parameter. The abscissa is the distance from the electrode, stretched by dividing by $\sqrt{t}$. When these profiles are compared with the theoretically calculated concentration profile from chapter 2, the results indicate that the concentration profile would not reach a steady condition until after a very long time. In other words, the similarity transformation, defined in Eqs. (2-6a, b), was not a suitable approach to predict concentration profiles although we have considered the variation of transport properties and nonzero interfacial velocity. This is because of the strong transient effect

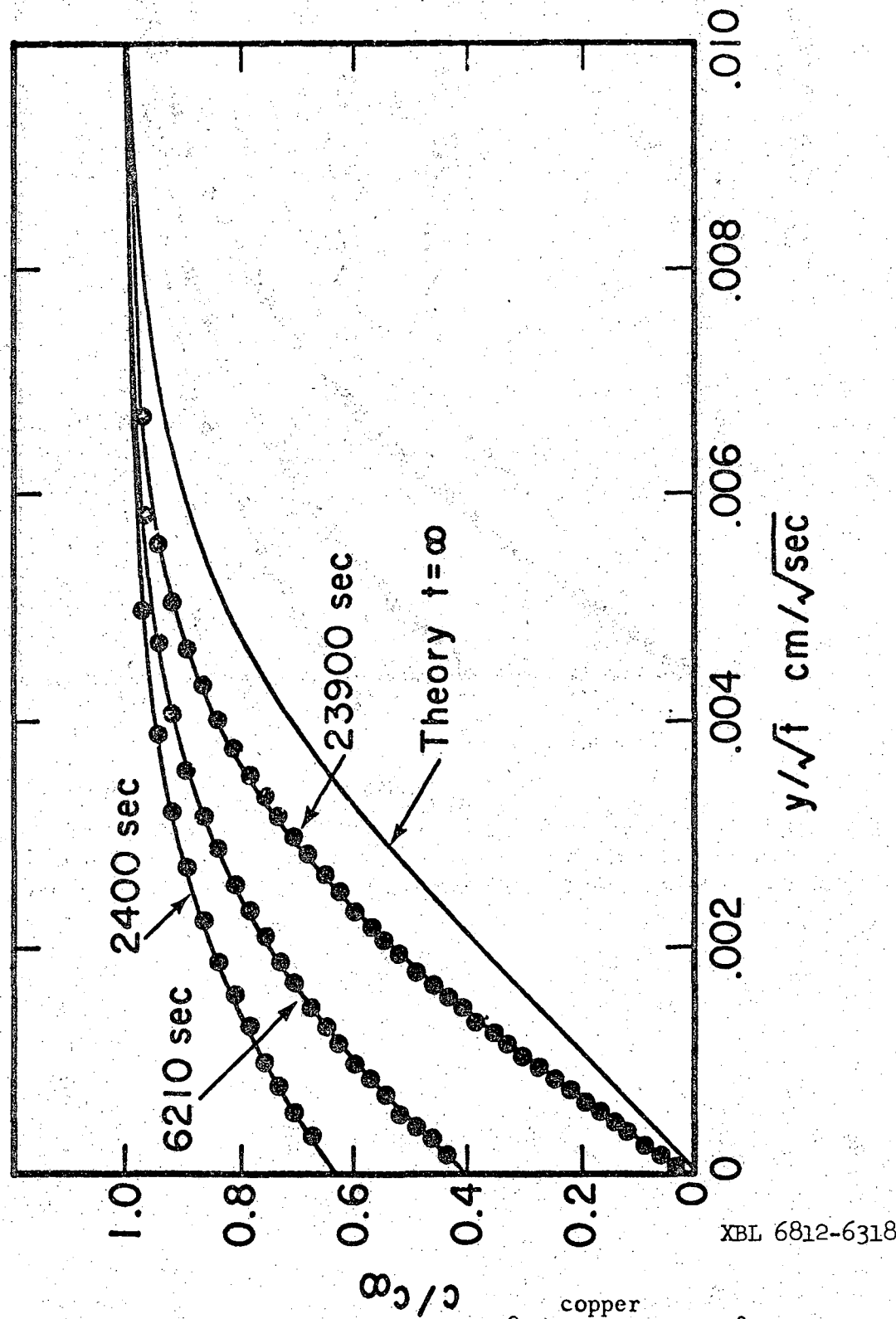

XBL 6812-6318

Fig. 7-11 Concentration profiles of 0.0385M copper/sulfate at 25°C with total applied voltage of 0.80 V (Run 24; curves from top to bottom correspond to film #F-7, F-11, F-15 and theoretical calculation from CONCEN program).

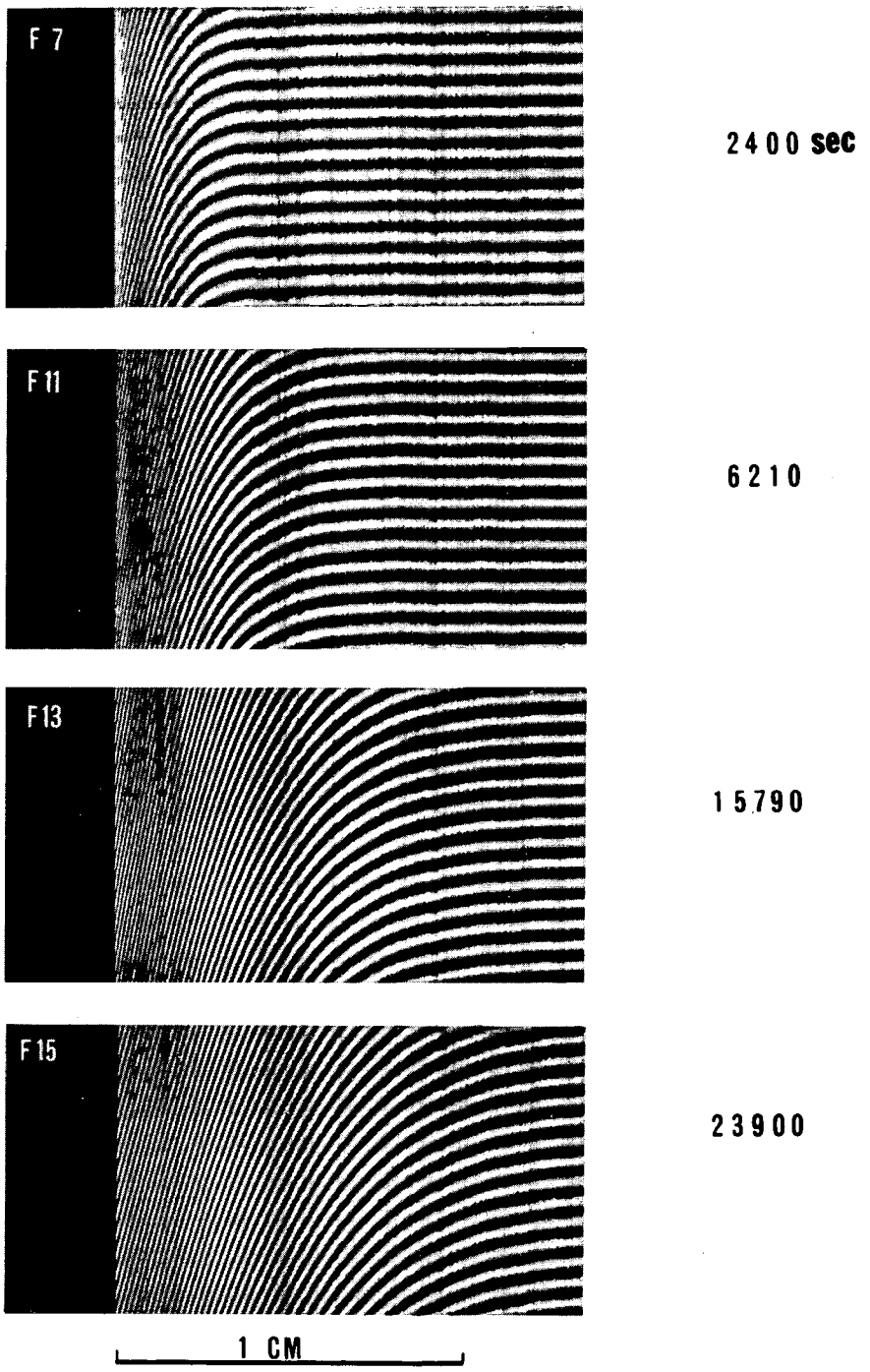

XBB 6811-7170

Fig. 7-12. Fringe patterns in a stagnant diffusion cell of a copper sulfate solution at 25°C (Run 24).

in a binary electrolyte of low conductivity which makes it difficult to achieve a constant concentration at the electrode.

For this mentioned solution, some interference fringe patterns, taken at various times, are shown in Fig. 7-12.

7.5 Surface Concentration in a Multicomponent Solution

In a well supported copper sulfate solution, the conductivity of the solution is high, the surface concentration of copper ions drops to zero much faster than in a binary electrolyte, and the transient behavior of the copper ion concentration is no longer of interest.

For many of the discharge reactions, the concentration of supporting electrolyte is higher at the electrode surface than in the bulk solution. The difference is of considerable interest in free convection problems since the convective velocity is due to the density difference in the solution produced by the electrode reaction, and these density differences are affected by the concentration of supporting electrolyte to roughly the same extent as by the concentration of the reactant.

There are two methods to determine the surface concentration of sulfuric acid interferometrically.

Direct Method: The refractive index of the bulk solution is first measured with the same light source as used in the interferometer. From the total number of fringe shifts at limiting current, it is possible to calculate the change of RI across the diffusion layer by Eq. (7-1). The concentration of sulfuric acid is then directly determined from the known correlation of its concentration and RI.

Indirect Method: The method is based on Eq. (7-7). No accurate RI data are needed except that the constants k_A and k_B have to be determined experimentally from solutions of known concentrations. The k_A and k_B are constant only within a small concentration range.

Two runs (#28, 29) were carried out in two different concentrations of copper sulfate at 1.0M of sulfuric acid. The total applied voltage across the optical cell was 0.15 V for both runs. The total number of fringe shifts across a diffusion layer was counted at different times. The numbers reached a constant after a certain amount of time (see Fig. 7-13). Presumably, the concentration of copper ions drops to zero at that time. The concentration of sulfuric acid at the electrode surface is then calculated from Eq. (7-7). The results are tabulated in Table 7-5 and compared with theoretical predictions of chapter 4.

The ratio $\Delta c_B/c_A^\infty$ of experimental results did not fall within the theoretical observed range of complete and no dissociation of bisulfate ions. The causes of this discrepancy may be attributed to the following reasons. Theoretically, because of the lack of concentration dependence data of ionic mobilities and ionic diffusivities, the concentration changes were calculated from the data at infinite dilution. The Nernst-Einstein relation was also assumed. Experimentally, the standard deviation of k_A and k_B are relatively high in Eq. (7-7). If the uncertainty is taken into account, the uncertainty in the experimentally measured concentration changes will allow some overlap with the theoretical results. Another possible cause of this deviation is that the total applied V voltage was not high enough. When the experiments were performed, the author was anxious to see some transient effect,

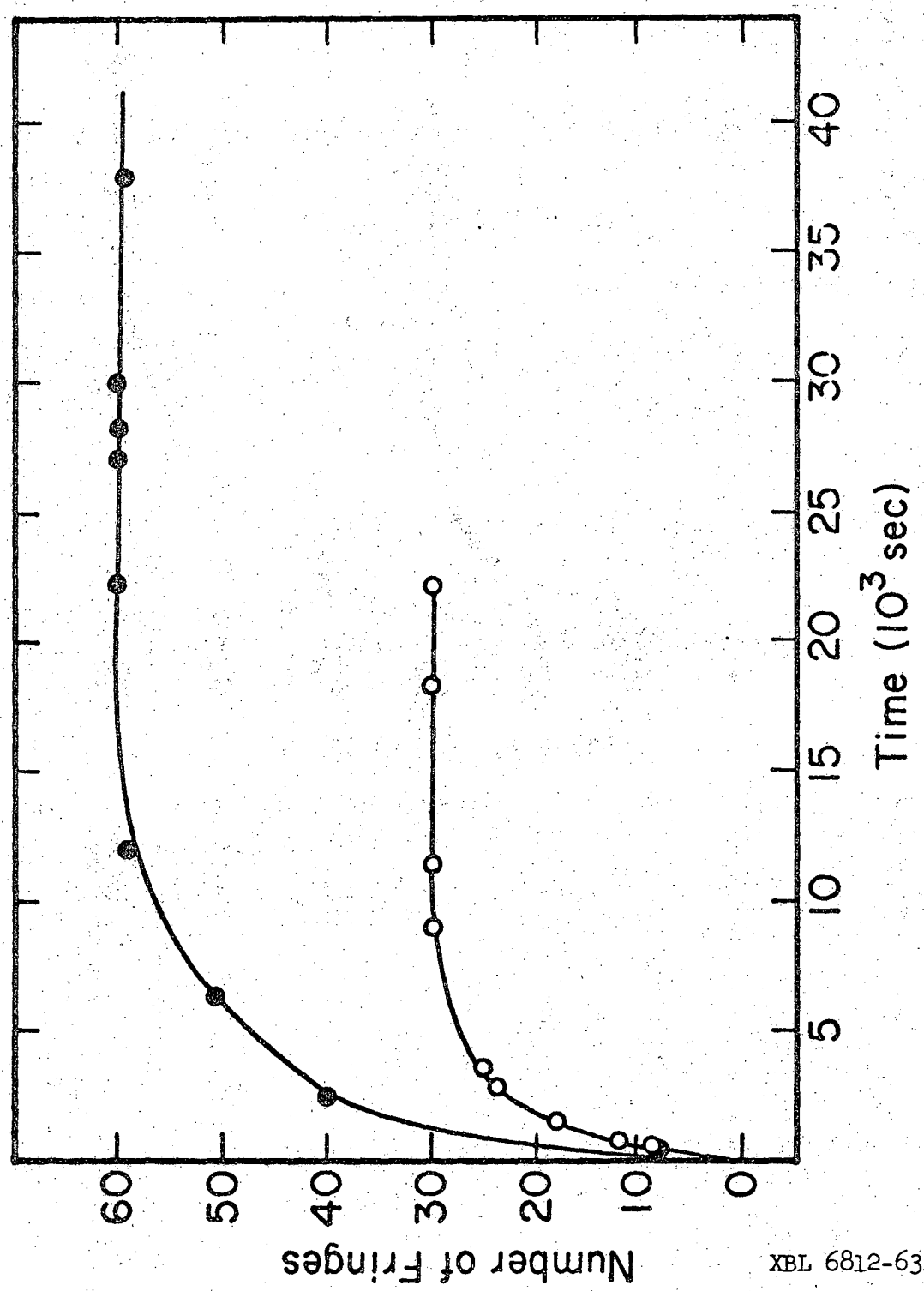

XBL 6812-6319

Fig. 7-13. Total number of fringe shifts across a diffusion layer.

Table 7-5. Surface concentration change of copper sulfate and sulfuric acid in a stagnant diffusion cell at 25°C.

	Run 28	Run 29
$[CuSO_4]$	0.1M	0.05M
$[H_2SO_4]$	1.0M	1.0M
total applied voltage	0.15V	0.15V
observed fringe shifts at steady value	60	30
$c_B^o - c_B^\infty$ calc. from Eq. (7-7)	0.0569M±0.0081	0.0284M
r Eq. (4-4)	0.909	0.952
$\frac{c_B^o - c_B^\infty}{c_A^\infty}$ observed	0.569	0.569
Theoretical predictions		
complete dissociation	0.48	0.49
no dissociation	0.22	0.24
incomplete dissociation		

the total applied voltage was only 0.15 V, compared with 0.6 to 0.8 V for copper sulfate solution and 0.35 V for most electrical measurements in chapter 6. Because of the voltage, the surface concentration of copper ions may not have dropped to zero but reached a constant value.

7.6 Concentration Profile in a Multicomponent Solution

The fringe patterns measured in a solution of 0.1M copper sulfate and 1.0M sulfuric acid are shown in Fig. 7-14. The molecular concentrations cannot be determined separately in a multicomponent solution by an interference method. It is possible to calculate the concentration profiles of ionic species from the computer program MIGR1 or MIGR2 and convert them to fringe profiles from the known concentration dependence of RI. However, the lack of RI data that are measured with a mercury light source detract from the value of comparing the observed profiles quantitatively.

Qualitatively, we may notice that there is a clear hump in the first two fringe patterns of Fig. 7-14 in contrast to the patterns in Fig. 7-12. This is because hydrogen ions move much faster than copper ions; hence the diffusion layer of sulfuric acid is thicker than that of copper sulfate. As a result, there is a maximum of refractive index in the direction of diffusion. Although there is no clear hump at the transition region in the next two fringe patterns, yet one may notice that the slope of fringe in that region is much steeper than those in Fig. 7-12.

In Fig. 7-15, two normalized fringe profiles are plotted as function of $y/\sqrt{t}$ at t = 11400 sec and t = 22080 sec. The two profiles

almost overlap each other, which means the fringe profiles have already reached steady condition.

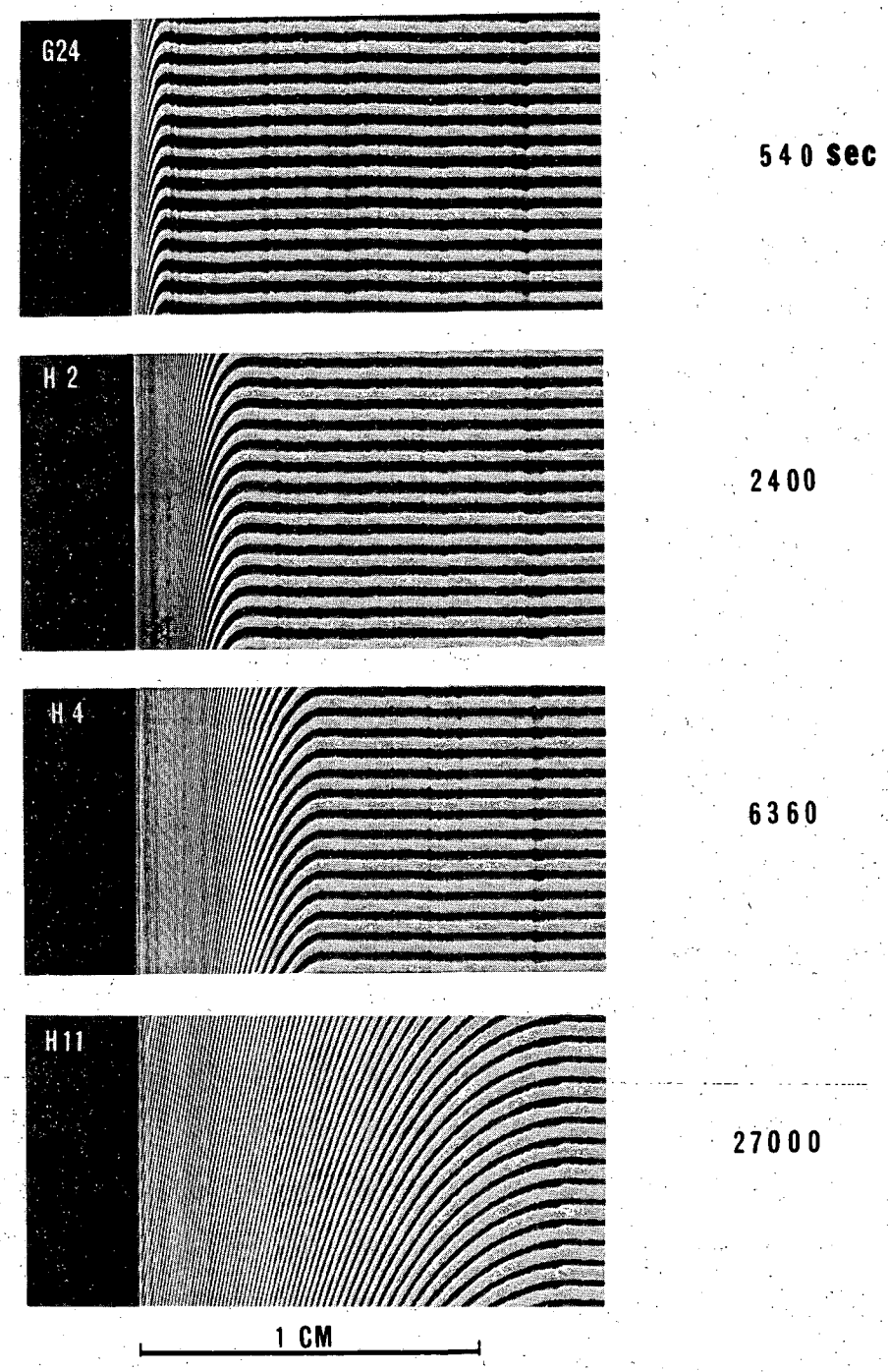

XBB 6811-7169

Fig. 7-14. Fringe patterns in a stagnant diffusion cell of a copper sulfate and sulfuric acid solution at 25°C (Run 28).

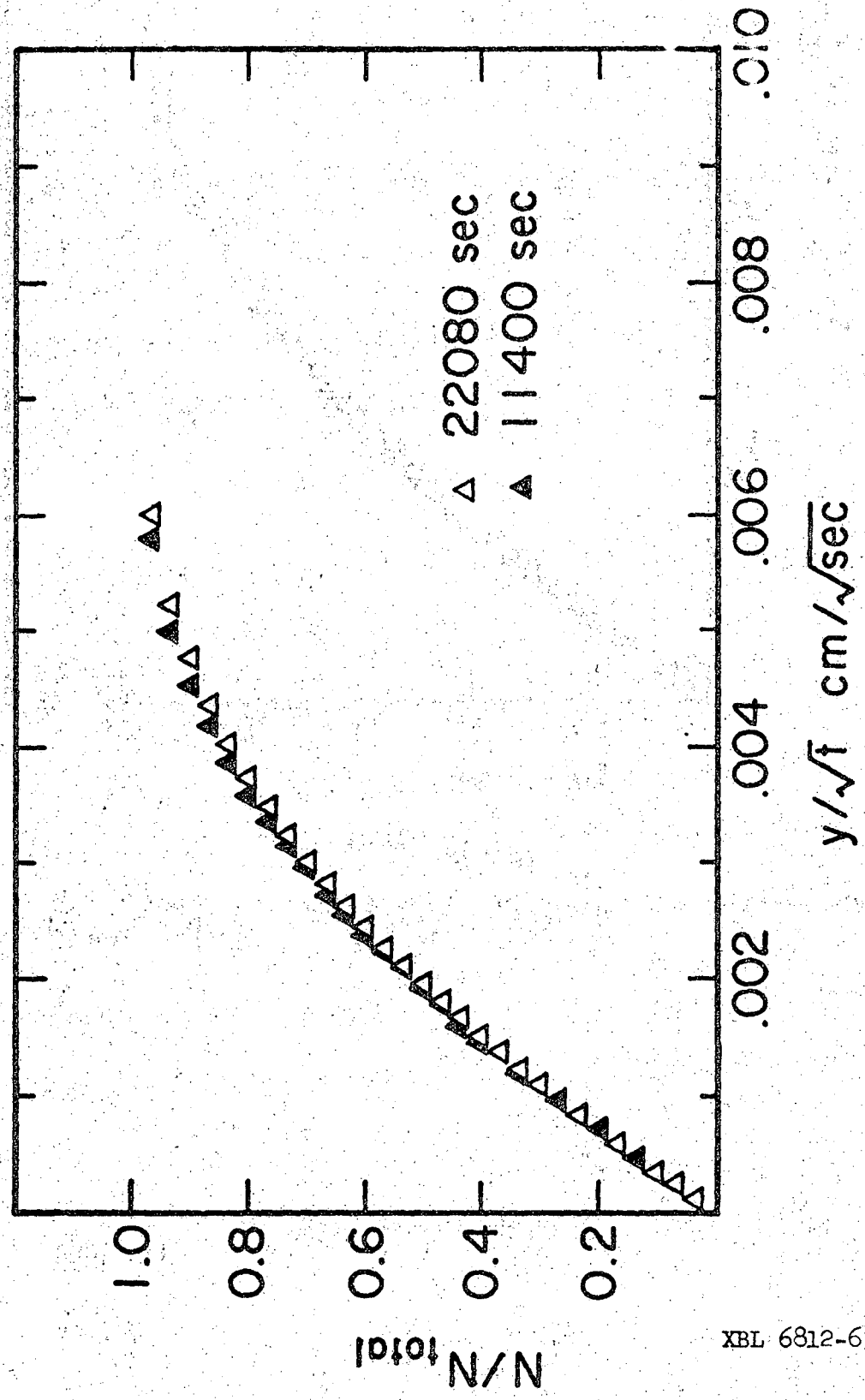

XBL 6812-6320

Fig. 7-15. Normalized fringe profiles in a supported copper sulfate solution. (run 29? 0.05M $CuSO_4$, 1M H_2SO_4.)

VIII. CONCLUSIONS AND RECOMMENDATIONS

The mass transfer rate and concentration profile in a stagnant diffusion cell have been calculated with consideration of the effect of variation of transport properties and nonzero interfacial velocity in a binary concentrated electrolyte. The work was essentially parallel to what has been done for a rotating disk.[3,5]

The inverse procedure of determining the differential diffusion coefficient as a function of concentration from the measured limiting currents has been worked out and tested. The method has the advantage of simplicity and efficiency in comparison with other methods, such as those utilizing an optical or diaphragm cell. The shortcoming that may limit the applicability of this method is the high ohmic potential drop associated with a binary electrolyte. A possible solution to this problem might be an elegant power source whose output voltage continuously or stepwise decreases with respect to the square root of time.

One of the original objectives of the concentration profile measurements was to see whether the variation of transport properties and nonzero interfacial velocity are the causes of the deviation observed in O'Brien's measurements.[6] Unfortunately, we could not make a definitive conclusion, because of the strong transient effect in a binary electrolyte of poor conductivity, which makes it difficult to achieve a constant concentration at the electrode surface.

For mass transfer in a multicomponent electrolyte at high Schmidt numbers, it is believed that an integral diffusion coefficient measured under one hydrodynamic condition would be directly applicable to others of the same classification. The integral diffusion coefficient

of copper ions in the copper sulfate and sulfuric acid system at 25°C has been measured for a wide range of concentrations in a stagnant diffusion cell (penetration-model classification) and a rotating disk electrode (boundary-layer classification).

Many previous workers have ignored the incomplete dissociation of bisulfate in solution of copper sulfate and sulfuric acid. Theoretical analysis indicated that incomplete dissociation has a drastic effect on the migration and the surface concentration of supporting electrolyte. The existence of bisulfate ions would increase the effect of migration and decrease the concentration difference of supporting electrolyte between the bulk solution and the electrode surface.

The limiting current measurements in a stagnant diffusion cell indicate that the actual effect of migration is higher than the theoretical predictions from the case of complete dissociation. The experimental results favor the theory of the existence of the bisulfate ion.

The experimental data on change of surface concentration of supporting electrolyte, sulfuric acid in this work, deviate significantly from the theoretical prediction. However the accuracy of the experiment is in doubt, and no definitive conclusion could be drawn from it.

For years, several of our co-workers in this laboratory have battled the quality of the polarization curves measured in a solution of <u>little</u> or <u>no</u> supporting electrolyte. Factors that affect the polarization curves in such a solution are

1. poor conductivity of the solution, the high ohmic resistance overshadowing the overpotential,

2. the nonuniformity of current distribution,

3. the transient effect.

In this work, the transient behavior has been worked out for a stagnant diffusion cell. The experimental work is essentially another version of testing our knowledge on the analysis of polarization and current distribution. The resulting current-time curves and the transient behavior of surface concentration of a binary electrolyte are found to agree with the theoretical predictions within the accuracy of available electrochemical kinetic parameters and experimental error.

For future work, the study of transient behavior should be extended to the case of a rotating disk, i.e.,

$$\frac{\partial c}{\partial t} + v_y \frac{\partial c}{\partial y} = D\frac{\partial^2 c}{\partial y^2}$$

or, to account for the variations in x direction (see Fig. 8-1) for a finite disk, i.e.,

$$\frac{\partial c}{\partial t} + v_x \frac{\partial c}{\partial x} + v_y \frac{\partial c}{\partial y} = D\frac{\partial^2 c}{\partial y^2}$$

with the boundary conditions similar to those discussed in chapter 5. This would provide a key to the paradox mentioned in the introduction, the change of limiting current density, or inflection point with respect to the rate of applied current.

Finally, for transport coefficient with a rotating disk electrode or a stagnant diffusion cell, several improvements are recommended for their design. (see Fig. 8-1).

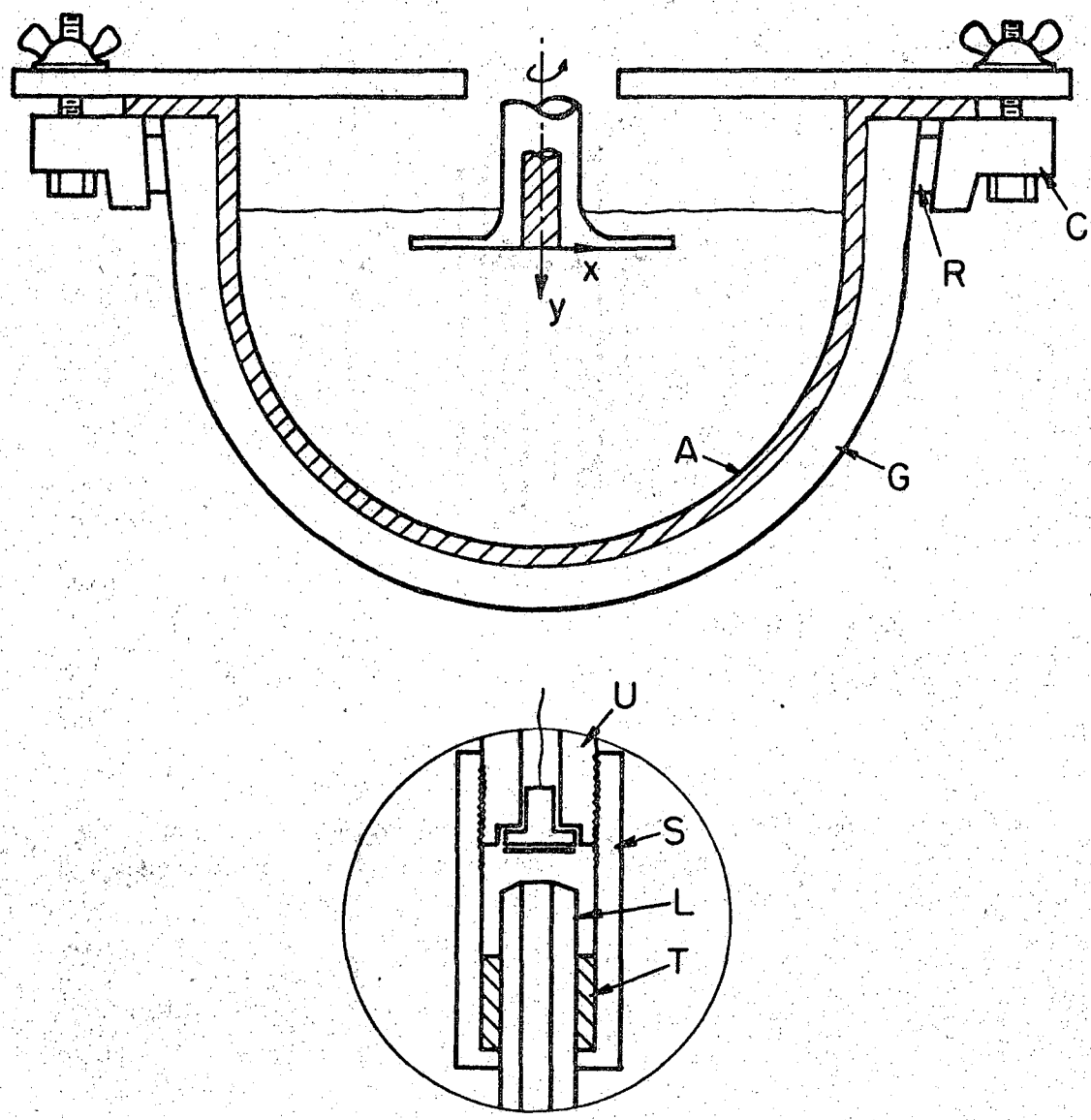

XBL6811-7245

Fig. 8-1. Modified design of a rotating disk (top) and a stagnant diffusion cell (bottom, see Fig. 6-1).

The cell (G) of the rotating disk should be made of glass of hemispherical shape, the counter electrode (A) be made of the proper electrode material by casting accordingly. For a finite disk imbedded in an infinite insulating plane, the equipotential contours approach hemispheres far from the disk.[40,33] This would not only reduce the wall effect on the current distribution, but also would minimize the problems of sealing, cleaning, and hydrodynamic distortion in a cylindrical cell. The cell would be held by a cast aluminum flange (C) with a rubber gasket(R).

The main part of the stagnant diffusion cell should still be made of true bore glass capillary (cf. Fig. 6-1). A large tube (T) is glued to the capillary (L). It is coupled to upper part (U) by a metal sleeve(S). The material of the sleeve and upper part could be any suitable metal. The advantages of this design are its ease of cleaning and the effective electrode area can be measured accurately.

ACKNOWLEDGMENTS

I would like to express my deep gratitude to Professor John Newman for his guidance and support throughout this project. The suggestions and critical review by Professors C. W. Tobias and D. R. Olander are greatly appreciated.

Thanks are also due to Mr. J. Robert Selman for generously sharing some of his apparatus, to Mr. Kong-Heong Tan for proof reading the manuscript, and to Mrs. Cross for typing this thesis.

I would like to express my appreciation to my wife, Yean Ming, for her encouragement and assistance in numerous small tasks during the preparation of this thesis.

This work was initially supported by the United States Atomic Energy Commission and, later, by the Petroleum Research Fund, administered by the American Chemical Society.

APPENDIX A

Physical Properties of $CuSO_4$ - H_2SO_4 Solutions at 25°C

Aqueous solutions of copper sulfate and sulfuric acid are commonly used in experimental studies of electrolytic mass transfer. The widespread use justifies a careful study of the relevant physical properties of this system.

A complete survey of literature from 1906 to 1966, done by Selman,[A27] revealed a total of 22 papers in addition to the data recently obtained in this laboratory by several of our co-workers.

In order to provide a correlation of the concentration dependence of these physical properties and to complement the existing data, additional measurements of density, viscosity, refractive index, and integral diffusion coefficients were conducted in this laboratory. All data which are used for the correlation will be tabulated by Selman.[A27] Additional data for binary electrolytes of $CuSO_4$ or H_2SO_4 in water may be found in the compilation of Chapman and Newman,[A28] and the physical properties of $CuSO_4$ in water are correlated as a function of concentration in the M.S. thesis of Hsueh.[A26]

1. Experimental methods used in this laboratory

   Density Densities were measured with 25 and 50ml Pyrex pycnometers which were calibrated with doubly distilled water.

   Viscosity Viscosities were measured with Ubbelohde viscometers, calibrated with distilled water.

   Refractive Index An Abbe refractometer with a sodium lamp (wave length 5893Å) was used for refractive index measurement.

   Integral Diffusion Coefficient See Refs. A25, A26.

Concentration Solutions were prepared from ACS reagent grade copper sulfate and sulfuric acid. Concentrations were determined by titration and electrogravimetric method. All weighing was done on an analytical balance of 0.1mg accuracy.

Temperature Control The measurements, except the integral diffusivity, were conducted in a constant temperature water bath controlled by a Sargent Model S "thermonitor" and measured with an N.B.S. Calibrated thermometer. The maximum temperature variation was less than ±0.02°C. The integral diffusivity measurements were carried out in a separate bath with temperature control of ±0.1°C.

2. Correlations

The reason for using a correlation equation is mainly a lack of experimental data at the concentrations of interest. In other cases a continuous set of data may be needed for a theoretical study in an electrolytic system. A deviation of the correlation equation from the original experimental values is almost inevitable for the majority of available data. However, the correlation equation does represent a smoothed curve as a result of least square fitting. An effort was made to include as many data as possible. Although many of the measurements may have been subject to systematic, experimental, or personal errors, the use of a large number of sets of data from various sources should guarantee that major systematic deviations do not persist in the correlation itself.

The correlation obtained by collecting all experimental data within the concentration range of interest at 25°C and subjecting them to

least square fitting. The deviation of every point was calculated and if any datum point deviated by more than 2.5 times the standard deviation or exceeded the specified maximum tolerable relative error, the datum was eliminated from the correlation. An improved fit was then obtained and again checked for excessive deviations. For the case of conductivity, the data are fit to minimize the relative error.

The physical properties of $CuSO_4$ - H_2SO_4 at 25°C have been correlated as functions of concentrations in the form

$$p = a_o + a_1[CuSO_4] + a_2[H_2SO_4] + a_{11}[CuSO_4]^2 + a_{22}[H_2SO_4]^2 + a_{12}[CuSO_4][H_2SO_4]$$

where p is the physical properties of the solution and the concentrations are in the unit of M. The constant a_o and the coefficients a_1 to a_{12} are tabulated in Table A-1.

It is generally true that the wider the concentration range which the correlation has to cover, the poorer the fit. Because of the large amount of density and viscosity data available, correlations for different concentration ranges were made:

i. the very dilute range,

ii. the saturation range, and

iii. in between these two extremes.

No attempt was made for a further division of concentration ranges at the risk of systematic error of individual workers and the discontinuity from one concentration range to the other.

The standard deviation, maximum absolute percentage deviation, the initial total number of data points that have been collected, the total number of data points involved in the final correlations and the source of data are also listed in Table A-1. The second correlations of density, viscosity and refractive index were taken from Ref. A24 for comparison.

There is a quite large difference of conductivity measurement between Richardson and Taylor[A14] and Kern and Chang[A23] at exact identical concentrations. Both data were included in the correlation. The correlated curves were compared with the experimental data shown in Fig. A-1.

For those who work in anodic dissolution the solubility of copper sulfate (in M) at 25°C is correlated as a function of concentration of sulfuric acid (in M) based on the saturated solution data given by Refs. A1 and A3. The experimental data and the correlation are plotted in Fig. A-2.

$$[CuSO_4] = 1.35158 + 1.28642\,[H_2SO_4]^{0.2} - 1.63073[H_2SO_4]^{\frac{1}{3}}$$

$$+ 2.10828 \times 10^{-3}[H_2SO_4]^2$$

where

$$0.01\underline{M} < [H_2SO_4] < 16\underline{M}$$

Table A-1. Coefficients of correlation of copper sulfate and sulfuric acid at 25°C.

$$p = a_o + a_1[CuSO_4] + a_2[H_2SO_4] + a_{11}[CuSO_4]^2 + a_{22}[H_2SO_4]^2 + a_{12}[CuSO_4][H_2SO_4]$$

	Density g/cm^3				Diffusivity (RDE) 10^{-5}cm^2/sec
$CuSO_4$	< 0.01	0.05-0.1M	0.01-saturated	saturated	0.01-0.65
H_2SO_4	< 0.01	0-2.5M	0.01-saturated	saturated	0.5-2.5
a_o	0.99705	0.99900	0.99837	1.1010[illegible]	0.597
a_1	0.16903	0.14219	0.15020	-	0.320
a_2	0.07565	0.061374	0.06240	0.0464[illegible]	-0.0656
a_{11}	-	-	0.002276	0.0578[illegible]	-0.306
a_{22}	-	-0.0003722	-0.000789	-0.0001[illegible]	-0.00585
a_{12}	-0.83954	-0.005536	-0.006921	-	-
std.dev.	1.00×10^{-5}	4×10^{-4}	1.60×10^{-3}	5.65×10^{-3}	3.45×10^{-2}
max.%dev.	0.0033%		0.35%		
data collected	66	30	141	22	25
data used	66	30	133	22	25
data source	A7	A24	A1-A3,A10,A24 A16-A19,A25	A1,A3	A25

Table A-1. (Continuted)

		Viscosity C.P.		Conductivity $\Omega^{-1}cm^{-1}$	Refractive Index
$CuSO_4$	< 0.01	0.05-0.1M	0.01-0.65	0-1.4M	0.05-0.1M
H_2SO_4	< 0.01	0-2.5M	0.01-2.5	0-2.0M	0-2.5M
a_o	0.89394	0.89864	0.90445	0.011163	1.33313
a_1	0.80030	0.45948	0.42999	0.030798	0.027952
a_2	0.27890	0.14068	0.13393	0.42355	0.010861
a_{11}	-14.0703	-	0.26385	-	-
a_{22}	-	0.027576	0.030696	-0.045224	-0.0002211
a_{12}	-30.4151	0.092374	0.10308	-0.135359	-0.003474
std. dev.	6.96×10^{-5}	1.9×10^{-3}	6.99×10^{-3}	9.22×10^{-3}	1×10^{-4}
max % dev.	0.02%		1%		
data collected	66	30	103	68	30
data used	66	29	97	68	28
data source	A7	A24	A16-A19 A10, A24, A25	A3,A14,A15, A23	A24

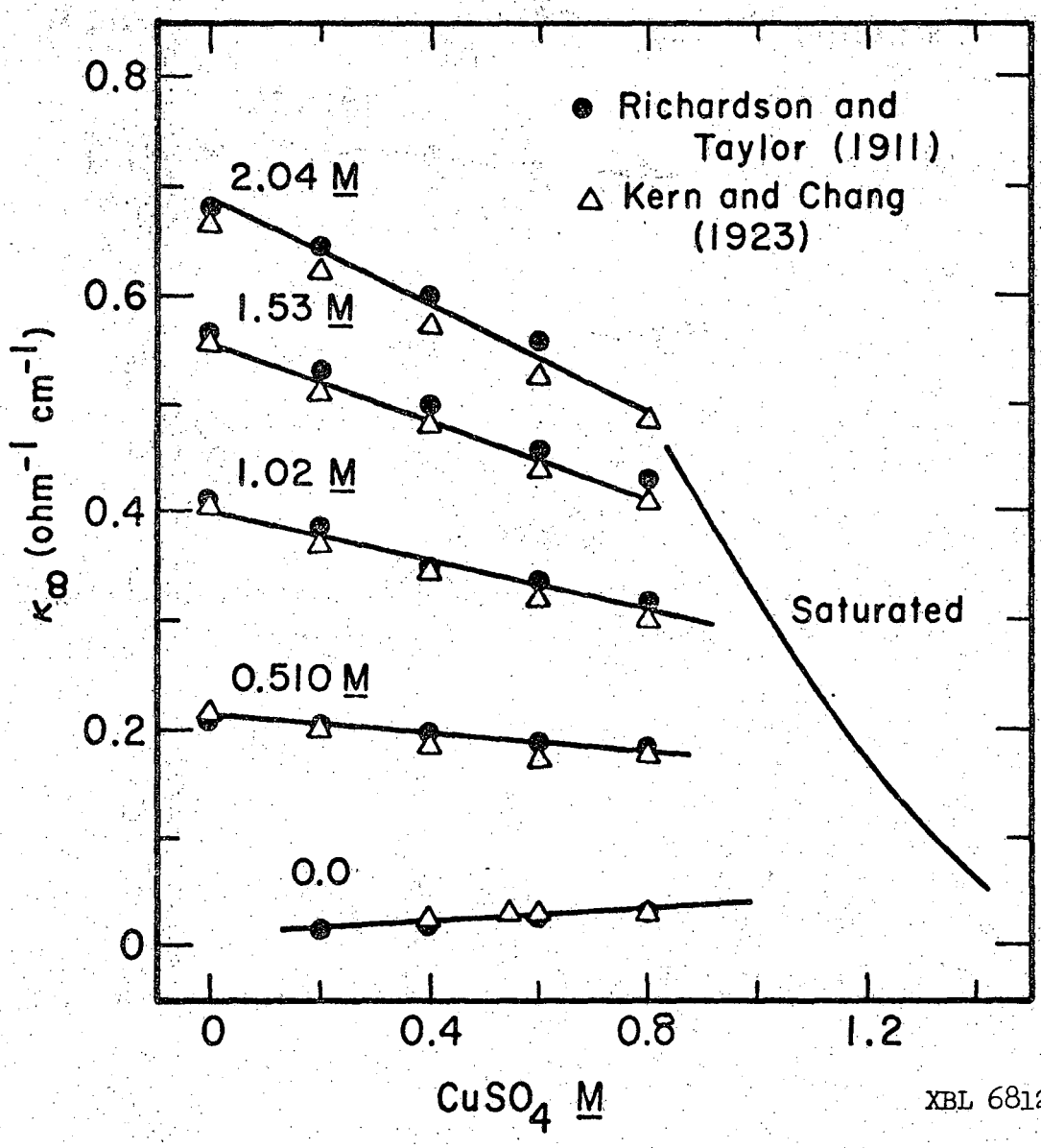

XBL 6812-6321

Fig. A-1. Conductivity of $CuSO_4$-H_2SO_4 at 25°C.

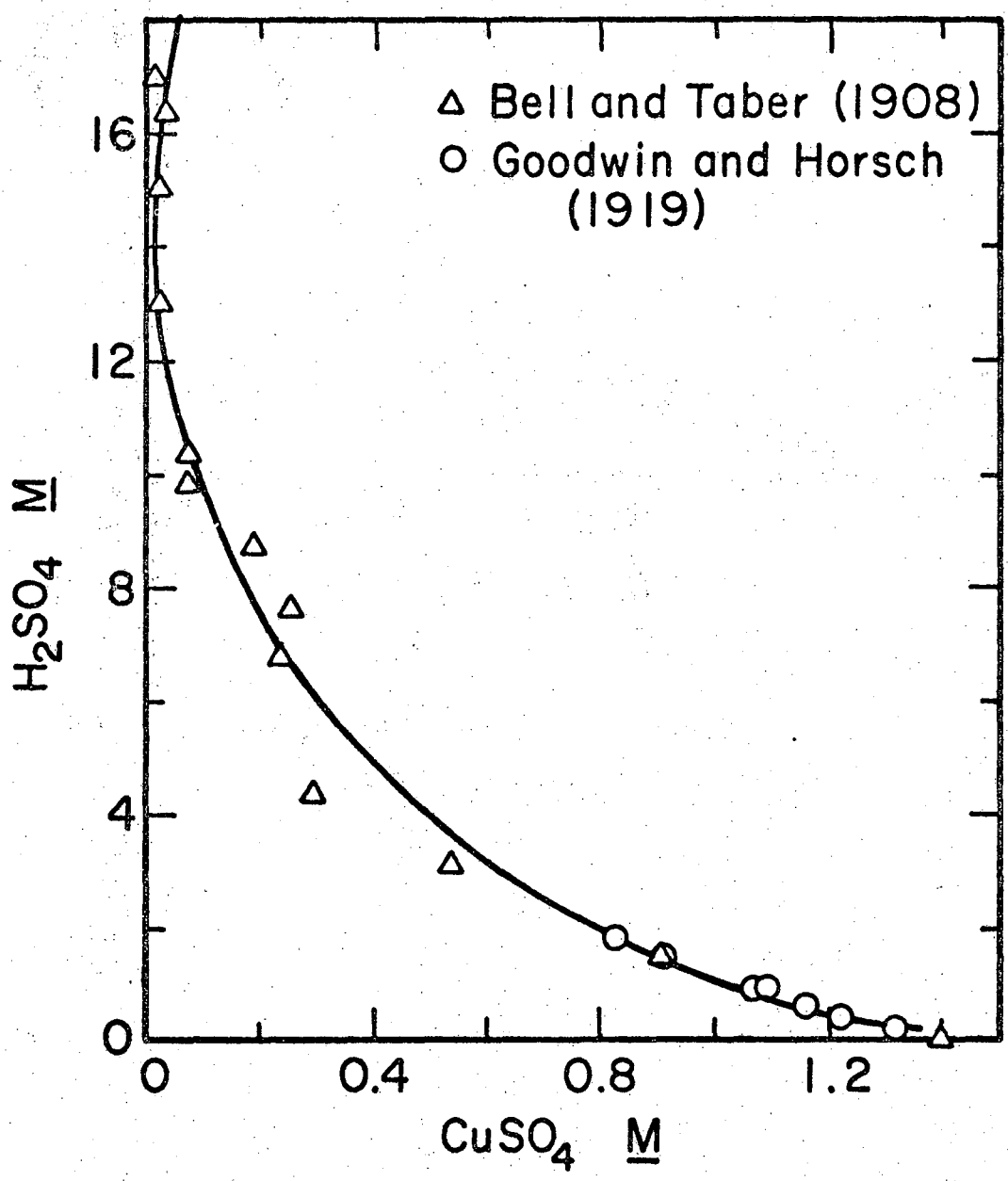

XBL 6812-6322

Fig. A-2. Solubility of $CuSO_4$ in H_2SO_4 at 25°C.

SOURCES OF DATA

A 1 J. M. BELL, W. C. TABER, J. PHYS. CHEM. 12,171-9 (1908)
A 2 H.D. HOLLER, E.L.PEFFER, J. AM. CHEM. SOC. 38,1021-9 (1916)
A 3 H. M. GOODWIN, W. G. HORSCH, CHEM. MET. ENG. 21,181-2 (1919)
A 4 G. AGDE, H. BARKHOLT, ZEIT. ANGEW. CHEM. 40,374-9 (1927)
A 5 W. J.MULLER, L.HOLLECK, MONATSH. 52,409-24 (1929)
A 7 E. ASMUS, ANN. D. PHYS. (5) 36, 166-32 (1939)
A 8 M.EISENBERG, C.W. TOBIAS, C.R. WILKE, J. ELECTROCHEM. SOC. 103, 413-6 (1956)
A 9 C. R. WILKE, M. EISENBERG, C. W. TOBIAS, J. ELECTROCHEM. SOC. 100, 513 (1953)
A10 G.M. HOMSY, J.R. SELMAN, UNPUBLISHED (1965)
A11 A. F. W. COLE, A. R. GORDON, J. PHYS. CHEM. 40, 733-7 (1936)
A12 M. HOLLARD, J. PHYS. THEOR. (4) 5, 654-67 (1906)
A12 M. HOLLARD, BL. SOC. CHIM. (3) 35, 1240-55 (1906)
A13 M.DEK.THOMPSON, E.R.HAMILTON, TRANS.AM.ELECTROCHEM. SOC. 17, 287-94 (1910)
A14 H.K. RICHARDSON, F.D. TAYLOR, TRANS.AM.ELECTROCHEM. SOC. 20, 179-84 (1911)
A15 S.SKOWRONSKI, E.A. REINOSO, TRANS.AM.ELECTROCHEM. SOC. 52, 205-31 (1927)
A16 S.K. GALLANTHINE, UNPUBLISHED (1965)
A17 J.R. SELMAN, J.S. NEWMAN, AND J. SCHEULER, UNPUBLISHED (1966)
A18 F. LEIF, UNPUBLISHED (1966)
A19 G.SCHUTZ, INT.J.HEAT MASS TRANSFER 6, 873-9 (1963)
A20 A.J.ARVIA, J.C.BAZAN AND J.S.W.CARROZZA, ELECTROCHIM.ACTA 11, 881-9 (1966)
A21 G.JANDER, H.MOHR, Z.PHYS.CH. A 190, 81-100 (1942)
A22 D.M. BRASHER, F.R. JONES, TRANS. FARADAY SOC. 42,775-9 (1946)
A23 E.F. KERN, M.Y. CHANG, TRANS. AM. ELECTROCHEM. SOC. 41, 181-96 (1923)
A24 S. CHIANG, J.R. SELMAN, UNPUBLISHED (1967)
A25 L.HSUEH, PH.D. THESIS, UCRL-18597 (1968)
A26 L.HSUEH, M.S. THESIS, UCRL-16607 (1966)
A27 J.R. SELMAN, UCRL- FORTHCOMING
A28 T.W. CHAPMAN, J. NEWMAN, UCRL-17767 (1968)

APPENDIX B

Analysis of Copper Sulfate and Sulfuric Acid Solutions

The principle of electrogravimetric analysis of $CuSO_4$ is simply to plate out electrochemically all copper to a platinum gauze electrode from a known amount of solution. For the general discussion of this method, one could refer to Ref. 41.

In order to avoid any mechanical loss of solution and to obtain a solid deposition film, the slow method of electrolysis was adopted. The electrolysis was performed at a current of 0.1 to 0.15 ampere for a sufficient amount of time until the blue color of the solution had entirely disappeared.

The electrolysis efficiency in a unstirred solution was very poor. A 25ml sample solution of copper sulfate concentration 0.1M theoretically requires only 80 minutes with sufficient stirring to deplete all copper at 0.1 ampere. Actually, it took 20 to 24 hours before all the copper was depleted. The excess electricity was wasted in water decomposition.

The completeness of deposition was tested by adding 2 to 3 drops of 1M potassium ferrocyanide $K_4Fe(CN)_6$, when deposition reaches end point, the solution becomes clear, homogeneous deep yellow color. Any brownish precipitation indicates the formation of complex ions of free copper ions and ferrocyanide ions. There was no way to redissolve the precipitation but to repeat the analysis.

There was no deep yellow coloring in a blank test (a solution containing everything except copper sulfate). However, after passing the

same amount of electricity in the blank solution, the solution does turn to yellow when potassium ferrocyanide is added.

The procedures of slow electrogravimetric method is summarized follows:

1. Remove the previous deposited copper by dipping the platinum electrodes into concentrated nitric acid. Wash them thoroughly with distilled water and dry in an oven.
2. Take the electrodes out of the oven, cool in a vacuum desiccator, weigh and record.
3. Sampling 25ml, or less depends on the approximate concentration, solution and dilute to 200ml, add a few drops of concentrated HNO_3.
4. Set up electrodes and make sure there is no short circuit. Start to electrolysis at 0.1-0.15 ampere per one set of electrode for at least 24 hours.
5. Lower the electrolyte container before turning off the current, check the residue solution with 1M potassium ferrocyanide, wait for 5 minutes to see if there is any brownish precipitation.
6. Before removing electrodes from the stands, rinse them with distilled water from a polyethylene wash bottle, then with clean pure acetone from a syringe. Dry the electrodes in an oven of 120°C for at least 5 minutes but not over 15 minutes. Cool in a desiccator, weigh and record.
7. The increased weight is the amount of copper in the solution.

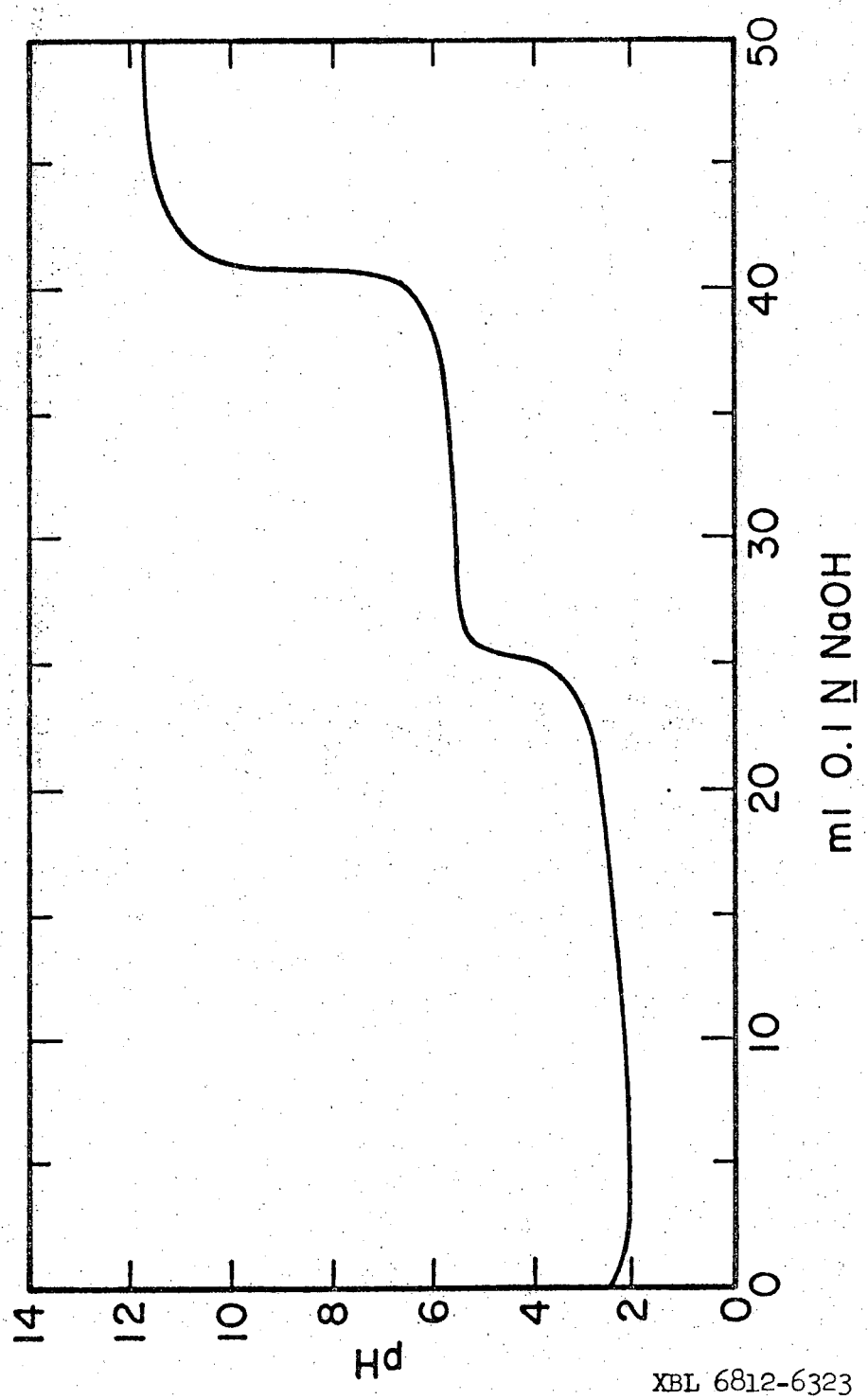

XBL 6812-6323

Fig. B-1. Titration curve of 10ml sample solution #106 with 0.1 N NaOH.

The sulfuric acid concentration was determined by titration with standardized 0.1N sodium hydroxide solution. A typical titration curve of 10ml sample solution of approximate 0.125M sulfuric acid and 0.100M copper sulfate is shown in Fig. B-1. The initial solution, 10ml sample solution diluted to 200ml, has pH value 2.2. The curve has a small dip at the very beginning and has three plateaus at pH approximately equal to 2.2, 5.5 and 11.8. The length of the first plateau is consistent with $CuSO_4$ if a simple reaction of formation of $Cu(OH)_2$ is assumed. It may be attributed to the complex ions formation of copper ions in an alkaline environment. The exact formation mechanism and its effect on determining the end point of H_2SO_4 were not investigated further. Without very strong reason, the end point in this titration was selected at pH 4.4.

APPENDIX C

Data Processing of a Magnetic Tape

Data from the digital voltmeter were either recorded by a FRANKLIN model 1030 D high speed digital printer or recorded on a magnetic tape for further mathematical treatments.

A section of paper tape from the printer (run 179, solution 106) is shown in Fig. C-1. Each row corresponds to one set of measurement of time and voltage at specified channel. To be consistent with the computer program, and to avoid any confusion on magnetic tape, from here on, each row of the data is called a LINE, each individual number or sign in the column is called a WORD. The sequence of words is given in Table C-1. For example, the first line in Fig. C-1 reads: at t=200.18sec the voltage of channel 21 is -0.0078701V, notice the decimal point was counted from right to left at 7th figure, i.e., the usual E format, with the exponent being negative. Similarly, line 20 reads; at t=500.93sec the voltage of channel 26 is 0.30873 volt which, incidentally, is the output voltage of constant voltage source.

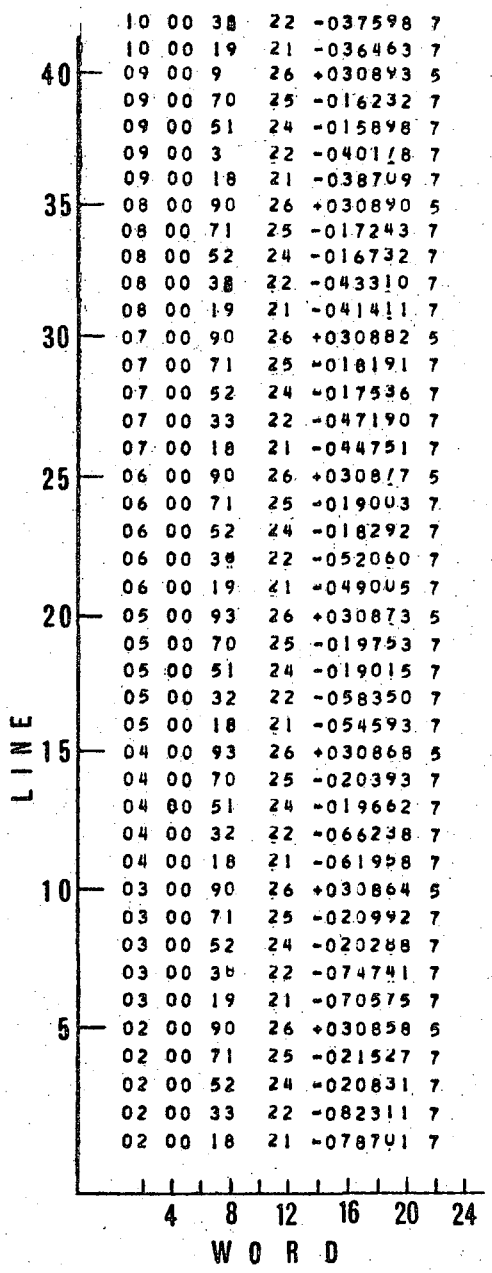

XBL692-180

Fig. C-1. A section of paper tape from Franklin Printer.

Table C-1.

WORD number	paper tape	magnetic tape
1,2	time: (10^3sec,10^2sec or 10 min,1 min)	BCD
3	Space	14B
4,5	time: (10 sec,sec)	BCD
6	Space	14B
7,8	time: (10^{-1}sec,10^{-2}sec)	BCD
9,10	Space	14B
11,12	Channel number	BCD
13	Space	14B
14	Polarity of voltage	12B or 15B or 17B
15-20	voltage mantissa	BCD
21	Space	14B
22	negative exponent voltage	BCD
23,24	end-of-line symbol	16B

Table C-2. Binary Coding on a Magnetic Tape

Octal BCD	Real	Octal BCD	Real
1B	1	10B	8
2B	2	11B	9
3B	3	12B	+, plus
4B	4	14B	space
5B	5	15B	*, overload
6B	6	16B	end of a line
7B	7	17B	-, minus

The measured data can simultaneously be transmitted to an Ampex RF-1 core memory. After 42 LINES are stored in the memory, they are then transferred to an Ampex 7211 Tape handler unit in batchwise and recorded on a magnetic tape of 1/2 inch width and approximate 5-6 inches in length. This batch is called one RECORD.

Each RECORD contains 512 rows of magnetic spots, see Fig. C-2 (only the first two rows of spots are drawn). In the computer program, each row of spots is called one MESSage.

Each MESSage has 60 magnetic spots, or BITS in computer terminology. Each WORD in the paper tape has to be store in six BITS in binary coding, magnetized or antimagnetized of each individual spot. The coding system of this apparatus is listed in Table C-2.

In paper tape, one line consists of 24 words, each MESSage can only store 10 words, therefore 2.4 MESSage units are needed to store one LINE, when the Ampex 7211 is operated at high density storage. The sequence of storages and their corresponding data line in a paper tape is also shown in Fig. C-2.

Accordingly, 42 lines occupy the first 100.8 message units in this RECORD, the remaining MESSage units are unused.

The computer program "PROCESS" consists of three parts:

1. ASCENTF SUBROUTINE IBITS: to convert these magnetic spots into real numbers.

2. TAPES: to check all words, to see if they are correctly spaced as they are specified in Table A-2 and convert them into actual numbers with decimal points. The data are then store in ARRAY of 60 spaces, 30 sets of times and voltages. The unused portions of ARRAY have

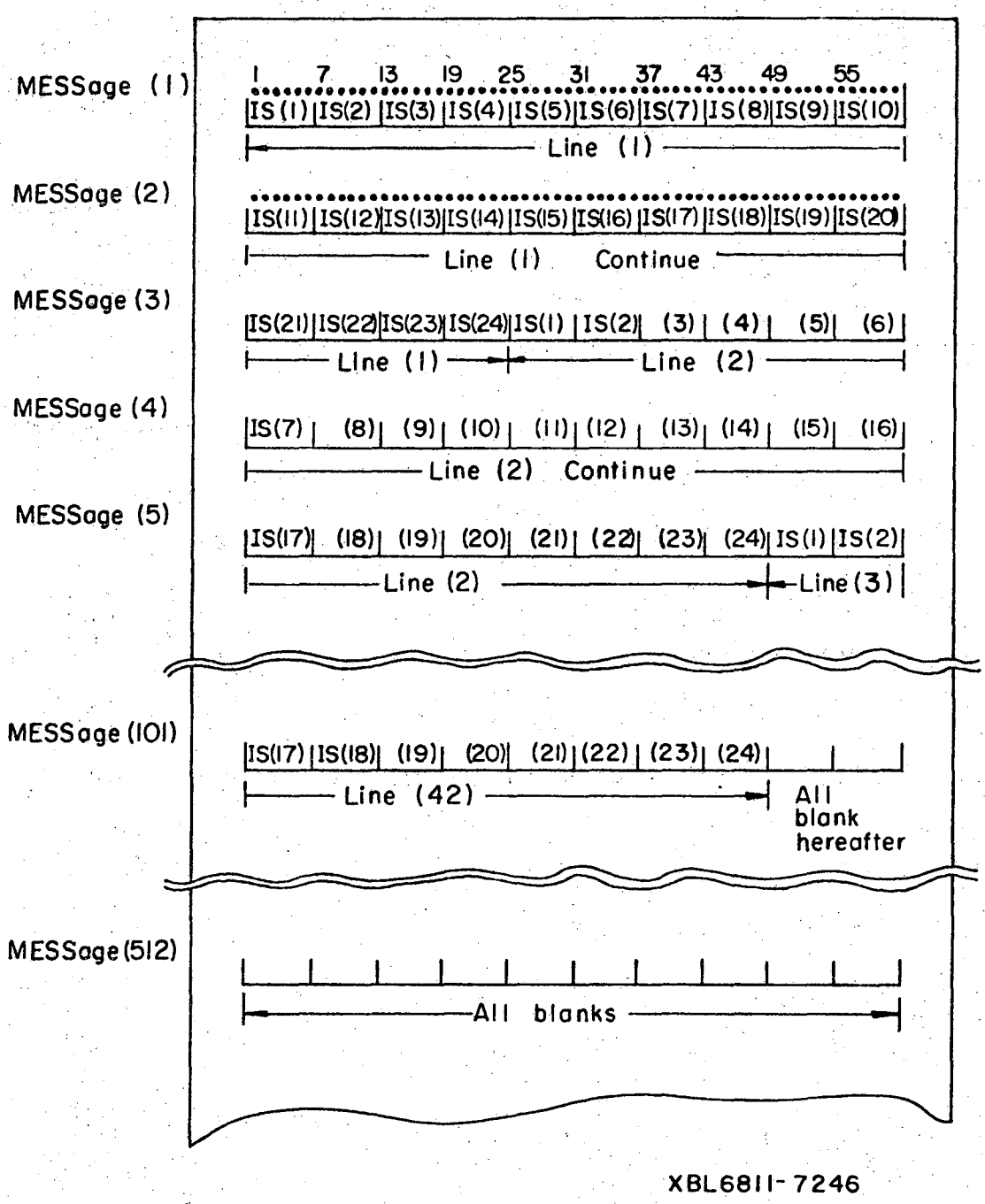

Fig. C-2. One RECORD of data on a magnet tape.

-10^6 in them. They are then written in the WRITE statement on Tape 6 ready to be used in the main program PROCESS.

To minimize the data lost in the storage because of parity error in one RECORD, the part of "SEARCH FOR A LEGAL LINE" was written for this purpose.

3. The main program "PROCESS" READ the data from Tape 6 and stores only the actual existing data and does all the mathematical treatment of data. For the special case of diffusion measurements, the mathematical treatment of data was discussed in section 6-2.

Whenever mathematical treatment of data is not needed, or very large amounts of data are recorded in one run, or when minimization of the computer storage is critically important, the second program "PROCESS" should be used. In the second program, the set of data are processed in groups each containing NMAX sets of data.

Summary of Input Data Notations in Program "PROCESS"

NRUN: total number of runs recorded on a tape roll

MINN: recorded time scale

MINN=0 the input time is in seconds

MINN=1 the input time is in minutes

NCHAN: total number of channels used in an experiment

NSUB: total number of subrun

NSUB=0 for a run lasting less than 10,000 sec.

NSUB=1 for a run lasting less than 20,000 sec.

NSUB=2 for a run lasting less than 30,000 sec.

etc.

NPASS: number of bypass or unwanted run between two good runs

M: experimental run number

ICHAN: channel numbers actually used in a run

NMAX: maximum number of data that can be mathematically treated in one batch.

```
      PROGRAM PROCESS(INPUT,OUTPUT,TAPE5,TAPE6,TAPE2=INPUT,TAPE3)
C     PROGRAM TO PROCESS THE DATA RECORDED ON TAPE FROM THE TAPE-RECORDER
C     OF THE DIGITAL VOLTMETER
C     PROGRAM LEADS TO DO ALL THE MATHEMATICAL TREATMENTS OF DATA
C     VOLTAGE FROM CHANNEL ICHAN(I) IS STORED IN V(I,ND).
      DIMENSION TIME(300),V( 5,300),ARRAY(2,30),ICHAN(30)
      DIMENSION JBEGIN(5),SUM(5),AVERAGE(5),CONST(5),COUNT(5),STD(5)
      DIMENSION NCHANG(5),SUMSQ(5)
      COMMON NRUN,MINN
  100 FORMAT (F9.2,4E14.5,I4)
  101 FORMAT (18I4)
  102 FORMAT (F9.2,5E14.4)
  103 FORMAT (7H    RUN ,I5)
  104 FORMAT(15X,I3,5I14)
  105 FORMAT (1H1)
  106 FORMAT (F9.2,4E14.5,I4)
  107 FORMAT (4E8.4)
  108 FORMAT (* TOTAL DATA COUNT*,F6.0,3F14.0)
  109 FORMAT (*      SUM=*,4E14.5)
  110 FORMAT (* AVERAGE=*,4E14.5)
  111 FORMAT(//10X,* THE INPUT TIME IS IN SECONDS.*)
  112 FORMAT(//10X,* THE INPUT TIME IS IN MINUTES.*)
  113 FORMAT (* THERE WAS MORE THAN 300 SETS OF DTAT,IT IS OUT OF CAPACI
     $TY OF STORAGE*)
  114 FORMAT (* STD DEV=*,4E14.5)
  115 FORMAT (1H0,* NUMBER OF ITERATIONS*,I5)
      READ 101,  NRUNS,MINN
      NRUN=0        $NC=5                $NMAX=300
      REWIND 5
    1 NRUN=NRUN+1
      IF (NRUN.GT.NRUNS) STOP
      READ 101,   NCHAN,NSUB,NPASS,M, (ICHAN(I),I=1,NCHAN)
      NCHM1=NCHAN-1
      READ 107,(CONST(I),I=1,NCHM1)
      NPASS=NPASS+1
      PRINT 105
      DO 7 I=1,NPASS
    7 CALL TAPES
      NSTART=1      $NS=0
      IF(NCHAN.GT.NC) NCHAN=NC
    2 DO 10 ND=NSTART,NMAX
    9 READ(6) (ARRAY(I),I=1,60)
      TIME(ND)=0.0
      IF (ENDFILE 6) 4,5
    5 DO 3 I=1,NCHAN
      J=ICHAN(I)
      T=ARRAY(1,J) + 10000.0*FLOAT(NS)
      IF (T.GE.0.0) TIME(ND)=T
    3 V(I,ND)=ARRAY(2,J)
      IF (TIME(ND).EQ.0.0) GO TO 9
   10 CONTINUE    $PRINT 113
    4 ND=ND-1
      IF (NS.GE.NSUB) GO TO 8
      CALL TAPES    $NS=NS+1             $NSTART=ND+1
      GO TO 2
    8 IF (MINN.EQ.1) PRINT 112           $IF (MINN.EQ.0) PRINT 111
      PRINT 103, M
      PRINT 104,  (ICHAN(I),I=1,NCHAN)
      DO 6 J=1,ND
    6 PRINT 102, TIME(J),(V(I,J),I=1,NCHAN)
```

```
C     MATHEMATICAL TREATMENTS OF PRCCESSED DATA
      PRINT 105     $PRINT 103,M
      PRINT 104,  (ICHAN(I),I=1,NCHM1)
      DO 11 J=1,ND
      SQT=SQRT(TIME(J))
      DO 11 I=1,NCHM1
      IF (V(I,J).LE.-1.0E+6) GO TO 11
      V(I,J)=ABS(V(I,J))*CUNST(I)*SQT
   11 CONTINUE
      ITERA=0
   12 ITERA=ITERA+1
      DO 16 I=1,NCHM1
      SUM(I)=0.0    $COUNT(I)=0.0
      SUMSQ(I)=0.0 $NCHANG(I)=0
      DO 15 J= 1,ND
      IF (V(I,J).LE.-1.0E+6) GO TO 15
      IF (ITERA.LE.1 .AND. TIME(J).LT.1000.0)  GO TO 15
      IF (ITERA.LE.1) GO TO 13
      IF (ABS(V(I,J)-AVERAGE(I)).GT. 3.*STD(I)) GO TO 14
   13 SUM(I)=SUM(I)+V(I,J)
      SUMSQ(I)=SUMSQ(I)+V(I,J)**2
      COUNT(I)=CCUNT(I)+1.0
      GO TO 15
   14 V(I,J)=-10.0**(5+ITERA)
      NCHANG(I)=NCHANG(I)+1
   15 CONTINUE
      IF (COUNT(I).LE.0.0) GO TO 16
      AVERAGE(I)=SUM(I)/COUNT(I)
      STD(I)=SQRT((SUMSQ(I)-SUM(I)**2/CCUNT(I))/(COUNT(I)-1.0))
   16 CONTINUE
      PRINT 115,ITERA
      PRINT 108, (COUNT(I), I=1,NCHM1)
      PRINT 109,(SUM(I), I=1,NCHM1)
      PRINT 110, (AVERAGE(I),I=1,NCHM1)
      PRINT 114, (STD(I),I=1,NCHM1)
      IF (ITERA.GE.10) GO TO 18
      IF (ITERA.LE.1) GO TO 12
      DO 17 I=1,NCHM1
   17 IF (NCHANG(I).GE.1) GO TO 12
   18 PRINT 105     $PRINT 103,M
      PRINT 104, (ICHAN(I),I=1,NCHM1)
      DO 19 J= 1,ND
   19 PRINT 106, TIME(J), (V(I,J),I=1,NCHM1),J
      PRINT 108, (COUNT(I), I=1,NCHM1)
      PRINT 109,(SUM(I), I=1,NCHM1)
      PRINT 110, (AVERAGE(I),I=1,NCHM1)
      PRINT 114, (STD(I),I=1,NCHM1)
C     END OF MATHEMATICAL TREATMENTS
      GO TO 1
      END
```

```
      SUBROUTINE TAPES
      DIMENSION ARRAY(2,30),MESS(512),IS(1010)
      COMMON NRUN,MINN
      DATA IGO, MAXCHAN, NREC, IEND/ 1, 30, 0, 60 /
  103 FORMAT(//10X,* THERE WAS A PARITY ERROR ON THE LAST READ.*)
  104 FORMAT(/10X,I3,* ERRORS OCCURRED IN READING THE INPUT TAPE.*)
      TO=0.0        $IO=0.0              $NERR=0
      DO 64 I=1,IEND
   64 ARRAY(I)= -1000000.
      REWIND 6
      GO TO (2,11) IGO
    1 NERR=NERR + NLINE-LINE
    2 NREC=NREC + 1
      BUFFER IN (5,1) (MESS(1),MESS(512))
   65 IF(UNIT,5) 66,3,15,67
   66 CALL RECALL(5)                    $GO TO 65
   67 PRINT 103
    3 LINE=0        $LL=LENGTHF(5)
      IF (LL.GT.101) LL=101
      IM=10*LL      $NLINE=IM/24        $IGO=2              $I=0
      DO 4 L=1,LL
      DO 4 K=1,10
      I=I+1
    4 IS(I)=IBITS(6*(K-1)+1, 6*K, MESS(L ))
      II=24

C     SEARCH FOR A LEGAL LINE
    5 IF (II.GT.IM) GO TO 1             $I=II-24
    6 IF(IS(I+24).EQ.16B) GO TO 7       $II=II+23           $GO TO 5
      IF(IS(I+23).EQ.16B) GO TO 6       $II=II+1            $GO TO 5
    7 IF(IS(I+3).NE.14B .OR. IS(I+ 6).NE.14B) GO TO 8
      IF(IS(I+9).NE.14B .OR. IS(I+10).NE.14B) GO TO 8
      IF(IS(I+13).EQ.14B.AND.IS(I+21).EQ.14B) GO TO 9
    8 II=II+24      $GO TO 5
    9 INDEX=10*IS(I+11) + IS(I+12)
      IF (IS(I+14).EQ.15B) GO TO 8
C     IS(I+14) EQUALS 15B IF THE VOLTAGE EXCEEDS ITS ALLOWABLE RANGE.
      IF(INDEX.LE.0 .OR. INDEX.GT.MAXCHAN) GO TO 8
      IF(IS(I+1).GT.9) GO TO 8
C     ALL THE CHECKS ARE CORRECT.

      TIME=FLOAT(10*IS(I+4)+IS(I+5))+0.01*FLOAT(10*IS(I+7)+IS(I+8))
      IF(MINN.EQ.0) TIME=TIME+100.0*FLOAT(10*IS(I+1)+IS(I+2))
      IF(MINN.EQ.1) TIME=TIME+60.0*FLOAT(10*IS(I+1)+IS(I+2))
      VOLT=0.0
C     THE MOST   LEFT      FIGURE IS THROWN AWAY. IF YOU WANT TO RETAIN
C     IT, SET VOLT EQUAL TO IS(I+15)*1.0E5 IN THE PRECEDING STATEMENT.
      LINE=LINE+1
      DO 10 K=1,5
      L=I+K+15
   10 VOLT=VOLT+FLOAT(IS(L))*10.**(5-K)
      IE=-IS(I+22)
      VOLT=VOLT*10.**(IE+3)
      IF (IS(I+14).EQ.17B) VOLT=-VOLT
C     THIS GIVES VOLT IN MILLIVOLTS. TO GET VOLT IN VOLTS, DELETE +3.

      IF(VOLT.EQ.0.0) GO TO 8
   11 IF(TIME.LE.TO-2.) GO TO 16
      IF(INDEX.LE.IO) GO TO 13
      IF(TIME.GE.TO+2.) GO TO 13
   12 ARRAY(1,INDEX)=TIME
```

```
      ARRAY(2,INDEX)=VOLT
      TO=TIME        $IO=INDEX              $GO TO 8
   13 WRITE(6) (ARRAY(I),I=1,IEND)
      DO 14 I=1,IEND
   14 ARRAY(I)= -1000000.                   $GO TO 12
   15 IGO=1
   16 IF(NERR.NE.0) PRINT 104, NERR
      WRITE(6) (ARRAY(I),I=1,IEND)
C     THE UNUSED PORTIONS OF ARRAY SHOULD HAVE -1000000. IN THEM.
      ENDFILE 6
      REWIND 6
      RETURN
      END
```

```
      ASCENTF SUBROUTINE IBITS(I1,I2,X)
         BSSZ 1              .THIS ROUTINE SELECTS BITS I1 TO I2 (INCLU000000000000
         BSSZ 1              .SIVE) OF X, AND STORES THEM (RIGHT ADJUST000000000000
         BSSZ 1              .WITH ZERO FILL) IN IBITS.                 000000000000
         BSSZ 1              .BITS ARE 1 TO 60 LEFT TO RIGHT            000000000000
         BSSZ 1                                                         000000000000
RET      BSSZ 1                                                         000000000000
         SA1  B1             .I1=(X1)                                   56110
         SB1= X1-1                                                      6211 777776
         SA2  B2             .I2=(X2)                                   56220
         IX2= X2-X1                                                     37221
         SB4= X2-59          .N=NUMBER OF BITS=I2-I1+1=(B4)-60          6242 777704
         SA3  B3             .X=(X3)                                    56330
         LX6= B1,X3          .LEFT SHIFT (X3), I1-1 BITS                22613
         EQ   B0,B4 RET      .DONE IF N=60                              0404 L00001
         LX6  B4,X6          .RIGHT SHIFT TO END OF WORD                22646
         MX0  1                                                         43001
         SB4  B4+1                                                      6144 000001
         LX0  B4,X0          .FORM 60-N BIT MASK                        22040
         BX6= -X0*X6                                                    15660
         EQ   B0,B0 RET                                                 0400 L00001
      END
```

```
      PROGRAM PROCESS(INPUT,OUTPUT,TAPE5,TAPE6,TAPE2=INPUT,TAPE3)
      DIMENSION TIME(200),V( 5,200),ARRAY(2,30),ICHAN(30)
      NC=5 $ NMAX=200
      COMMON NRUN,MINN
  101 FORMAT (18I4)
  102 FORMAT(F9.2,6E14.5)
  103 FORMAT (7H   RUN ,I5)
  104 FORMAT(15X,I3,5I14)
  105 FORMAT (1H1)
  106 FORMAT (7H  NTOT=,I6)
      READ 101,  NRUNS,MINN $ NRUN=0 $ REWIND 5
    1 NRUN=NRUN+1 $ IF(NRUN.GT.NRUNS) GO TO 99 $ PRINT 105
      READ 101,   NCHAN,NSUB,NPASS,M $ NPASS=NPASS+1 $ DO 7 I=1,NPASS
    7 CALL TAPES $ READ 101,   (ICHAN(I),I=1,NCHAN)
      MORE=0 $ NTOT=0 $ NS=0
      IF(NCHAN.GT.NC) NCHAN=NC
    2 DO 10 ND=1,NMAX
    9 READ(6) (ARRAY(I),I=1,60) $ TIME(ND)=0.0 $ IF(ENDFILE 6) 4,5
    5 DO 3 I=1,NCHAN $ J=ICHAN(I) $ T=ARRAY(1,J) + 10000.0*FLOAT(NS)
      IF(T.GE.0.0) TIME(ND)=T
    3 V(I,ND)=ARRAY(2,J) $ IF(TIME(ND).EQ.0.0) GO TO 9
   10 CONTINUE $ MORE=1 $ ND=NMAX+1
    4 ND=ND-1 $ NTOT=NTOT + ND
C
C     DO YOUR THING
      PRINT 103, M
      PRINT 104 , (ICHAN(I),I=1,NCHAN)
      DO 6 J=1,ND
    6 PRINT 102, TIME(J),(V(I,J),I=1,NCHAN)
      PRINT 106, NTOT
C
      IF(MORE.EQ.0) GO TO 8 $ MORE=0 $ GO TO 2
    8 IF(NS.GE.NSUB) GO TO 1 $ NS=NS+1 $ CALL TAPES $ GO TO 2
C     VOLTAGE FROM CHANNEL ICHAN(I) IS STORED IN V(I,ND).
C     IF A RUN HAS MORE DATA SETS THAN NMAX, THE SETS ARE PROCESSED IN
C     GROUPS EACH CONTAINING NMAX SETS.
C
C     ALTERNATELY, INSTEAD OF SPECIFYING THE CHANNELS, ONE COULD SEARCH
C     FOR CHANNELS WITH INFORMATION.  FOR A CHANNEL I WITH NO
C     INFORMATION, ARRAY(1,I) AND ARRAY(2,I) HAVE BEEN SET EQUAL TO
C     -1.0E6
   99 STOP $ END
```

(Pages 154 and 155 are the original programs written by John Newman. For processing the data tapes, these programs were modified by the author, eventually coming to the form on pages 150 to 153.)

```
      SUBROUTINE TAPES $ DIMENSION ARRAY(2,30),MESS(512),IS(1010)
      COMMON NRUN,MINN
      DATA IGO, MAXCHAN, NREC, IEND/ 0, 30, 0, 60 /
   17 FORMAT(//10X,* THE INPUT TIME IS IN SECONDS.*)
   18 FORMAT(//10X,* THE INPUT TIME IS IN MINUTES.*)
   19 FORMAT(///,10X,*THERE WAS A PARITY ERROR ON THE LAST READ.*)
   20 FORMAT(/10X,I3,* ERRORS OCCURRED IN READING THE INPUT TAPE.*)
      TO=0.0 $ IO=0.0 $ DO 21 I=1,IEND
   21 ARRAY(I)= -1000000. $ NERR=0 $ REWIND 6
      IF(IGO.EQ.2) GO TO 2 $ IF(IGO.EQ.1) GO TO 11
      IF(MINN.EQ.1) PRINT 18 $ IF(MINN.EQ.0) PRINT 17 $ GO TO 2
    1 NERR=NERR + NLINE-LINE
    2 NREC=NREC + 1 $ BUFFER IN(5,1) (MESS(1),MESS(512))
   65 IF(UNIT,5) 66,3,15,67
   66 CALL RECALL(5) $ GO TO 65
   67 PRINT 19
    3 LINE=0 $ LL=LENGTHF(5) $ IF(LL.GT.101) LL=101 $ IM=10*LL
      NLINE=IM/24 $ IGO=1
      I=0 $ DO 4 L=1,LL $ DO 4 K=1,10 $ I=I+1
    4 IS(I)=IBITS(6*(K-1)+1, 6*K, MESS(L ))  $ II=24
C     SEARCH FOR A LEGAL LINE
    5 IF(II.GT.IM) GO TO 1 $ I=II-24
    6 IF(IS(I+24).EQ.16B) GO TO 7 $ II=II+23 $ GO TO 5
      IF(IS(I+23).EQ.16B) GO TO 6 $ II=II+1 $ GO TO 5
    7 IF(IS(I+3).NE.14B .OR. IS(I+6).NE.14B) GO TO 8
      IF(IS(I+9).NE.14B .OR. IS(I+10).NE.14B) GO TO 8
      IF(IS(I+13).EQ.14B . AND. IS(I+21).EQ.14B) GO TO 9
    8 II=II+24 $ GO TO 5
    9 INDEX=10*IS(I+11) + IS(I+12) $ IF(IS(I+14).EQ.15B) GO TO 8
C     IS(I+14) EQUALS 15B IF THE VOLTAGE EXCEEDS ITS ALLOWABLE RANGE.
      IF(INDEX.LE.0 .OR. INDEX.GT.MAXCHAN) GO TO 8
      IF(IS(I+1).GT.9) GO TO 8
C     ALL THE CHECKS ARE CORRECT.
      TIME=FLOAT(10*IS(I+4)+IS(I+5))+0.01*FLOAT(10*IS(I+7)+IS(I+8))
      IF(MINN.EQ.0) TIME=TIME+100.0*FLOAT(10*IS(I+1)+IS(I+2))
      IF(MINN.EQ.1) TIME=TIME+60.0*FLOAT(10*IS(I+1)+IS(I+2))
      VOLT=0.0
C     THE MOST SIGNIFICANT FIGURE IS THROWN AWAY. IF YOU WANT TO RETAIN
C     IT, SET VOLT EQUAL TO IS(I+15)*1.0E5 IN THE PRECEDING STATEMENT.
      LINE=LINE+1 $ DO 10 K=1,5 $ L=I+K+15
   10 VOLT=VOLT+FLOAT(IS(L))*10.**(5-K) $ IE=-IS(I+22)
      VOLT=VOLT*10.**(IE+3) $ IF(IS(I+14).EQ.17B) VOLT=-VOLT
C     THIS GIVES VOLT IN MILLIVOLTS. TO GET VOLT IN VOLTS, DELETE +3.
      IF(VOLT.EQ.0.0) GO TO 8
   11 IF(TIME.LE.TO-2.) GO TO 16  $ IF(INDEX.LE.IO) GO TO 13
      IF(TIME.GE.TO+2.) GO TO 13
   12 ARRAY(1,INDEX)=TIME$ TO=TIME $ ARRAY(2,INDEX)=VOLT $ IO=INDEX
      GO TO 8
   13 WRITE(6) (ARRAY(I),I=1,IEND) $ DO 14 I=1,IEND
   14 ARRAY(I)= -1000000. $ GO TO 12
   15 IGO=2
   16 IF(NERR.NE.0) PRINT  20, NERR $ WRITE(6) (ARRAY(I),I=1,IEND)
C     THE UNUSED PORTIONS OF ARRAY SHOULD HAVE -1000000. IN THEM.
      ENDFILE 6 $ REWIND 6 $ RETURN $ END
```

APPENDIX D

Magnetic Tape Handling

In the Ampex 7211 tape unit, the two-channel-photosense-unit automatically stops tape motion and gives a signal to a remote equipment, a digital voltmeter or a computer, when reflective tabs are sensed. In other words, two reflective tabs are essentially the points where the recording starts and ends.

The tabs have a size of 3/16 inch by 1 inch, and are made of aluminum foil. They are located 1/32 inch from the lower edge of tape as an indication of the starting point, 1/32 inch from the upper edge of tape as an indication of the end point.

For the purpose of economizing the use of magnetic tape and saving the cost of tape cleaning and the storage spaces, the tape can be left on the tape recording unit without rewinding between two runs whenever it is possible. If it becomes necessary to remove it from the tape unit, a tab of the above size should be put at the lower edge of the tape as a second starting point at the position of recording-head where the tape stopped.

When the remaining part of the tape is being used again, skip the first tab by pushing the "FORWARD" button once. The tape unit automatically stops at the second starting point and recording will start to record at the second tab.

Remove the first tab, when the tape is sent to be processed, or remove the second tab and set NSUB in program "PROCESS" equal to the total number of runs previously recorded.

APPENDIX E1

"CONCEN" program notes

Program "CONCEN" was written for calculating the velocity and concentration profiles and dimensionless current density on a stagnant diffuscion cell when the variation of transport properties and nonzero interfacial velocity are taken into consideration. The program notations are:

N	number of iterations
DY	mesh size
ERR	relative tolerable error
GNUP	$M_+ \nu_+ / M_s$
CINF	c_∞
CZERO	c_o
AMP	I (see Eq. (2-9))

```
      PROGRAM CONCEN (INPUT,OUTPUT, TAPE2=INPUT, TAPE3=OUTPUT)
      DIMENSION B(1001),H(1001),W(1001),C(1001),RATIO(1001),SLOPE(1001)
  101 FORMAT (4I4,5F8.0)
  102 FORMAT (1H1, 69H INPUT DATA....  N     DY     W-INF      W-ZERO
     $ ERROR    M+*NO+/MS / 15X,I4,F6.3,1P3E11.3,1PE11.4//)
  103 FORMAT (I5,1P5E15.4)
  104 FORMAT (1H0/ 84H     I        V-PROFILE        W-PROFILE       C (MOLE/L)
     $          C/CINF      C/CINF/DY*I       /)
  105 FORMAT (15X,8H D-INF = ,E11.4, 5X, 8H C-INF = E11.4  / 15X,
     $ 8H D-ZERO= , E11.4,5X,8H C-ZERO= ,E11.4/ 19X,4H I= ,1PE11.4/
     $ 9X,14HNO. ITERATION= ,I6  /9X, 14HTIME IN SECOND, F9.2 )
  106 FORMAT (5X,18HD(INTEGRAL)/DINF=    ,1PE11.4,//)
    8 READ (2,101) N,N1,NP,M,CINF,CZERO,DY,ERR,GNUP
      IF (N.EQ.0) GO TO 6
      CALL SECOND(TIME)
      RINF=1.0
   10 ROLD=RINF
      WINF=CINF/RINF*0.15961
      RINF=RHO(WINF)
      TEST1=ROLD/RINF-1.0
      IF (ABS(TEST1).GT.ERR) GO TO 10
      WZERO=CZERO*0.15961
      AMP=0.0
      RO=RHO(WZERO)
      TPO=TP(WZERO)
      TMO=TM(WZERO)
      DO=D(WZERO)
      DINF=D(WINF)
      SO=RO/RINF*DO/DINF
      DO 1 J=1,N
      W(J)=WINF
    1 H(J)=0.0
      ITERA=0
    2 AO=AMP
      HINF=H(N)
      ITERA=ITERA+1
      W(1)=0.0
      B(1)=0.0
      S1=SO
      P1=RO/RINF*H(1)+AMP*TPO
      ADD1=P1/S1
      DO 3 J=2,N
      S2=RHO(W(J))/RINF*D(W(J))/DINF
      P2=RHO(W(J))/RINF*H(J)+AMP*TP(W(J))
      ADD2=P2/S2-2.0/D(W(J))*DINF*(J-1)*DY
      B(J)=B(J-1)+DY/2.0*(ADD1+ADD2)
      W(J)=W(J-1)+DY/2.0*(EXPF(B(J))/S2+EXPF(B(J-1))/S1)
      ADD1=ADD2
    3 S1=S2
      CONST =(WINF-WZERO)/W(N)
      DO 4 J=1,N
    4 W(J)=CONST*W(J)+WZERO
      AMP=-CONST/TMO
      H(1)=AMP*GNUP*RINF/RO
      SUM=0.0
```

```
      RHO1=RO
      DO 5 J=2,N
      RHO2=RHO(W(J))
      SUM=SUM+DY/2.0*(RHO1+RHO2)
      H(J)=2.0*(J-1)*DY-2.0/RHO2*SUM+H(1)*RO/RHO2
    5 RHO1=RHO2
      IF (ITERA.EQ.1) GO TO 2
      TEST1=AMP/AO-1.0
      TEST2=H(N)/HINF-1.0
      IF (ABS(TEST1).GT.ERR) GO TO 2
      IF (ABS(TEST2).GT.ERR) GO TO 2
      DO 9  I=1,N
      C(I)=W(I)*RHO(W(I))/0.15961
    9 RATIO(I)=C(I)/CINF
      DOD=3.1415927*(AMP/2.0*TM(WINF)/WINF)**2
      SLOPE(1)=RO/SO/0.15961/CINF*CONST
      DO 7 I=2,N
    7 SLOPE(I)=RATIO(I)/DY/(I-1)
      WRITE (3,102) N,DY,WINF,WZERO,ERR,GNUP
      WRITE (3,105) DINF,CINF, DO,CZERO,AMP,ITERA,TIME
      WRITE (3,106) DOD
      WRITE (3,104)
      WRITE (3,103) (I,H(I),W(I),C(I),RATIO(I),SLOPE(I), I=1,N1)
      WRITE (3,104)
      WRITE (3,103) (I,H(I),W(I),C(I),RATIO(I),SLOPE(I), I=N1,NP,M)
      GO TO 8
    6 STOP          $END


      FUNCTION RHO(W)
      RHO=0.99669+0.026901*W**0.5+0.74771*W+0.80718*W**1.5
      RETURN        $END


      FUNCTION TM(W)
      TM=0.597063+3.57889*W-8.21995*W**1.5
      RETURN        $END


      FUNCTION TP(W)
      TP=-3.57889+12.329925*W**0.5
      RETURN        $END


      FUNCTION D(W)
      D=0.207*EXPF(-29.0*W**0.5)+0.638-0.580*W**0.5
      D=D*1.0E-5
      RETURN        $END
```

APPENDIX E2

"DIFF" Program notes

Program "DIFF" was written for obtaining differential diffusion coefficients from the limiting current measurements. The program notations are:

MAXIT	maximum number of iterations, e.g. 15
TOL	tolerable error in differential diffusion coefficients, e.g., 10^{-8} cm^2/sec
NVAR	number of variables in correlations, e.g., 5 (see Eq. (2-19))
NDATA	total number of input experimental data
SALTMW	molecular weight of salt
GNUP	$M_+\nu/M_s$
ETRON	n
AREA	area of capillary (cm^2)
N	number of mesh points, e.g. 501
DY	mesh size, e.g. 0.01
ERR	relative tolerable error, e.g. 10^{-4}
CDATA	concentration of solutions (M)
SQRIT	experimental result of $I\sqrt{t}$ ($mA\sqrt{sec}$)
AMP	I (see Eq. (2-9))
DD(I)	differential diffusion coefficients at ITERA th iterations
DPRED	predicted diffusivities from Eq. (2-19))

```
      PROGRAM DIFF (INPUT,OUTPUT, TAPE2=INPUT,TAPE3=OUTPUT)
      DIMENSION COF(10),X(60,10),WDATA(60),DD(60),CDATA(60),SQRIT(60),
     $          DEN(60),DDO(60)
      COMMON NVAR,NDATA,SALTMW,COE,X,WDATA,DD
  101 FORMAT (I4,E8.2)
  102 FORMAT (2I4,4F8.0)
  104 FORMAT (1H0, 10X,20H NO. OF ITERATION=   ,I4,/14X,16H TIME  IN SECO
     $ND ,F8.2// 7X,2H I , 9X, 3HAMP,12X, 2HDD,15X,1HD,14X,4HTIME   )
  105 FORMAT (5X,I4,3E16.4,F16.2)
  106 FORMAT (1H0,5X, 20H STANDARD DEVIATION=    , E11.4)
  107 FORMAT (90H THE NUMBER OF ITERATIONS HAS EXCESSED THE NUMBER OF
     $MAX ITERATION, PROBLEM TERMINATED      )
  108 FORMAT (6E10.4)
  109 FORMAT (I4,3E10.4)
  110 FORMAT (3E15.4)
      READ(2,101) MAXIT,TOL
      READ(2,102) NVAR,NDATA,SALTMW,GNUP,ETRON,AREA
      READ(2,109) N, WZERO,DY,ERR
      READ(2,108) (CDATA(I),SQRIT(I),I=1,NDATA)
      WRITE(3,116)
      CALL SECOND(TIME)
      DO 1 I=1,NDATA
      DD(I)=SQRIT(I)/(ETRON*96500.0*AREA*CDATA(I))
      WDATA(I)=CDATA(I)/DEN(I)*SALTMW/1000.0
      DD(I)=TM(WDATA(I))*DD(I)
      DD(I)=3.14159*DD(I)**2
    1 WRITE(3,110) WDATA(I),DEN(I),DD(I)
      ITERA=0
    2 DO 3 I=1,NDATA
    3 DDO(I)=DD(I)
      ITERA=ITERA+1
      CALL DMATRX
      CALL CORREL
      WRITE(3,104) ITERA,TIME
      STDD=0.0
      DO 4 I=1,NDATA
      WINF=WDATA(I)
      CALL AMPERE (N,WZERO,WINF,DY,ERR,GNUP,AMP)
      CALL SECOND(TIME)
      DPRED=D(WINF)
      WRITE(3,105) I,AMP,DD(I),DPRED,TIME
      STDD=STDD+(DD(I)-DPRED)**2
      DD(I)=2.0/ETRON*SALTMW/1000.0*SQRIT(I)/AREA/DEN(I)
    4 DD(I)=(DD(I)/96500.0/AMP)**2
      STDD=SQRT(STDD/(NDATA-1))
      WRITE (3,106) STDD
      IF (ITERA.LT.MAXIT) GO TO 5
      WRITE(3,107)
      GO TO 100
    5 DO 6 I=1,NDATA
    6 IF(ABS(DD(I)-DDO(I)).GT.TOL) GO TO 2
  100 STOP
      END
```

```
      SUBROUTINE AMPERE (N,WZERO,WINF,DY,ERR,GNUP,AMP)
      DIMENSION B(1001), H(1001),W(1001)
      AMP=0.0
      R0=RHO(WZERO)
      TP0=TP(WZERO)
      D0=D(WZERO)
      RINF=RHO(WINF)
      DINF=D(WINF)
      S0=R0/RINF*D0/DINF
      DO 1 J=1,N
      W(J)=WINF
    1 H(J)=0.0
    2 A0=AMP
      HINF=H(N)
      W(1)=0.0
      B(1)=0.0
      S1=S0
      P1=R0/RINF*H(1)+AMP*TP0
      ADD1=P1/S1
      DO 3 J=2,N
      S2=RHO(W(J))/RINF*D(W(J))/DINF
      P2=RHO(W(J))/RINF*H(J)+AMP*TP(W(J))
      ADD2=P2/S2-2.0/D(W(J))*DINF*(J-1)*DY
      B(J)=B(J-1)+DY/2.0*(ADD1+ADD2)
      W(J)=W(J-1)+DY/2.0*(EXPF(B(J))/S2+EXPF(B(J-1))/S1)
      ADD1=ADD2
    3 S1=S2
      CONST =(WINF-WZERO)/W(N)
      DO 4 J=1,N
    4 W(J)=CONST*W(J)+WZERO
      AMP=-CONST/TM(WZERO)
      H(1)=AMP*GNUP*RINF/R0
      SUM=0.0
      RHO1=R0
      DO 5 J=2,N
      RHO2=RHO(W(J))
      SUM=SUM+DY/2.0*(RHO1+RHO2)
      H(J)=2.0*(J-1)*DY-2.0/RHO2*SUM+H(1)*R0/RHO2
    5 RHO1=RHO2
      IF(ABS(AMP-A0).GT.ERR*ABS(AMP)) GO TO 2
      IF (ABS(H(N)-HINF).GT.ERR*ABS(H(N))) GO TO 2
      RETURN
      END
```

```
      SUBROUTINE CORREL
      DIMENSION COE(10),X(60,10),B(10),A(10,10)
      COMMON NVAR,NDATA,SALTMW,COE,X
  101 FORMAT (2I4)
  103 FORMAT (35H ONE OF THE DIAGONAL ELEMENTIS ZERO          )
  104 FORMAT (1H1, 10( 15H COEF. OF  X ( , I3, 4H) = , E12,4/))
  111 FORMAT (1H1)
      NVAR1=NVAR+1
      DO 3 K=1,NVAR
      B(K)=0.0
      DO 2 I=1,NVAR
    2 A(K,I)=0.0
      DO 3 J=1,NDATA
      B(K)=B(K)+X(J,NVAR1)*X(J,K)
      DO 3 I=1,NVAR
    3 A(K,I)=A(K,I)+X(J,K)*X(J,I)
      DO 4 I=1,NVAR
    4 IF (A(I,I).NE.0.0) GO TO 5
      WRITE (3,103)
      GO TO 100
    5 INM1=NVAR-1
      DO 12 I=1,INM1
      IP1=I+1
      A(I,I)=1.0/A(I,I)
      B(I)=B(I)*A(I,I)
      DO 11 K=IP1,NVAR
   11 A(I,K)=A(I,K)*A(I,I)
      DO 12 J=IP1,NVAR
      B(J)=B(J)-B(I)*A(J,I)
      DO 12 K=IP1,NVAR
   12 A(J,K)=A(J,K)-A(I,K)*A(J,I)
        B(NVAR)=B(NVAR)/A(NVAR,NVAR)
      DO 13 JJ=2,NVAR
      J=NVAR-JJ+1
      JP1=J+1
      DO 13 K=1,J
   13   B(K)=B(K)-A(K,JP1)*B(JP1)
      WRITE (3,111)
      DO 14 I=1,NVAR
      COE(I)=B(I)
   14 WRITE (3,104) I, COE(I)
  100 RETURN
      END
```

```
      SUBROUTINE DMATRX
      DIMENSION COE(10),X(60,10),WDATA(60),DD(60)
      COMMON NVAR,NDATA,SALTMW,COE,X,WDATA,DD
       NVAR1=NVAR+1
      DO 1 J=1,NDATA
      X(J,NVAR1)=DD(J)
      X(J,1)=1.0
      X(J,2)=WDATA(J)**0.5
      X(J,3)=WDATA(J)
      X(J,4)=WDATA(J)**1.5
    1 X(J,5)=WDATA(J)**2.0
      RETURN
      END


      FUNCTION D(W)
      DIMENSION COE(10)
      COMMON NVAR,NDATA,SALTMW,COE
      D=COE(1)+COE(2)*W**0.5+COE(3)*W+COE(4)*W**1.5+COE(5)*W**2
      RETURN
      END


      FUNCTION RHO(W)
      RHO=0.99669+0.026901*W**0.5+0.74771*W+0.80718*W**1.5
      RETURN
      END


      FUNCTION TM(W)
      TM=0.597063+3.57889*W-8.21995*W**1.5
      RETURN
      END


      FUNCTION TP(W)
      TP=-3.57889+12.329925*W**0.5
      RETURN
      END
```

APPENDIX E3

"MIGR1" and MIGR2" Program notes

Programs MIGR1 and MIGR2 were written by Newman;[14,27] MIGR2 is transferred here for easy reference. MIGR1 was written for calculation of the effect of migration on the limiting current and surface concentration changes for the cases of no or complete dissociation of bisulfate ions. MIGR2 was written for the case of incomplete dissociation of bisulfate ions. The programs notations are:

MODE	MODE=1 Nernst diffusion,
	MODE=2 Stagnant diffusion or penetration model,
	MODE=3 Rotating disk or boundary layer model
NJ	total number of mesh points, maximum capacity 403
N	total number of ionic species, maximum capacity 5
H	mesh size, e.g., 0.24
STRI	ionic strength of solution (see Eq. (4-8))
R	r (see Eq. (4-4))
AK	K_2 (see Eq. (4-5))
CRO	concentration of reacting ion at electrode surface
CUSO4	concentration of copper sulfate in bulk solution
H2SO4	concentration of sulfuric acid in bulk solution
CIN(I)	concentration of individual ionic species

One blank card terminates a system, two blank cards stop the program. The built-in relative tolerable error in iteration is 0.00001 of calculated current.

```
      PROGRAM MIGR2 (INPUT,OUTPUT)
C     PROGRAM FOR EFFECT OF MIGRATION ON LIMITING CURRENT
C     INCOMPLETE DISSOCIATION
      DIMENSION A(6,6),B(6,6),C(6,403),D(6,13),G(6),X(6,6),Y(6,6),U(6),
     1V(403),DIF(6),Z(6),S(6),CIN(6),REF(6)
      COMMON A,B,C,D,G,X,Y,N,NJ
  101 FORMAT (3I4,3E8.4)
  102 FORMAT (4E8.4,A6)
  103 FORMAT (4HONJ=,I4,5H,  H=,F6.4/34HOSPECIES       U       DIF     Z
     1 S/(3X,A6,2F8.5,2F5.1))
  104 FORMAT (32H1NERNST STAGNANT DIFFUSION LAYER)
  105 FORMAT (32H1GROWING DROP OR PLANE ELECTRODE)
  106 FORMAT (14H1ROTATING DISK)
  107 FORMAT (5E8.4)
  108 FORMAT (30HOTHE NEXT RUN DID NOT CONVERGE)
  109 FORMAT (1HO,26X,2F10.6, F8.2/(3X,A6,2F9.5))
  110 FORMAT (54HOSPECIES      CINF      CZERO      AMP     AMP/AMPD       R)
  111 FORMAT (* THERE ARE TWO IMAG.OR NEGA. CONC.*/4E15.4)
  113 FORMAT ( ///// 10X,*CUSO4=*,1PE14.4,9X,*H2SO4=*,1PE14.4/
     $   * IONIC STRENGTH=*,1PE14.4,4X,*DISC. CONST=*, 1PE14.4          )
   99 READ 101, MODE,NJ,N,H
      IF (MODE.EQ.0)  STOP
      GO TO (1,2,3),MODE
    1 H=1.0/(NJ-2)
      CONST=0.0      $AMPD=1.0            $PRINT 104           $GO TO 4
    2 CONST=2.0      $AMPD=1.12838        $PRINT 105           $GO TO 4
    3 CONST=3.0      $AMPD=1.1198         $PRINT 106
    4 NM1=N-1        $NM2=N-2
      READ 102, (U(I),DIF(I),Z(I),S(I),REF(I),I=1,NM1)
      PRINT 103, NJ,H,(REF(I),U(I),DIF(I),Z(I),S(I),I=1,NM1)
    5 READ 107,STRI,R,AK,CRO
      IF (STRI.LE.0.0) GO TO 99
      CUSO4=(1.0-R)/(4.0-R)*STRI
      H2SO4=R/(4.0-R)*STRI
      PRINT 113, CUSO4,H2SO4,STRI,AK
      Q2=-CUSO4-3.0*H2SO4-AK              $Q3=2.0*H2SO4*(CUSO4+H2SO4)
      D=Q2*Q2-4.0*Q3                      $SQD=SQRT(ABS(D))
      ROOT1=(-Q2+SQD)/2.0                 $ROOT2=(-Q2-SQD)/2.0
      IF (ROOT1.LT.0.0 .AND. ROOT2.LT.0.0) GO TO 33
      CSUM=CUSO4+H2SO4
      IF (ROOT1.LT.0.0.OR.ROOT1.GE.CSUM) GO TO 31
      CIN(1)=ROOT1 $CIN(4)=CUSO4          $CIN(5)=0.0          $GO TO 32
   31 CIN(1)=ROOT2 $CIN(4)=CUSO4          $CIN(5)=0.0
   32 CIN(2)=CUSO4+H2SO4-CIN(1)           $CIN(3)=2.0*H2SO4-CIN(1)
      GO TO 6
   33 PRINT 111,ROOT1,ROOT2               $GO TO 5
    6 PRINT 110
      DO 7 J=1,NJ
      V(J)= CONST*(H*(NJ-J-1))**(MODE-1)*DIF(NM1)
      C(NM1,J)= CRO + (CIN(NM1) - CRO)*(NJ-J-1)/(NJ-2)
      C(N,J)= 0.0
      DO 7 I=1,NM2
    7 C(I,J)= CIN(I)
      JCOUNT=0       $AMP=0.0
    8 JCOUNT= JCOUNT + 1
      J= 0
      DO 9 I=1,N
      DO 9 K=1,N
      Y(I,K)= 0.0
    9 X(I,K)= 0.0
   10 J= J + 1
```

```
      DO 11 I=1,N
      G(I)= 0.0
      DO 11 K=1,N
      A(I,K)= 0.0
      B(I,K)= 0.0
   11 D(I,K)= 0.0
      IF (J-1)  12,12,14
   12 DO 13 I=1,N
      B(I,I)= 1.0
   13 G(I)= CIN(I)
      CALL BAND(J)                          $GO TO 10
   14 DO 15 K=1,NM1
   15 B(N,K)= Z(K)
      IF (J-NJ)  16,18,18
   16 DO 17 I=1,NM1
      PP= U(I)/DIF(I)*(C(N,J+1)-C(N,J-1))/2.0
      PPP= U(I)/DIF(I)*(C(N,J+1)+C(N,J-1)-2.0*C(N,J))
      CP= (C(I,J+1) - C(I,J-1))/2.0
      A(I,I)= - 1.0 + PP/2.0 - H*V(J)/2.0/DIF(I)
      B(I,I)= 2.0 - PPP
      D(I,I)= - 1.0 - PP/2.0 + H*V(J)/2.0/DIF(I)
      A(I,N)= U(I)/DIF(I)*(CP/2.0 - C(I,J))
      B(I,N)= 2.0*U(I)/DIF(I)*C(I,J)
      D(I,N)= - U(I)/DIF(I)*(CP/2.0 + C(I,J))
   17 G(I)= - PPP*C(I,J) - PP*CP
      DO 23 I=2,3
      A(I,1)=A(1,1)            $B(I,1)=B(1,1)        $D(I,1)=D(1,1)
      A(I,N)=A(I,N)+A(1,N)
      B(I,N)=B(I,N)+B(1,N)
      D(I,N)=D(I,N)+D(1,N)
   23 G(I)=G(I)+G(1)
      A(1,1)=0.0    $B(1,1)=-AK          $D(1,1)=0.0
      A(1,N)=0.0    $B(1,N)=0.0          $D(1,N)=0.0
      G(1)= C(3,J)*C(2,J)
      B(1,3)=C(2,J)
      B(1,2)=C(3,J)
      CALL BAND(J)                          $GO TO 10
   18 DO 19 I=2,NM2
      PP= U(I)/DIF(I)*(C(N,NJ)-C(N,NJ-2))
      Y(I,I)= - 1.0            $A(I,I)=PP            $B(I,I)=1.0
      Y(I,NM1)= S(I)*DIF(NM1)/S(NM1)/DIF(I)
      B(I,NM1)= - Y(I,NM1)
      Y(I,N)= (S(I)/S(NM1)*U(NM1)*CRO-U(I)*C(I,NJ-1))/DIF(I)
      B(I,N)= - Y(I,N)
   19 G(I)= PP*C(I,NJ-1)
      A(NM1,NM1)= 1.0          $G(NM1)=CRO
      G(1)=C(3,J)*C(2,J)
      B(1,1)=-AK    $B(1,2)=C(3,J)        $B(1,3)=C(2,J)
      CALL BAND(J)
      AMPO= AMP
      AMP= (L(NM1)*CRO*(C(N,NJ-2)-C(N,NJ))+DIF(NM1)*(C(NM1,NJ-2)-C(NM1,
     1NJ)))/2.0/H/(CIN(NM1)-CRO)/DIF(NM1)
      RAMP=AMP/AMPO
      IF (ABSF(AMP-AMPO)-0.00001 *ABSF(AMP))  22,22,20
   20 IF (JCOUNT-10)  8,8,21
   21 PRINT 108
   22 PRINT 109, AMP,RAMP,R,(REF(I),C(I,1),C(I,NJ-1), I=1,NM1)
      GO TO 5
      END
```

```
      SUBROUTINE BAND(J)
      DIMENSION A(6,6),B(6,6),C(6,403),D(6,13),G(6),X(6,6),Y(6,6),
     $E(6,7,403)
      COMMON A,B,C,D,G,X,Y,N,NJ
  101 FORMAT (15HODETERM=0 AT J=,I4)
      IF (J-2)  1,6,8
    1 NP1= N + 1
      DO 2 I=1,N
      D(I,2*N+1)= G(I)
      DO 2 L=1,N
      LPN= L + N
    2 D(I,LPN)= X(I,L)
      CALL MATINV(N,2*N+1,DETERM)
      IF (DETERM)  4,3,4
    3 PRINT 101, J
    4 DO 5 K=1,N
      E(K,NP1,1)= D(K,2*N+1)
      DO 5 L=1,N
      E(K,L,1)= - D(K,L)
      LPN= L + N
    5 X(K,L)= - D(K,LPN)
      RETURN
    6 DO 7 I=1,N
      DO 7 K=1,N
      DO 7 L=1,N
    7 D(I,K)= D(I,K) + A(I,L)*X(L,K)
    8 IF (J-NJ)  11,9,9
    9 DO 10 I=1,N
      DO 10 L=1,N
      G(I)= G(I) - Y(I,L)*E(L,NP1,J-2)
      DO 10 M=1,N
   10 A(I,L)= A(I,L) + Y(I,M)*E(M,L,J-2)
   11 DO 12 I=1,N
      D(I,NP1)= - G(I)
      DO 12 L=1,N
      D(I,NP1)= D(I,NP1) + A(I,L)*E(L,NP1,J-1)
      DO 12 K=1,N
   12 B(I,K)= B(I,K) + A(I,L)*E(L,K,J-1)
      CALL MATINV(N,NP1,DETERM)
      IF (DETERM)  14,13,14
   13 PRINT 101, J
   14 DO 15 K=1,N
      DO 15 M=1,NP1
   15 E(K,M,J)= - D(K,M)
      IF (J-NJ)  20,16,16
   16 DO 17 K=1,N
   17 C(K,J)= E(K,NP1,J)
      DO 18 JJ=2,NJ
      M= NJ - JJ + 1
      DO 18 K=1,N
      C(K,M)= E(K,NP1,M)
      DO 18 L=1,N
   18 C(K,M)= C(K,M) + E(K,L,M)*C(L,M+1)
      DO 19 L=1,N
      DO 19 K=1,N
   19 C(K,1)= C(K,1) + X(K,L)*C(L,3)
   20 RETURN
      END
```

```
      SUBROUTINE MATINV(N,M,DETERM)
      DIMENSION A(6,6),B(6,6),C(6,403),D(6,13),ID(6)
      COMMON A,B,C,D
      DETERM= 1.0
      DO 1 I=1,N
    1 ID(I)= 0.0
      DO 18 MM=1,N
      BMAX= 0.0
      DO 6 I=1,N
      IF (ID(I))  2,2,6
    2 DO 5 J=1,N
      IF (ID(J))  3,3,5
    3 IF (ABSF(B(I,J)) - BMAX)  5,5,4
    4 BMAX= ABSF(B(I,J))
      IROW= I
      JCOL= J
    5 CONTINUE
    6 CONTINUE
      IF (BMAX)  7,7,8
    7 DETERM= 0.0
      RETURN
    8 ID(JCOL)= 1
      IF (JCOL-IROW)  9,12,9
    9 DO 10 J=1,N
      SAVE= B(IROW,J)
      B(IROW,J)= B(JCOL,J)
   10 B(JCOL,J)= SAVE
      DO 11 K=1,M
      SAVE= D(IROW,K)
      D(IROW,K)= D(JCOL,K)
   11 D(JCOL,K)= SAVE
   12 F= 1.0/B(JCOL,JCOL)
      DO 13 J=1,N
   13 B(JCOL,J)= B(JCOL,J)*F
      DO 14 K=1,M
   14 D(JCOL,K)= D(JCOL,K)*F
      DO 18 I=1,N
      IF (I-JCOL)  15,18,15
   15 F= B(I,JCOL)
      DO 16 J=1,N
   16 B(I,J)= B(I,J) - F*B(JCOL,J)
      DO 17 K=1,M
   17 D(I,K)= D(I,K) - F*D(JCOL,K)
   18 CONTINUE
      RETURN
      END
```

APPENDIX E4

"CURD1" program notes

The first input data card is the six parameters ALPHA, BETA, GAMMA, TPLUS, V corresponding to α, β, γ, t_+, V mentioned in chapter 5, and EXCH = 1/J, TAF = 1.0 for Tafel polarization.

The second (third etc., if change of mesh size is necessary) input data card is

MAXI maximum allowed number iterations, e.g. 50

DAMPE exponential in damping factor, see n in P. 64

e.g., DAMPE=2.0 to 3.0 at small times

DAMPE=1.0 at large times

H mesh size of time scale, e.g., 0.0001, 0.001, 0.01, 0.1 etc.

ERR relative tolerable error, e.g. 0.0001

The actual numbers of iterations of each mesh point are printed in the last column under the heading I. If I=MAXI, the calculations were not converged at that particular mesh point. Thus, either adjust DAMPE or increase MAXI. Increase DAMPE, if I=MAXI occurs at the beginning of a cycle, decrease DAMPE, if I=MAXI occurs at the end of a cycle.

If the mesh size H and/or DAMPE is too large, the dimensionless surface concentration θ(CJ) may overshoot and become negative. In this case, either reduce H or DAMPE or both.

One blank card terminates a system; two blank cards stop the program.

```
      PROGRAM CURD1 (INPUT,OUTPUT)
      DIMENSION A(101), B(101),C(101),CUR(101),ETA(101)
  101 FORMAT (8F8.2)
  102 FORMAT (I8, F8.2,F8.3,F8.4)
  103 FORMAT (1H1,*    ALPHA     BETA    GAMMA    TPLUS     EXCH      TAF   V*)
  104 FORMAT (1H0,*     MAXI   DAMP E       H      ERR                        *)
  105 FORMAT (E10.2,F10.4,1P2E14.4,I4)
  106 FORMAT (1H0,*     TAO       C(J)        ETA(J)          CUR(J)        I*)
  107 FORMAT (1H0,* CJ OVERSHOT,NEGATIVE, REDUCE  INPUT H OR DAMPE.    *)
  108 FORMAT (1H0,* IF I=MAXI, CALC.WAS NOT CONVERGED,  ADJUST  DAMPE *)
      C1=0.0          $C2=1.0
      DO 3 J=1,101
      C3=J+1          $C3=C3**0.5
      A(J)=2.0*C2-C1-C3
      B(J)=C2-C1      $C1=C2
    3 C2=C3
    1 READ 101,ALPHA,BETA,GAMMA,TPLUS,EXCH,TAF,V
      IF(V.EQ.0.0) STOP                  $JBEGIN=1
      IF(EXCH.LE.400.0) GO TO 2
      TAF=0.0         $EXCH=1.0
    2 READ 102,MAXI,DAMPE,H,ERR
      IF (H.EQ.0.0) GO TO 1
      PRINT 103       $PRINT 101,ALPHA,BETA,GAMMA,TPLUS,EXCH,TAF,V
      PRINT 104       $PRINT 102,MAXI,DAMPE,H,ERR
      PRINT 106
      IF (JBEGIN.NE.1) GO TO 10          $CJ=1.0              $ETAJ=V
   10 C1=H**0.5/2.0
      DO 8 J=JBEGIN,101
      IF(J.EQ.1) GO TO 5
      SUM=C(1)*B(J-1)
      IF (J.EQ.2) GO TO 5                $JM1=J-1
      DO 4 K=2,JM1
    4 SUM=SUM+C(K)*A(J-K)
      SOLVE ETA(J) BY NEWTON-RAPHSON METHOD (SEE E.G. LAPIDUS)
    5 DO 6 I=1,MAXI
      IF (J.EQ.1) GO TO 9
      DAMPIN=(1.0-CJ)**DAMPE
      CJ=CJ*DAMPIN+(C1*CURJ+SUM)*(1.0-DAMPIN)
      IF (CJ.LT.0.0) PRINT 107
    9 C2=ETAJ+TPLUS*(CJ-1.0)
      X1=CJ**(GAMMA-ALPHA)*EXP(ALPHA*C2)*TAF
      X2=CJ**(GAMMA+BETA )*EXP(BETA*(-C2))
      F=X1-X2-EXCH*(V-ETAJ)
      DF=ALPHA*X1+BETA*X2+EXCH
      ETAP=ETAJ-F/DF
      CURJ = V-ETAP
      IF (ABS(ETAJ-ETAP).LE.ERR*ABS(ETAP)) GO TO 7
    6 ETAJ=ETAP
    7 C(J)=CJ         $ETA(J)=ETAP         $CUR(J)=CURJ          $TAO=(J-1)*H
    8 PRINT 105,TAO,C(J),ETA(J),CUR(J),I
      DO 11 K=1,11
      J=K*10-9        $C(K)=C(J)           $ETA(K)=ETA(J)
   11 CUR(K)=CUR(J)
      JBEGIN=12       $PRINT 108
      GO TO 2         $END
```

APPENDIX F

Control Panel in Electrical Measurement

The circuit diagram of the control panel is shown in Fig. F-1. The "VOLT SOURCE" is connected to a constant voltage power supply which serves as a constant voltage source for all five cells connected in parallel. The inlet voltage is measured at V6.

Three precision resistors of 100 ohms were built inside the control panel for measuring the current of the first three cells C1, C2, and C3. For the flexibility of measuring any special electrolytic solution with an extremely low or high conductivity solution in cells C4 and C5, the two other resistors were not put into the control panel; external decade resistor boxes can be connected for measuring the current to these cells. On the rear panel, V1 to V6 were connected to a VIDAR 12361-1 scanner at selected channels which gives the current flowing through cells 1 to 5 and the source voltage.

The accuracy of the three built in resistors (Shallcross Mfg. Co. Wire wound type BX 110, 100ohms resistor, Accuracy ±0.05%) were checked one by one with a standard resistor. (Leeds and Northrup Co. Catalog #4030B, serial #1692170 terminal resistance at 25°C 99.9999 ohms, uncertainty 0.001%). The voltage drop across the resistor and standard resistor, connected in series, were measured by a digital voltmeter. Four dry cells connected in parallel were used as the current source. The measured resistances are

#1	100.06±0.01 ohms
#2	100.07±0.01 ohms
#3	100.07±0.01 ohms

The deviation from 100.0 ohms was neglected in all previous calculations.

The four push-button-switches (START, STOP, RESET, and MANUAL ENTRY) located in the front of the panel have the same functions as those located inside the electronic clock drawer. They take over the function when the local-remote switch is at "RMT" position. The "START" switch on the panel will not only start the clock but also switch on the power source and start the current flowing through the cells. The "STOP" switch, on the other hand, stops the clock and switches off the current. These control signals are transmitted to the clock through a cable with an AMPHENOL 165-15 plug at one end and an AMPHENOL 57-30360 plug at the other end.

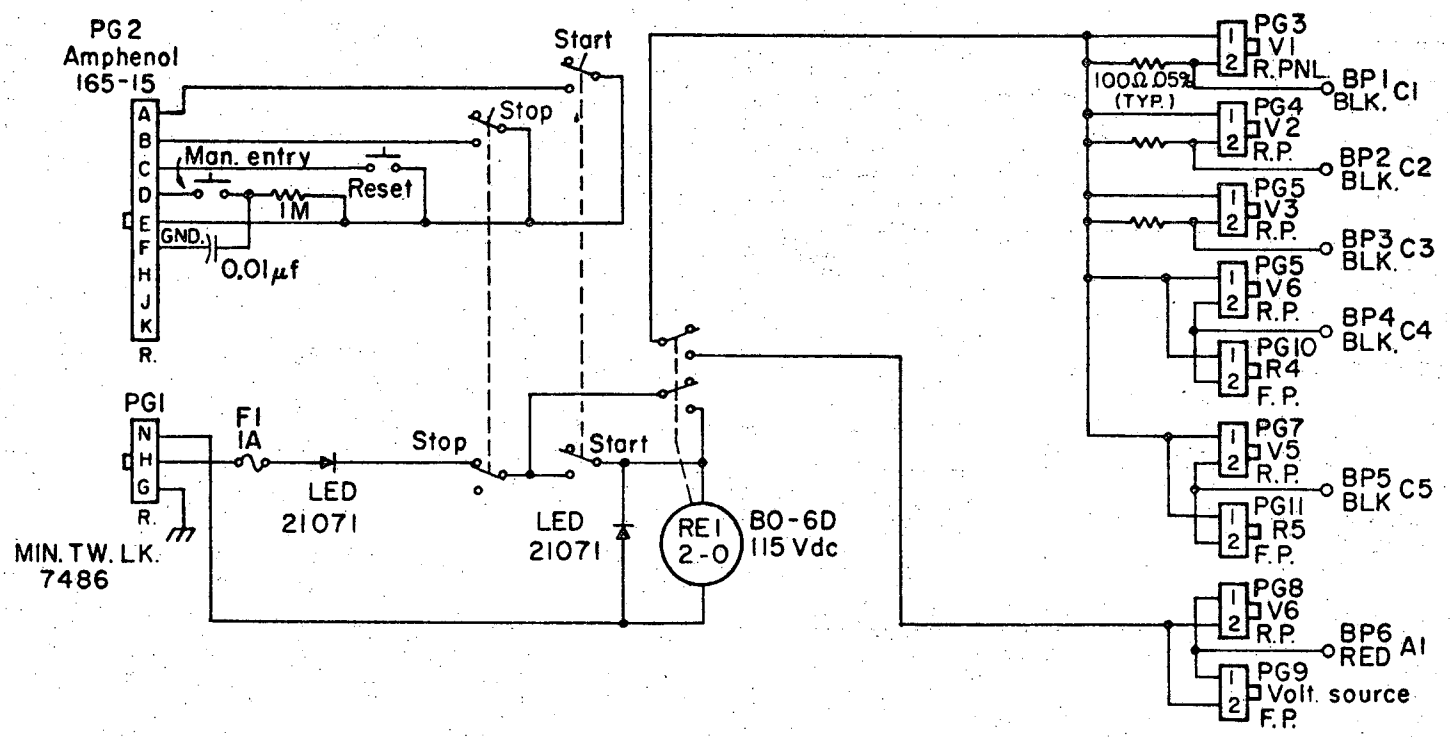

Fig. F-1. Stagnant diffusion measurement and clock control circuit diagram.

APPENDIX G

Analytic Solution of the Effect of Migration in Nernst Diffusion Layer

An analytic solution to the effect of migration was found possible when $k = 0$ in Eq. (4-1). Physically it is a steady diffusion in a motionless layer of thickness δ. A simpler case that all ions are monovalent was given by Levich[28] and Eucken.[29] Here we extend the treatment to the more general case.

Let the subscript 3 denote the reacting ion, 1 and 2 denote the remaining two species of indifferent ions (see Table 4-1). Integrating Eq. (4-1) once with k=0 gives

$$-D_i \frac{dc_i}{dy} - z_i u_i F c_i \frac{d\phi}{dy} = N_i \qquad i=1,2,3 \tag{G-1}$$

For a metal deposition reaction, $N_1 = N_2 = 0$, thus the current and flux relation (3-5) becomes

$$i = F z_3 N_3 \tag{G-2}$$

The three ionic species have also to satisfy the electroneutrality Eq. (4-2); thus it is possible to solve the three equations (G-1) and Eq. (4-2) simultaneously with the following boundary conditions

$$c_i = c_i^{\infty} \quad \text{and} \quad \phi = 0 \quad \text{at } y = \delta \quad i = 1,2,3 \tag{G-3a}$$

$$c_3 = 0 \quad \text{at } y = 0 \text{ and } i = i_L \tag{G-3b}$$

Integrating Eqs. (G-1) for i=1, 2 with boundary conditions (G-3a) gives

$$c_1 = c_1^{\infty} e^{-\psi_1} \quad ; \quad c_2 = c_2^{\infty} e^{-\psi_2} \tag{G-4}$$

where $$\psi_i = \frac{z_i u_i F}{D_i} \phi \quad . \tag{G-5}$$

Substituting into Eq. (4-2) we obtain c_3,

$$z_3 c_3 = -z_1 c_1^{\infty} e^{-\psi_1} - z_2 c_2^{\infty} e^{-\psi_2} \quad . \tag{G-6}$$

If we replace N_3 in Eq. (G-1), i=3, by Eq. (G-2) and replace c_3 by Eq. (G-6) and replace dc_3/dy by the derivative of Eq. (G-6), we obtain

$$\frac{i}{D_3 F}\, dy = \left[z_1 F c_1^{\infty} e^{-\psi_1} \left(\frac{z_3 u_3}{D_3} \right) - \frac{z_1 u_1}{D_1} + z_2 F c_2^{\infty} e^{-\psi_2} \left(\frac{z_3 u_3}{D_3} - \frac{z_2 u_2}{D_2} \right) \right] d\phi \quad .$$

Finally, we integrate the above equation with boundary conditions (G-3a) and use the equation of electroneutrality (4-2) and Eq. (G-4) to simplify the integrated equation, the final result being

$$\frac{i(y-\delta)}{z_3 D_3 F} = c_3^{\infty} - c_3 + \frac{u_3 D_1}{u_1 D_3} c_1^{\infty} (1-e^{-\psi_1}) + \frac{u_3 D_2}{u_2 D_3} c_2^{\infty} (1-e^{-\psi_2}) \tag{G-7a}$$

$$= c_3^{\infty} - c_3 + \frac{u_3 D_1}{u_1 D_3} (c_1^{\infty} - c_1) + \frac{u_3 D_2}{u_2 D_3} (c_2^{\infty} - c_2) \quad . \tag{G-7b}$$

1. Complete Dissociation of Bisulfate Ion

At the electrode surface, y=0, where $c_3=0$, $i=i_L$, we define

$$q = -\frac{z_2 c_2^{\infty}}{z_1 c_1^{\infty}} \tag{G-8}$$

$$R = 1 - \frac{z_2 u_2 D_1}{z_1 u_1 D_2} \quad . \tag{G-9}$$

The equation of electroneutrality at y=0 becomes $z_1 c_1 = -z_2 c_2$. From Eq. (G-4), we can prove the following relations at y=0

$$e^{-\psi_1} = q^{\frac{1}{R}} \quad , \tag{G-10}$$

$$e^{-\psi_2} = q^{\frac{1}{R} - 1} \tag{G-11}$$

If we evaluate Eq. (G-7a) at y=0 with all the relations we have got from Eqs. (G-8) to (G-11), and with elaborate algebraic rearrangements and simplifications, we then obtain

$$-\frac{i_L \delta}{z_3 D_3 F c_3^{\infty}} = 1 + \frac{z_3 u_3 D_1}{z_1 u_1 D_3} \frac{1}{1-R} \left[R \frac{1-q^{\frac{1}{R}}}{1-q} - 1 \right] \quad . \tag{G-12}$$

When Eq. (4-1) is solved without the migration term, we obtain the limiting diffusion current

$$-\frac{i_D \delta}{z_3 D_3 F c_3^{\infty}} = 1 \quad .$$

Therefore the ratio of limiting current to the limiting diffusion current is the right hand side of Eq. (G-12).

The surface concentration of each ionic species is calculated from the combination of Eqs. (G-4) and (G-10) or (G-11)

$$c_1^o = c_1^\infty q^{\frac{1}{R}} \quad ; \quad c_2 = c_2^\infty q^{\frac{1}{R}-2} \tag{G-13}$$

For the electrolytic system of copper sulfate and sulfuric acid with complete dissociation, the relation of ionic concentration and molecular concentration is shown in Table 4-1. We can prove that q=r in this case, where r is the concentration ratio defined in Eq. (4-4) and R = 1.5. If the Nernst-Einstein relation is assumed,

$$\frac{I_L}{I_D} = 3\frac{1-r^{\frac{2}{3}}}{1-r} - 1$$

and

$$\frac{c_B^o - c_B}{c_A} = \frac{1}{1-r}\left(r^{\frac{2}{3}} - r\right) .$$

Numerical plots and tabulations of these two ratios have been given in Figs. G-1 and G-2, and Tables 4-2 and 4-3.

2. <u>No Dissociation of Bisulfate Ion, when $r \geq 0.5$</u>

The mathematics are essentially the same as in the previous case, except that q is now $(c_B - c_A)/(c_B + c_A)$. In order to be comparable to the previous case, q is related to r by q = 2r - 1. Again if the Nernst-Einstein relation (4-2) is assumed, we obtain

$$\frac{I_L}{I_D} = 4\frac{1-\sqrt{q}}{1-q} - 1 \quad .$$

The same equations (G-13) of surface concentration are also valid in this case. If the ionic concentration is replaced by molecular concentration (see Table 4-1) and we are able to solve for c_B^o, there follows

$$c_B^o = \frac{1}{2}q^{\frac{1}{R}-1}(c_B^\infty - c_A^\infty) + \frac{1}{2}q^{\frac{1}{R}}(c_A^\infty + c_B^\infty)$$

3. <u>No Dissociation of Bisulfate Ion, when $r < 0.5$</u>

In this case the copper ion is the only cation; when its concentration drops to zero at the electrode surface, the remaining two anions have to be zero too, so that electroneutrality would be preserved. If c_1, c_2, and c_3 are set to equal zero at y=0 in Eq. (G-7b) and ionic concentrations are replaced by molecular concentrations of c_A and c_B, and the Nernst-Einstein relation is assumed, the ratio of limiting current is then reduced to

$$\frac{I_L}{I_D} = 1 + 2\left(\frac{r}{1-r}\right) + \left(\frac{1-2r}{1-r}\right) \quad ,$$

and the ratio of concentration change

$$\frac{c_B^o - c_B^\infty}{c_A^\infty} = -\frac{r}{1-r}$$

Numerical tabulations and plots of these two ratios have been given in Figs. G-1 and G-2 and in Table 4-1 and 4-2.

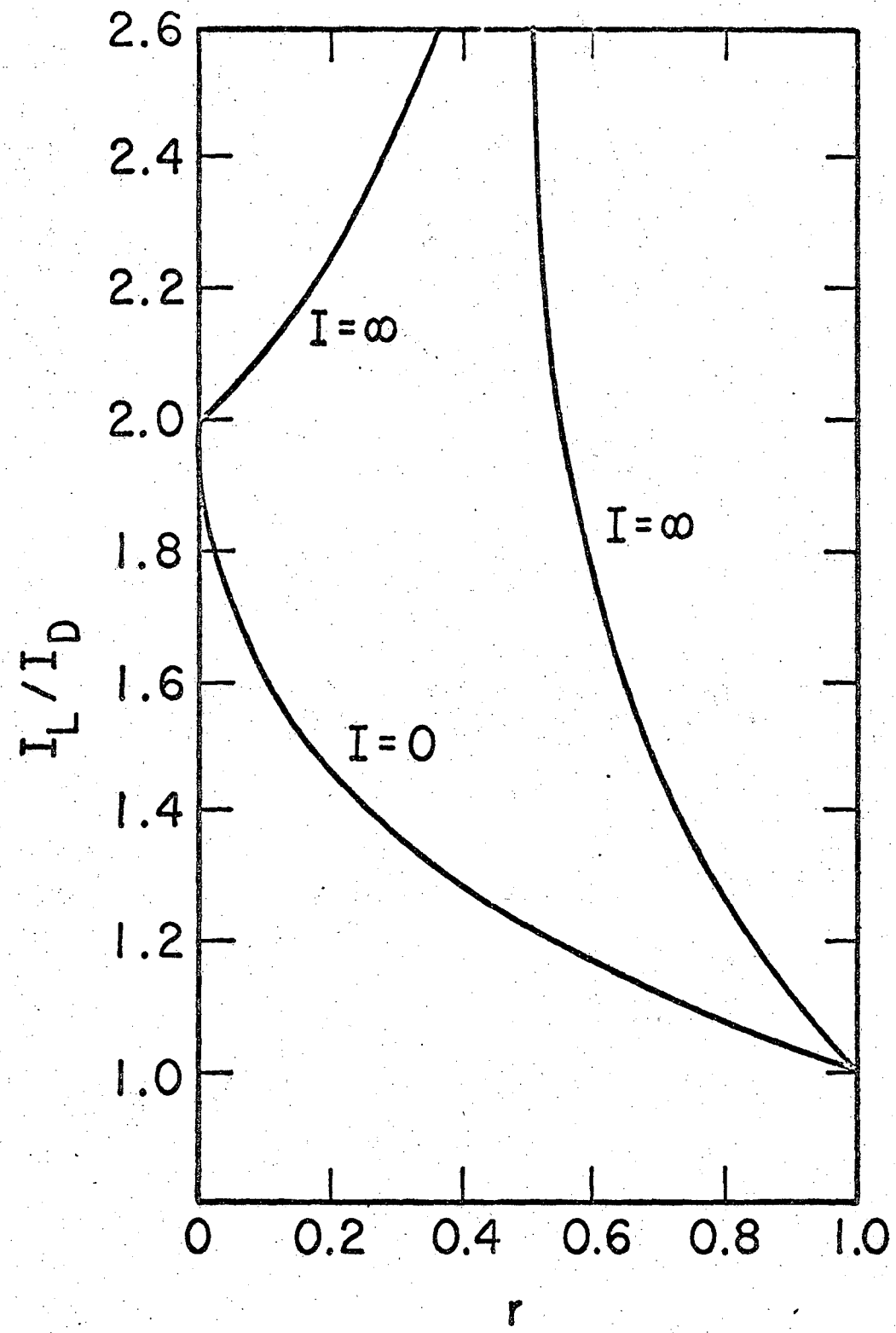

XBL 6812-6325

Fig. G-1. The effect of migration in a Nernst diffusion layer.

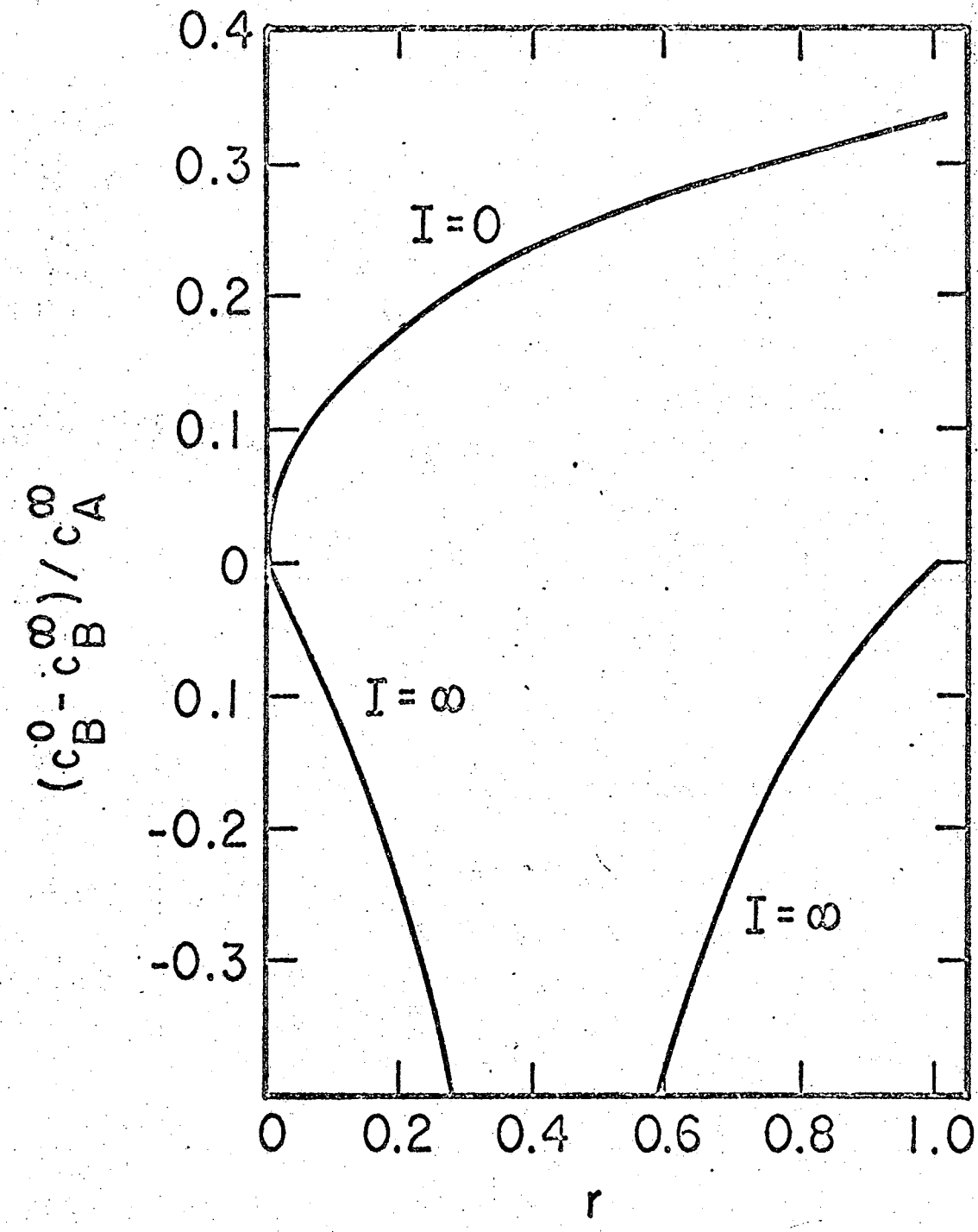

XBL 6812-6324

Fig. G-2. The surface concentration change in a Nernst diffusion layer.

NOMENCLATURE

(The numbers in parentheses refer to equation numbers)

a	constants (Table 3-1)
c_i	concentration of species i (mole/cm^3)
c_A	concentration of copper sulfate (mole/l)
c_B	concentration of sulfuric acid (mole/l)
D	molecular diffusivity (cm^2/sec)
$\bar{D}$	integral diffusion coefficient (cm^2/sec)
d	a damping factor
F	Faraday's constant (coul/equiv)
f	F/RT
H	function expressing dimensionless velocity in y direction
h	distance between two parallel plates of flow channel (cm)
I	dimensionless current (2-9), (5-10)
I	ionic strength of solution (4-8)
I_L	dimensionless limiting current
i	current density
i_o	exchange current density
J	dimensionless exchange current density (5-11)
$K_{1,2}$	first and second stage ionization constants
k	a constant (4-1)
$k_{1,2}$	ionization reaction kinetics constants
$k_{A,B}$	constants (7-3)
L	length of capillary tube (cm)
l	length of light path across an optical cell

M_i	molecular weight of species i
m	an exponent (4-1)
m	number of fringe shift
n	change of refractive index (7-1)
N_i	flux of species i (mole/cm^2-sec)
Q	a ratio of fluxes (3-11b)
q	an ionic concentration ratio (G-8)
R	universal gas constant (joule/mole-deg)
R	a ratio (G-9)
R	radius of growing mercury drop, cylinder, sphere (Table 3-1)
RI	Refractive index
r	concentration ratio of supporting electrolyte (4-4)
r	defines position of surface for an axisymmetric body (cm)
r_i	rate of ionic production (mole/cm^3-sec)
S	fluid velocity normal to the interface
Sc	Schmidt number
s_i	stoichiometric coefficient of species i in electrode reaction
T	temperature (deg K)
t	time (sec)
t_i	transference number of species i
t_c	characteristic time (5-14)
u_i	mobility of species i (cm^2-mole/joule-sec)
$\langle v \rangle$	average velocity in a conduit (cm/sec)
V	dimensionless total applied voltage (5-8)
x	distance measured along an electrode surface (cm)
y	distance normal from electrode (cm)
Z	(5-7)
z_i	valence or charge number of species i

α, β, γ	electrochemical reaction kinetic parameters (5-5)
$\beta(x)$	velocity derivative at electrode surface (sec^{-1})
Γ	the gamma function
δ	thickness of Nernst diffusion layer (cm)
η	dimensionless distance (Table 3-1)
η	dimensionless total overpotential (5-9)
η_c	concentration overpotential
η_s	surface overpotential
θ	dimensionless surface concentration (5-6)
κ	conductivity (mho/cm)
κ	ratio of radii of inner to outer cylinder
λ	wavelength of light (cm)
μ	viscosity (g/cm-sec)
ν	kinetic viscosity (cm^2/sec)
ν_+, ν_-	number of cations and anions produced by dissociation of one molecule of electrolyte
ξ	dimensionless variable (3-10) and (3-14)
ρ	density (g/cm^3)
τ	dimensionless time
ϕ	electrostatic potential (volt)
ψ_i	dimensionless electrostatic potential
Ω	rotation speed (radian/sec)
ω	mass fraction of salt in binary electrolyte

Subscripts or Superscripts

+,-	cation, anion
∞	in the bulk of solution
o	at electrode surface
D	diffusion current
L	limiting current
R	reactant

REFERENCES

1. John Newman "Engineering Design of Electrochemical Systems". Ind. Eng. Chem. 60, (No. 4) 12-27 (1968).
2. N. Ibl "Probleme des Stofftransports in der Angewandten Elektrochemie." Chemie-Ingenieur-technik, 35, 353-361 (1963).
3. John Newman and Limin Hsueh "The Effect of Variable Transport Properties on Mass Transfer to a Rotating Disk." Electrochim. Acta 12, 417-427 (1967).
4. John Newman "Transport Processes in Electrolytic Solutions." C. W. Tobias, ed., Advances in Electrochemistry and Electrochemical Engineering, 5, 87-135 (1967).
5. Limin Hsueh "Mass Transfer and Polarization at a Rotating Disk Electrode." (M.S. Thesis), UCRL-16607, January 1966.
6. R. N. O'Brien, "Concentration Gradients at Horizontal Electrodes," J. Electrochem. Soc., 113, 389-392 (1966).
7. N. Ibl and G. Trumpler "Uber zwei Elektrolyseprobleme mit linearer Diffusion bei Abwesenheit von Konvektionen." Helvetica Chimica Acta 34, 1217-1223 (1951).
8. V. G. Levich "The Theory of Concentration Polarization." Acta Physicochimica USSR, 17, 257-307 (1942).
9. R. Byron Bird, Warren E. Stewart, and Edwin N. Lightfoot. Transport Phenomena. New York: John Wiley & Sons, Inc., 1960.
10. R. E. Davis, G. L. Horvath and C. W. Tobias. "The Solubility and Diffusion Coefficient of Oxygen in Potassium Hydroxide Solutions," Electrochimica Acta, 12, 287-297 (1967).

11. M. v. Stackelberg, M. Pilgram and V. Toome."Bestimmung von Diffusions -koeffizientzen einiger Ionen in wässriger Lösung in Gegenwart von Fremdelektrolyten. I" Zeitschrift für Elektrochemie. 57, 342-350 (1953).

12. Andreas Acrivos. "Solution of the Laminar Boundary Layer Energy Equation at High Prandtl Numbers." The Physics of Fluids, 3, 657-658 (1960).

13. John Newman. "Schmidt Number Correction for the Rotating Disk," J. Phys. Chem., 70, 1327-1328 (1966).

14. John Newman. "Effect of Ionic Migration on Limiting Currents." Ind. Eng. Chem. Fundamentals 5, 525-529 (1966).

15. Andreas Acrivos. "The Asymptotic Form of the Laminar Boundary-layer Mass-Transfer Rate for Large Interfacial Velocities." J. Fluid Mech., 12, 337-357 (1962).

16. E. E. Stewart, J. B. Angelo and E. N. Lightfoot. "Forced Convection in Three Dimensional Flows: II. Asymptotic Solution For Mobile Interfaces." A. I. Ch.E. Journal, to be published.

17. John Newman. "The Effect of Migration in Laminar Diffusion Layers." Intern. J. Heat Mass Transfer, 10, 983-997 (1967).

18. D. R. Olander. "The Influence of Physical Property Variations on Liquid-phase Mass Transfer for Various Laminar Flows." Intern. J. Heat Mass Transfer, 5, 765-780 (1962).

19. William H. Smyrl and John Newman. "Potentials of Cells with Liquid Junctions." J. Phys. Chem., 72, 4660-4671 (1968).

20. M. J. Lighthill. "Contributions to the Theory of Heat Transfer through a Laminar Boundary Layer." Proceedings of the Royal Society A 202, 369-377 (1950).

21. J. B. Angelo, E. N. Lightfoot and D. W. Howard. "Generalization of the Penetration Theory for Surface Stretch: Application to Forming and Oscillating Drops." A. I. Ch.E. Journal, 12, 751-760 (1966).

22. H. Schlichting. Boundary Layer Theory. New York: McGraw-Hill Book Company, Inc., 1960 a. pp. 78-79 b. pp. 146-153.

23. L. Rosenhead. Laminar Boundary Layers. Oxford University Press, 1963, pp. 231-234.

24. J. C. Knudsen and D. L. Katz. Fluid Dynamics and Heat Transfer. New York. McGraw-Hill Book Company, Inc., 1958.

25. D. Ilkovic. "Polarographic Studies with the Dropping Mercury Kathode. - Part XLIV. - The Dependence of Limiting Currents on the Diffusion Constant, on the Rate of Dropping and on the Size of the Drops." Collection of Czechoslovak Chemical Communications, 6, 498-513 (1934).

26. R. A. Robinson and R. H. Stokes. Electrolyte Solutions. London: Butterworths Company, Inc., Revised ed. 1965 a. chapter 15 b. p. 463

27. John Newman. "Numerical Solution of Coupled, Ordinary Differential Equations." Ind. Eng. Chem. Fundamentals 7, 514-517 (1968).

28. V. G. Levich. Physicochemical Hydrodynamics. Englewood Cliffs: Prentice-Hall, Inc., 1962 Section 53.

29. Arnold Eucken. "Uber den stationären Zustand zwischen polarisierten Wasserstoffelektroden." Z. physik. Chem. 59, 72-117 (1907).

30. Andreas Acrivos and Paul L. Chambré. "Laminar Boundary Layer Flows with Surface Reactions." Ind. Eng. Chem., 49, 1025-1029 (1957).

31. Leon Lapidus. Digital Computation for Chemical Engineers. New

York: McGraw-Hill Book Company, Inc., 1962.

32. E. Mattsson and J. O'M. Bockris. "Galvanostatic Studies of the Kinetics of Deposition and Dissolution in the Copper + Copper Sulphate System." Transactions of the Faraday Society, 55, 1586-1601 (1959).

33. John Newman. "Current Distribution on a Rotating Disk below the Limiting Current." J. Electrochem. Soc., 113, 1235-1241 (1966).

34. W. R. Parrish and John Newman. "Current Distribution on a Plane Electrode below the Limiting Current." J. Electrochem. Soc., 116, 169-172 (1969).

35. A. J. Arvia, J. C. Bazan and J. S. Carrozza. "Electrochemical Study of Cupric Ion in Aqueous and Aqueous-Glycerol Solutions Containing Sulphuric Acid." Electrochimica Acta, 11, 881-889 (1966).

36. R. N. O'Brien. "Some Electrolyte Solution Refractive Indices at 5893 and 6328 A" J. Chem. Eng. Data 13, 2-5 (1968).

37. T. W. Chapman. "Transport Properties of Concentrated Electrolytic Solutions." (Ph.D. Thesis), UCRL-17768, November, 1967.

38. J. J. Fritz and C. R. Fuget. "Measurement of the Transference Numbers of Aqueous Cupric Sulfate Solutions by the Moving Boundary Method." J. Phys. Chem., 62, 303-304 (1958).

39. Benton Brooks Owen and Robert W. Gurry. "The Electrolytic Conductivity of Zinc Sulfate and Copper Sulfate in Water at 25°." J. Am. Chem. Soc. 60, 3074-3078 (1938).

40. John Newman. "Resistance for Flow of Current to a Disk." J. Electrochem. Soc. 113, 501-502 (1966).

41. A. I. Vogel. Quantitative Inorganic Analysis, 3rd ed., John Wiley and Sons, Inc., New York, N. Y. 1961.

42. D. M. Brasher and F. R. Jones. "The Effect of Viscosity of the Solution on Polarographic Diffusion Currents." Transactions of the Faraday Society, 42, 775-779 (1946).

43. W. G. Eversole, H. M. Kindsvater, and J. D. Peterson. "The Diffusion Coefficient of Cupric Sulfate from 0.0 to 0.35 Molar at 25°C." J. Phys. Chem., 46, 370-375 (1942).

44. Milton Abramowitz and Irene A. Stegun. eds. Handbook of Mathematical Functions. Washington, D. C.: NBS, 1964 p. 310 and p. 320.

LEGAL NOTICE

This report was prepared as an account of work sponsored by the United States Government. Neither the United States nor the United States Atomic Energy Commission, nor any of their employees, nor any of their contractors, subcontractors, or their employees, makes any warranty, express or implied, or assumes any legal liability or responsibility for the accuracy, completeness or usefulness of any information, apparatus, product or process disclosed, or represents that its use would not infringe privately owned rights.

TECHNICAL INFORMATION DIVISION
LAWRENCE RADIATION LABORATORY
UNIVERSITY OF CALIFORNIA
BERKELEY, CALIFORNIA 94720